Quantum Fluctuations in Two-Dimensional Metals with Singular Forward Scattering

Von der Fakultät Mathematik und Physik der Universität Stuttgart
zur Erlangung der Würde eines Doktors der Naturwissenschaften
(Dr. rer. nat.) genehmigte Abhandlung

vorgelegt von

Tobias Holder

aus Stuttgart

Hauptberichter:	Prof. Dr. Walter Metzner
Mitberichter:	Prof. Dr. Maria Daghofer
Tag der mündlichen Prüfung:	9. Dezember 2015

Max Planck Institut für Festkörperforschung
Stuttgart 2015

Universität Stuttgart

Max Planck Institute for Solid State Research

For my family

How many are your works, Lord!
In wisdom you made them all;
the earth is full of your creatures.

Psalm 104,24

Contents

1 Introduction

In the field of correlated many-body systems continuous quantum phase transitions have in the last few decades become a persistent source of rich and unconventional phyics [1–6]. A quantum phase transition (QPT) takes place at zero temperature if tuning a non-thermal control parameter like pressure or magnetic field leads to a significant change in the ground state wave function with respect to symmetry or degeneracy. If the phase transition spontaneously breaks a symmetry of the Hamiltonian, a description in terms of a Landau order parameter is possible. The expectation value of the order parameter may change discontinuously at the phase transition, making the transition of first order. A continuous onset of the order parameter on the other hand is associated with a second order phase transition. In the phase diagram, a second order quantum phase transition is denoted a *quantum critical point* (QCP), at which correlations span all energy scales and the thermodynamics and transport obey universal scaling laws. In high dimensions the exponents of this critical scaling follow mean field behavior. In low dimensions quantum fluctuations become important and affect the critical exponents. By definition, a QPT and thus the QCP is always restricted to zero temperature. Quantum criticality on the other hand is determined by a precedence of quantum fluctuations over thermal fluctuations and other disturbances, a condition which can be fulfilled even at comparatively high temperatures. In a number of materials, the influence of the quantum critical scaling laws are thus visible in a large area of the phase diagram around the QCP (Fig. 1.1).

Quantum criticality

Quantum criticality and thus the existence of a QCP has been put forward for many unconventional condensed matter systems, among them heavy fermion compounds [7, 8], and the high-temperature superconductors of the cuprate and pnictide families [9–11]. Quantum critical behavior also surfaces in the study of fractional quantum Hall systems at half filling [12] and doped Mott insulators [13, 14]. More recently, experiments with ultracold gases have gained a lot of attention as a possible way to engineer and tune many-body systems at will, which opens a route to recreate QCPs and entire phase diagrams in a controlled way [15, 16]. Additionally, the dilute Fermi gas itself provides with the BCS-BEC crossover a textbook case of quantum criticality without a QPT at strong coupling [17].

Apart from the experimental input, the theoretical interest in quantum criticality is also fueled by the intricate difficulties one faces in the treatment of quantum fluctuations [2, 6, 18]. By conventional wisdom, a QCP in d spacetime dimensions should behave like a corresponding $d + z$-dimensional classical critical point, where an additional z dimensions account for the quantum degrees of freedom. In this case a straightforward analysis in terms of a Landau-Ginzburg-Wilson (LGW) action of the order parameter would be possible [19–21]. Since a couple of years it is known that this identification fails in a number of important cases, a particular notorious offender being a metal near a QCP [22, 23]. The problems are related to the presence of a Fermi surface: The Landau quasiparticles in a metal are gapless and contribute additional soft modes to the action. An expansion of an LGW-action solely in terms of the gapless order parameter fields then contains effective interactions which are singular due to low energy quasiparticle excitations, with potentially catastrophic consequences [24, 25]. But not only the order parameter field is strongly affected by the Fermi surface, there is also a back-reaction on the quasiparticles which can significantly shorten their lifetime, effectively undermining the notion of a Fermi liquid. These overdamped quasiparticles are frequently referred to as a "singular Fermi liquid" or "non-Fermi liquid" [7, 26–28]. Both the singular interactions and the interplay of multiple soft modes with very dissimilar characteristics lie at the very heart of many issues of understanding metallic quantum criticality. Since the first appearance of non-Fermi liquids (NFL) in two dimensions in the mid-nineties many attempts were made to capture the essential physics featuring a plethora of methods and approximations. While a lot of progress was made, a universal tool to tackle the coupling of a Fermi surface to gapless bosons is presently unknown.

A popular way to treat multiple gapless modes is a parametrization in terms of a combined fermion-boson low energy effective action. Such an action can keep track of both fermionic and bosonic dynamics, which allows for a more granular control of singular terms.

To illustrate this concept, we consider a generic single band metal with fermionic fields ψ, a four-fermion interaction V and a number of discrete or continuous degrees of freedom x, (usually momentum, frequency and spin)

$$S[\psi, \bar{\psi}] = \sum_x \bar{\psi}_x G_x^{-1} \psi_x + \tfrac{1}{4} \sum_{x,x',x'',x'''} V_{x,x',x'',x'''} \bar{\psi}_x \psi_{x''} \bar{\psi}_{x'} \psi_{x'''}. \tag{1.1}$$

The Stoner criterion for a critical phase transition tells us that the susceptibility which is sensitive to the symmetry breaking diverges at criticality. Therefore, the physics is dominated by scattering processes which mediate the symmetry breaking. After restricting the four fermion interaction to this interaction channel, it is then useful to decouple the four fermion term by introducing a Hubbard-Stratonovich field ϕ

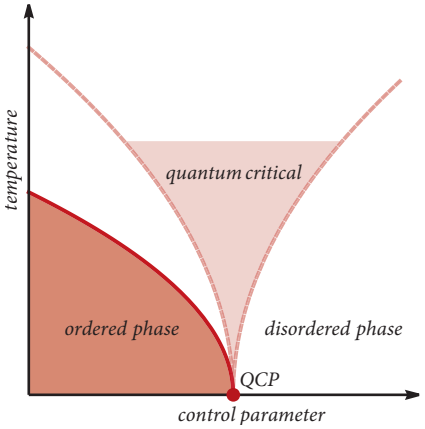

(a) Schematic phase diagram around the continuous onset of an ordered phase. The phase transition line (dark red) can be classical critical or first order. In 2d dimension the ordered phase is usually destroyed by thermal fluctuations and only exists at zero temperature.

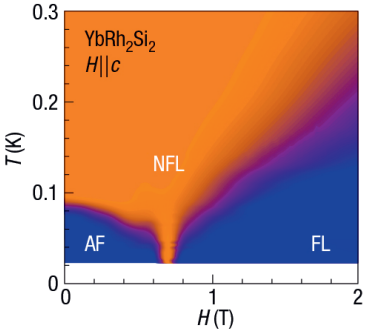

(b) Quantum criticality in the heavy fermion compound $YbRh_2Si_2$, when the ordered phase is suppressed with a magnetic field. The temperature exponent of the resistivity is 1 in the quantum critical regime (orange) and 2 otherwise (blue). From [8], see also [29].

Figure 1.1 The phase diagram in proximity of a quantum critical point. The presence of the QCP leads to a quantum critical "fan" at finite temperatures, in which the disordered phase exhibits universal scaling with unusual exponents. On the left a schematic view is shown and on the right an experimental example.

of the corresponding singular channel. The resulting fermion-boson action retains only kinetic terms and a Yukawa coupling g,

$$S[\psi, \bar{\psi}, \phi] = \sum_x \bar{\psi}_x G_x^{-1} \psi_x + \tfrac{1}{2} \sum_{x,x'} \phi_x^* D_{x,x'}^{-1} \phi_{x'} + \sum_{x,x',x''} g_{x,x',x''} \phi_x \bar{\psi}_{x'} \psi_{x''}. \quad (1.2)$$

While this step is formally exact for the critical channel, in a practical calculation certain approximations are necessary for the matrix elements of G, D and g. The most straightforward derivation of such a fermion-boson model is therefore done in terms of a low energy effective theory, which could be justified phenomenologically or derived by a renormalization flow which integrates modes successively. An action of the form of Eq. 1.2 is nowadays almost universally employed to deal with metallic quantum criticality. We stress that the exclusive focus on the singular channel is a severe restriction in any practical instability analysis, as it favors one interaction

channel over the others [30]. It is also important to keep in mind that the issue of singular interactions is not solved by the combined fermion-boson approach, it persists in any formulation. Quantum criticality is inherently a strong coupling problem and always requires some manually introduced control on interactions to allow a perturbative or renormalization group treatment. Much of the literature deals exactly with this quest.

Motivations

This thesis will focus on a particular fermion-boson action in 2D which was a long time ago proposed as a minimal model to couple fermions to a fluctuating U(1) gauge field, but has more recently resurfaced as the low-energy effective theory for a nematic QCP in two dimensions. The model describes fermions at finite density which couple to a bosonic field via forward scattering (zero momentum transfer scattering) in the charge channel. At zero temperature the action is in momentum space and imaginary frequencies given by

$$S[\psi,\bar{\psi},\phi] = \sum_{k,\sigma} \bar{\psi}_{k,\sigma}(ik_0 - \epsilon(\mathbf{k}))\psi_{k,\sigma} + \tfrac{1}{2}\sum_{q} \phi(q)\mathbf{q}^2\phi(-q) + \sum_{q,k,\sigma} g(\mathbf{k})\phi(q)\bar{\psi}_{k-\frac{q}{2},\sigma}\psi_{k+\frac{q}{2},\sigma} \tag{1.3}$$

where σ is the spin index and spins are trivially summed as the interaction is spin independent. $\epsilon(\mathbf{k})$ is the dispersion with respect to the Fermi surface, the vertex g varies only slowly along the Fermi surface and is independent of the transmitted momentum q. One might also want draw a connection from the model defined by Eq. 1.3 to the low-energy theory of a ferromagnetic QCP in 2D, which features critical forward scattering in the spin channel, but both models do not share the same universality class [31].

In the last three decades, the action in Eq. 1.3 was suggested as the proper low-energy theory for a large number of strongly coupled condensed matter systems, in most cases ultimately unsuccessfully. On a formal level, the model comprises only two physically distinct cases, depending on the structure of the interaction $g(\mathbf{k})$. In the following, we briefly present the history of the model and the different motivations for its study. The review is grouped with regards to the symmetry properties of $g(\mathbf{k})$.

If $g(\mathbf{k}) = -g(-\mathbf{k})$, the action describes fermions coupled to a random $U(1)$ gauge field. In two dimensions such a system was first discussed in the early days of high temperature superconductors after Anderson suggested the enigmatic resonating valence bond (RVB) state as a core mechanism in the hole-doped cuprates [28, 32–34]. An RVB state might arise if antiferromagnetically coupled spins can gain energy by

forming a liquid of singlet dimers compared to a static Néel order. Low dimensions and frustration helps to form an RVB state, the former of which holds for cuprates as doped antiferromagnetic Mott insulators with small interlayer hopping. At the time, the slave-boson method was extensively used to treat the t-J model of the cuprates, and it was soon realized that the redundancy which is introduced with the slave-boson approach leads to an additional gauge degree of freedom [35–38]. The simplest choice for the gauge field is abelian ($U(1)$), which leads directly to Eq. 1.3. While the physical origin of the model is unrelated to quantum phase transitions, the appearance of a massless gauge field ensures the emergence of quantum critical scaling. The spinon-gauge system, as it was called at the time [39] was later abandoned as a candidate to explain the physics of the normal state of high temperature superconductors, but it helped to boost the study of what is nowadays known as spin liquids and deconfined quantum criticality [13, 40, 41].

The $U(1)$-gauge action has ever since enjoyed a fair share of attention. It was invoked to explain experiments on certain frustrated magnets [42–44], which contain spinon excitations like the cuprates but no charge modes, thus simplifying the situation considerably [45–47]. Deconfined quantum criticality associated with the spinon-gauge model was also theorized for heavy fermion systems [48]. More recently, it was also proposed for underdoped cuprates in a scenario which was termed an "algebraic charge liquid" [49, 50].

The $U(1)$ gauge theory is also featured in Quantum Hall physics. The action Eq. 1.3 describes fermions at a finite density coupled to an abelian gauge field, this also describes normal electrons at a finite density coupled to the transverse component (vector potential) in conventional quantum electrodynamics (QED). Unsurprisingly, the QED case was studied a long time ago in three dimensions [51, 52], already pointing towards a breakdown of Fermi liquid theory. However, due to the suppression with the speed of light, for a magnetic field these effects only become visible at extremely low temperatures, rendering the impact of transverse fluctuations in a metal a mere academic exercise. The situation changes dramatically if the transverse fluctuations are the result of an emergent gauge field with comparatively higher scales. This is the case for a half filled Landau level ($\nu = \frac{1}{2}$) in fractional quantum Hall systems [12, 53–55]. At half filling the two-dimensional electron gas combines with the external magnetic field to form composite electrons which experience a mean magnetic field equal zero [56]. Gauge fluctuations on top of the mean field solution are then governed by the much larger energy scale of the cyclotron motion and no longer negligible. [1]

[1] We point out, however, that the $\nu = \frac{1}{2}$ state usually features an electron liquid where the Coloumb interaction is unscreened, in which case the kinetic energy of the bosons is proportional to $|\mathbf{q}|$ instead of $\mathbf{q}^2$, the latter of which applies to a screened Coloumb interaction only.

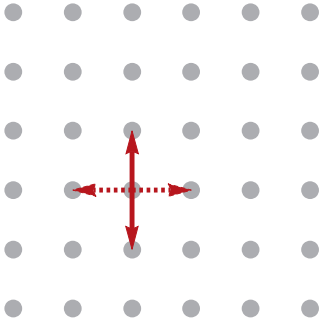

(a) Real space. The electrons spontaneously favor one direction of movement over the other, breaking the symmetry between horizontal and vertical hopping amplitudes.

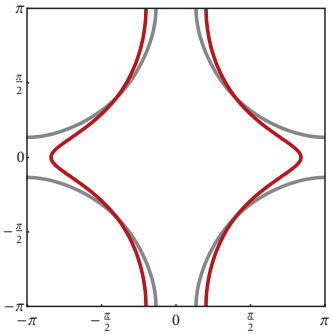

(b) Momentum space. The original C_4 symmetric Fermi surface (gray) turns into a C_2 symmetric one (red). Depending on the original shape of the Fermi surface, the resulting Fermi surface can be quasi-one-dimensional.

Figure 1.2 Nematic ordering in a square lattice. The reduction of the C_4 rotational symmetry is shown in real space and momentum space.

If the interaction in Eq. 1.3 fulfills $g(\mathbf{k}) = g(-\mathbf{k})$, i.e., if it is even with respect to momentum, the model can describe a nematic instability in a Fermi liquid. Nematic ordering appears if the electronic motion spontaneously develops a rotational anisotropy in the system. In a tight-binding picture, this means that the hopping amplitude for bonds of a certain direction are enhanced, while the remaining ones are decreased (Fig. 1.2). This behavior can also be seen as a uniform *bond order*. In momentum space, nematic order reduces the rotational symmetry of the Fermi surface, creating a preferred axis along which more states are occupied. Electronic nematicity is therefore a spontaneous symmetry breaking of the rotational symmetry, but without breaking any translational symmetry. The adjective "nematic" was chosen in analogy to liquid crystal nematicity, a famous example of spontaneous rotational symmetry breaking in a classical system [57].

The nematic transition is of the Pomeranchuk type [58, 59], i.e., it leads to a Fermi surface deformation while preserving the Fermi surface topology. The paradigmatic case considered in the literature is a d-wave Pomeranchuk instability, where the interaction $g(\mathbf{k})$ contains a d-wave form factor, thus changing sign upon a $\frac{\pi}{2}$ rotation in momentum space. For an isotropic Fermi liquid, the corresponding Landau parameter belongs to the charge channel with angular momentum $\ell = 2$.

In a lattice, the nematic instability breaks a discrete rotational symmetry. In contrast, for metals with a circular Fermi surface a continuous rotational symmetry is broken by nematic order. To distinguish the two classes of symmetry breaking in lattice systems and isotropic Fermi liquids respectively, the former is called "Ising nematic" [60] and the latter "quadrupolar" [61].

Electronic nematicity was first considered in the context of cuprate superconductivity. This connection can best be understood by looking at the transient nature of rotational symmetry breaking. On the one hand, the anisotropy of the correlation functions in a nematic phase can be seen as an intermediate between a true two-dimensional lattice and weakly coupled chains, which are quasi one-dimensional. Nematic order is thus important in the dimensional crossover from two to one dimension. On the other hand, coupled chains also emerge when a density wave order becomes pinned in a unidirectional manner, creating characteristic stripes in the real space electronic density which break both translational and rotational symmetry. Nematicity then emerges when the translational symmetry is restored in a process which is known as a "melting" of stripes. After the observation of stripes in a narrow region of the phase diagram of some cuprates, the melting of stripes and the resulting nematic correlations were proposed as an important factor in the normal state of cuprate superconductors [57]. Subsequent experiments confirmed the presence of uniform anisotropic correlations in cuprates [62–65], but the interplay of possible stripes and nematicity in the vicinity of superconductivity remains difficult to disentangle [66–70]. More recently, nematicity was reported in several iron-based superconductors (pnictides) in close proximity to the superconducting dome [71–74]. The phenomenology mentioned so far point out nematic correlations, but not necessarily a nematic QCP. It is the conjoint occurrence of charge anisotropies, high-temperature superconductivity and the existence of a so called strange metal region that has fueled speculations about the interplay of these orders and the presence of a nematic QCP. More precisely, in the phase diagram of many unconventional superconductors one finds a broad region directly above the superconducting dome, termed strange metal, in which the electrical resistivity has an unusual linear temperature dependence (Fig. 1.3a). This linear power law can be identified with quantum critical scaling and consequently with the presence of a QCP below the superconducting dome [11, 77]. The common idea is now to trace the origin of the high superconducting transition temperatures back to strong correlations arising from critical fluctuations [67, 78]. Many suggestions are abound for the nature of the QCP point (or even a multitude of QCPs) below the superconducting dome [79, 80]. Among these suggestions also nematic order was studied intensely as a possible candidate [81–84].

Apart from the high-temperature superconductors, nematic ordering is a recurrent topic in a number of other systems with strong interactions. Nematicitiy was for

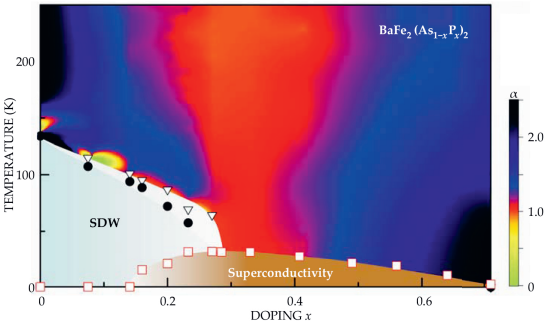

(a) Linear-T resistivity above the superconducting dome in the pnictide $BaFe_2(As_{1-x}P_x)_2$. The quantum critical region terminates near the onset of spin density wave order, which coincides with the maximal superconducting transition temperature.

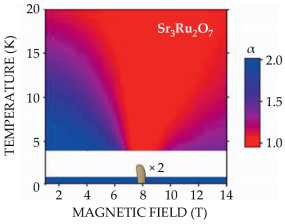

(b) Temperature exponent of the electrical resistivity. The small brown area at 8T marks the nematic phase (doubled in size for better visibility) with a region of metamagnetic criticality above.

Figure 1.3 Examples of strange metal regions in an iron-based superconductor (a) and the ruthenate $Sr_3Ru_2O_7$ (b). In both figures the temperature exponent α of the electrical resistivity in the normal phase is shown, where a red color indicates a linear temperature dependence. The red regions clearly resemble a quantum critical "fan" of the form drawn in Fig. 1.1a. Figures taken from [11], based on the experimental data of [75] and [76].

example suggested as a possible candidate for the "hidden order" in the heavy fermion compound URu_2Si_2 [85]. In Quantum Hall systems, an anisotropic state has been found for high Landau levels [86, 87].

A particularly clear example for nematic ordering is believed to be given by $Sr_3Ru_2O_7$, for which a small nematic phase and a surrounding quantum critical "fan" was measured at high magnetic fields [60, 88, 89] (Fig. 1.3b).

On a more theoretical side, instability analyses of the t-J model [90, 91] and the Hubbard model [92] pointed out tendencies to nematic ordering in these microscopic models. The nematic instability was also studied more directly in a tight binding model containing a phenomenological d-wave density-density interaction [93]. Within mean field theory a nematic dome is present for a range of fillings and hopping amplitudes [94–96]. At zero temperature, the phase transition is generically first order, but fine-tuning or the inclusion of order parameter fluctuations can drive the transition to second order [96, 97]. In the latter case, the nematic phase as a whole is suppressed, and can even vanish entirely, leaving an isolated QCP without any adjacent ordered phase [98].

A breaking of the rotational symmetry of the Fermi surface was also studied as a secondary instability, a nodal superconductor for example can develop a nematic QCP [83, 99]. Similarly, nematic order can form after the destruction of a classical [100, 101] or a quantum [102, 103] antiferromagnetic order.

As was mentioned briefly, in very low density electron systems like ultracold fermion gases the Pomeranchuck instability distorts an isotropic Fermi surface, which falls into a different universality class (quadrupolar order). The fluctuation dynamics then features not one but two critical modes with dissimilar critical scaling, which leads to multiscale quantum criticality [104–109]. We do not pursue this case further.

Previous works and outline

While the impressive popularity of both, the $U(1)$ gauge theory and the nematic QCP, is certainly motivated by the multitude of applications which have been discussed over the years, an important contribution is also the theoretical significance of the solution of Eq. 1.3. This action can be seen as a minimal model of metallic criticality, coupling a single-band fermion non-spin selectively to one gapless abelian boson, which is arguably the simplest possible choice. In this thesis, we will refer to this action as the "spinless critical metal" (SCM), and distinguish both physical cases - fermions coupled to a $U(1)$ gauge field and the nematic instability - only when it is necessary. Here, the attribute "spinless" is not with regards to the fermionic spinors, which have spin $1/2$, but with regards to the nature of the coupling. We further adopt a differentiation with respect to the symmetry of the interaction $g(\mathbf{k})$ under inversion of momentum, calling the case $g(\mathbf{k}) = g(-\mathbf{k})$ "even coupling" and likewise $g(\mathbf{k}) = -g(-\mathbf{k})$ "odd coupling".

Despite intense effort, the physics associated with the spinless critical metal is not fully understood. It is known from a perturbative calculation that already at one loop level fluctuations produce strong self-energy corrections, leading to a non-Fermi liquid [110, 111]. This result is not changed at two loops [39, 112, 113] and was considered stable until logarithmically divergent diagrams were found recently at three loops [114]. In a renormalization group treatment, these singular contributions introduce anomalous scaling exponents. At the same time it was realized that the SCM action cannot be controlled by a large-N limit, making any expansion very difficult [114, 115]. Still, the three loop result suggested only a small anomalous dimension for the fermionic field strength renormalization and found no correction at all for the dynamical critical exponent $z = 3$. Subsequent works confirmed this, exploring a number of different avenues to regain a small parameter [116–118].

This thesis aims to contribute a small step in understanding the SCM action, with a special focus on the magnitude of quantum fluctuations directly at the critical point.

We derive a number of exact analytical results which expose and explain the peculiar behavior of the loop expansion, paving the way to the prediction and confirmation of a renormalization of the dynamical critical exponent at four loops. Furthermore, we offer new insights why the anomalous terms are so small and provide conditions under which the loop expansion is viable. Our results at four loop call the stability of the nematic QCP into question, and we explore several possible consequences.

The present analysis will be restricted to zero temperature. We stress that the usual identification of $\omega \sim T$ which is often used to extend $T = 0$ results to finite temperatures fails for the SCM [111], so that no conclusions about the quantum critical region at finite temperature can be drawn from the QCP directly.

For even coupling, the model is also constrained to the nematic channel, thus completely neglecting the dynamics of a competition with other instabilities. Competing orders, especially the interplay of charge fluctuations and the onset of superconductivity has recently attracted attention [119–121]. A different possibility is a spatially modulated Pomeranchuk instability, i.e., an incommensurate nematic order, also called modulated bond order, which was recently proposed to be important in the cuprates [122–124]. The mostly analytical treatment presented here expands around zero momentum transfer and is therefore incapable to account for ordering at a finite momentum, something which would require a different expansion point or a more numerical approach.

In low dimensional systems disorder can have a huge impact, possibly also near criticality. Only few studies investigated the effects of disorder on a nematic phase, but the results indicate already that there are situations when disorder is a relevant perturbation. A random chemical potential for example can destabilize a nematic QCP, disorder and impurities generally also affect the transition temperatures and transport [125–127]. We will not consider disorder in this work.

In the first part of this thesis we derive general improved power counting rules for higher order corrections. These rules retroactively explain previous explicit results and suggest that the conjectured stability of $z = 3$ breaks down at four loops.

For this, we briefly review in chapter 2 the Eliashberg approach to the SCM and critically examine the Fermi surface patching and the integration techniques which are commonly employed. Special attention is given to the incorporation of vertex corrections and the lines of arguments which were put forth historically to rationalize the usability of partial resummations. In chapter 3 we derive an explicit expression for the effective N-point density vertices and generalize results from free fermions in 2D and the Tomonaga-Luttinger model in 1D to the present problem. By combining the various limiting cases in a suitable way, we improve the power counting estimate and develop a classification scheme which allows to easily differentiate between finite and singular fluctuation corrections. A comparison with various related treatments reveals that the singularity structure presented here is most likely not altered by any

additional "hidden symmetries". The results for the density-density vertices are not only applicable to the present case of an SCM, but offer a straightforward way to deal with higher order corrections in other non-Fermi liquids. We show that the power counting improvement rules out power law divergences, which could previously not be excluded and are present in the related problem of the 2d ferromagnetic QCP [31]. These findings are published in a preprint [128].

While the power counting results strongly hint at a renormalization flow away from $z = 3$ at loop order four and higher, this conclusion is not mandatory: The identification of the cancellations up to three loops and the absence of the same type of cancellation starting with four loops only negates that the same mechanism is present for arbitrary high fluctuation corrections, it does not prove the actual presence of singular terms. The second part of the thesis resolves this issue. In chapter 4 we calculate a certain subset of four-loop contributions to the susceptibility whose divergence is sufficient to show that $z = 3$ is violated either for the nematic QCP or the U(1)-gauge system or probably both. The evaluation is done in parts analytically with the final integrations being performed numerically. We find a singular term at four-loop which carries a multi-logarithmic divergence, indicating a breakdown of the original scaling ansatz. Several possible consequences of this unexpected behavior are investigated, among them quantum anomalies, spontaneous symmetry breaking and a destruction of the QCP. We argue for the latter by illustrating how the order parameter field might acquire a mass, driving the continuous phase transition to a fluctuation induced weak first order transition. Parts of these results were published recently [129].

We summarize in chapter 5, offering possible avenues to improve on the presented results.

2 The spinless critical metal

In this chapter we present the ingredients and approximations used to derive a set of renormalization group equations for the spinless critical metal. In Sec. 2.1 the Fermi liquid picture of a QCP is introduced, which views the system at criticality as a deformed Fermi liquid with anomalous low quasiparticle lifetimes. We document how the Hertz-Millis-Moriya theory of quantum criticality fails for the SCM and exemplify the general mechanisms of this failure with the examples of other critical metals like the critical ferromagnet or antiferromagnet. The resolution to these problems in form of an effective low-energy action is presented in Sec. 2.2. At one-loop level, this action leads to unusual renormalizations which enforce a special low-energy limit of 321-scaling (Sec. 2.2.1). As a consequence, the forward scattering limit becomes so strong that the Fermi surface effectively decouples into distinct local patches, and we explain in detail how this happens in Sec. 2.2.2. The decoupling allows for an efficient formulation of the SCM in a two-patch approximation, which only retains the Fermi surface near an arbitrary expansion point $\mathbf{k}_F$ and its antipode $-\mathbf{k}_F$. Based on this approximation, a perturbative expansion around the one-loop result is formulated in Sec. 2.2.3, which essentially amounts to next-to-leading order calculations within RPA. This perturbation theory can then easily be generalized to a renormalization group flow which tracks the evolution of anomalous exponents due to fluctuations (Sec. 2.2.4). An important issue is the absence of a small parameter in the SCM. In the low-energy limit it is also not possible to expand in a large number N_f of fermion flavors, as is discussed in Sec. 2.2.5. In the absence of a small parameter, general arguments for the smallness of vertex corrections, as they were sought historically, fall short. In Sec. 2.2.6, we calculate the full frequency and momentum dependence of the one-loop vertex correction and use this to present an alternative line of arguments which supports the smallness of vertex corrections.

The two-patch approximation entails a parabolic Fermi surface with a linear momentum dependence perpendicular to the Fermi surface. This linearity plays a crucial role for all calculations, because it allows for an easy integration by residues. In Sec. 2.3 we state results for diagrams which only contain fermions from one Fermi surface patch. A simple proof is given for the nonrenormalization theorem of chiral fermions.

A few special notations will be used throughout the text. Fermionic variables usually are denoted by k or p, bosonic ones by q. Frequencies k_0 and two dimensional

momenta $\mathbf{k}$ will often be jointly denoted by $k \equiv (\mathbf{k}, k_0)$ in indexes and arguments. The standard volume integral in frequency-momentum space is abbreviated by

$$\int_k \equiv \int \frac{\mathrm{d}^2\mathbf{k}\mathrm{d}k_0}{(2\pi)^3}. \tag{2.1}$$

A prominent role is played by a fractional exponent $2/3$. We therefore use the notation

$$\{x\} \equiv \mathrm{sgn}\,(x)|x|^{2/3}. \tag{2.2}$$

2.1 Singular Fermi liquids

In the following we will restrict the discussion to a system in two dimensions and zero temperature. A normal Fermi liquid is an interacting gas of fermions in which basic excitations retain their fermionic character. If this is the situation, it is possible to adiabatically connect the noninteracting system with the fully interacting one. Given second-quantized electron creation and annihilation operators $c^\dagger_{\mathbf{k}\sigma}$ and $c_{\mathbf{k}\sigma}$, where σ is the spin index, the free Hamiltonian is

$$H = \sum_{\mathbf{k}\sigma} \varepsilon(\mathbf{k}) c^\dagger_{\mathbf{k}\sigma} c_{\mathbf{k}\sigma}. \tag{2.3}$$

$\varepsilon(\mathbf{k})$ is the electron dispersion. We choose a definition of the dispersion which already contains the chemical potential μ. At the Fermi surface, the dispersion including the chemical potential is $\varepsilon(\mathbf{k}) = 0$. A low energy excitation is given by the creation of a particle with $\varepsilon(\mathbf{k}) > 0$ or the annihilation of a particle (creation of a hole) with $\varepsilon(\mathbf{k}) < 0$. In the vicinity of the Fermi surface, these excitations follow a linear dispersion $v(\hat{\mathbf{k}})k_r$, where the unit vector $\hat{\mathbf{k}} = \mathbf{k}/|\mathbf{k}|$ points perpendicular to the Fermi surface. $|k_r|$ measures the distance to the Fermi surface, where $k_r > 0$ corresponds to particles and $k_r < 0$ to holes. The noninteracting Green's function in imaginary times is defined as

$$G_0(k)\delta_{\sigma\sigma'} = -\int \mathrm{d}\tau \langle \mathcal{T}[c_{\mathbf{k}\sigma}(\tau) c^\dagger_{\mathbf{k}\sigma'}(0)]\rangle e^{ik_0\tau}, \tag{2.4}$$

and thus

$$G_0(k) = \frac{1}{ik_0 - v(\hat{\mathbf{k}})k_r}. \tag{2.5}$$

For a Fermi liquid, the low-energy excitations share the same quantum numbers, but the Green's function is instead

$$G(k) = \frac{Z(\hat{\mathbf{k}})}{ik_0 - \bar{v}(\hat{\mathbf{k}})k_r}, \tag{2.6}$$

meaning that they have a renormalized quasiparticle residue $Z(\hat{\mathbf{k}})$ and a renormalized Fermi velocity $\bar{v}(\hat{\mathbf{k}})$. The interpolation between the free and the fully interacting system is conveniently realized by a renormalization group flow which successively integrates out high energy electronic states. The result of this RG is a low-energy effective action with the quadratic part

$$\mathcal{S}[\bar{\psi}, \psi] = \sum_{\sigma} \int_k \bar{\psi}_{k,\sigma} G^{-1}(k) \psi_{k,\sigma}. \tag{2.7}$$

Within Fermi liquid theory, the residual interactions of the quasiparticles ψ are of vanishing strength and only mediate scattering between points near the Fermi surface. From the RG, one can then conclude that only two interaction types are not irrelevant, namely zero momentum scattering (also termed forward scattering) and the BCS channel [130, 131]. To see how this argument goes, we concentrate on an isotropic system and adopt a scaling which successively approaches the Fermi surface as a whole. With the vector $\mathbf{k}_r = \mathbf{k} - \mathbf{k}_F$ and using the renormalization scale $\lambda \to 0$, the scaling is

$$\mathbf{k}_F \to \mathbf{k}_F \qquad \mathbf{k}_r \to \lambda \mathbf{k}_r \qquad k_0 \to \lambda k_0, \tag{2.8}$$

the quasiparticle field thus scales like $\lambda^{-3/2}$. The four fermion interaction is generally

$$\sum_{\sigma,\sigma'} \int_{k_1,k_2,k_3,k_4} V(k_1,k_2,k_3,k_4) \bar{\psi}_{k_1,\sigma} \psi_{k_3,\sigma} \bar{\psi}_{k_2,\sigma'} \psi_{k_4,\sigma'} \delta^3(k_1 + k_2 - k_3 - k_4). \tag{2.9}$$

When disregarding the δ-function, this scales as λ^2, which is irrelevant. Taking into account that the δ-function for energy conservation contains a vanishing argument with regards to all frequencies, this scaling is enhanced by one to λ^1. Resolving the scaling of the remaining δ-function for momentum conservation is more subtle as a scattering event must go from one point near the Fermi surface to another. Momentum conservation therefore requires that

$$(\mathbf{k}_{F,3} - \mathbf{k}_{F,1}) + (\mathbf{k}_{F,4} - \mathbf{k}_{F,2}) + (\mathbf{k}_{r,3} - \mathbf{k}_{r,1}) + (\mathbf{k}_{r,4} - \mathbf{k}_{r,2}) = 0. \tag{2.10}$$

For a general momentum transfer, the $\mathbf{k}_F$ do not cancel and the argument of the δ-function does *not* vanish equivalently in the low-energy limit. The electron-electron interaction is thus generically of order λ^1 and stays irrelevant. On the other hand, for special momentum combinations which lead to a cancellation of all $\mathbf{k}_F$ in the δ-function, one additional power of λ is gained from the vanishing x-momenta, making the interaction marginal. These special combinations are forward scattering $\mathbf{k} \to \mathbf{k}; \mathbf{k}' \to \mathbf{k}'$ and the BCS channel $\mathbf{k} \to \mathbf{k}'; -\mathbf{k} \to -\mathbf{k}'$.

The forward scattering interaction V^{FS} can be further decomposed into a charge channel (V^c) and a spin channel (V^σ),

$$V^{FS}_{\alpha\beta;\gamma\delta}(\hat{\mathbf{k}}, \hat{\mathbf{k}}'; \hat{\mathbf{k}}, \hat{\mathbf{k}}') = \delta_{\alpha\gamma}\delta_{\beta\delta} V^c(\hat{\mathbf{k}}, \hat{\mathbf{k}}') + (2\delta_{\alpha\delta}\delta_{\beta\gamma} - \delta_{\alpha\gamma}\delta_{\beta\delta})\, V^\sigma(\hat{\mathbf{k}}, \hat{\mathbf{k}}'). \quad (2.11)$$

The BCS interaction V^{BCS} can likewise be separated into a singlet (V^s) and a triplet interaction (V^t),

$$\begin{aligned} V^{BCS}_{\alpha\beta;\gamma\delta}(\hat{\mathbf{k}}, -\hat{\mathbf{k}}; \hat{\mathbf{k}}', -\hat{\mathbf{k}}') &= (\delta_{\alpha\gamma}\delta_{\beta\delta} - \delta_{\alpha\delta}\delta_{\beta\gamma})\, V^s(\hat{\mathbf{k}}, \hat{\mathbf{k}}') \\ &\quad + (\delta_{\alpha\gamma}\delta_{\beta\delta} + \delta_{\alpha\delta}\delta_{\beta\gamma})\, V^t(\hat{\mathbf{k}}, \hat{\mathbf{k}}'). \end{aligned} \quad (2.12)$$

The momentum dependence of the interactions $V^{c,\sigma,s,t}$ is completely determined by the scattering angle along the Fermi surface, so that an expansion in terms of angular harmonics is possible. A hallmark of Fermi liquid theory are the RG equations which govern the scaling of the interactions in the different angular momentum channels with index m,

$$\frac{\mathrm{d}V^{c,\sigma}_m}{\mathrm{d}\lambda} = 0 \quad (2.13)$$

$$\frac{\mathrm{d}V^{s,t}_m}{\mathrm{d}\lambda} = -N(0)\left(V^{s,t}_m\right)^2. \quad (2.14)$$

$N(0)$ is the density of states at the Fermi energy. The solution of these equations shows that in the weak coupling limit, only the BCS channel can lead to an instability. On the other hand, the susceptibilities of the forward scattering channels are given by

$$\chi^{c,\sigma}_m = \frac{N(0)}{1 + N(0)V^{c,\sigma}_m}. \quad (2.15)$$

A diverging susceptibility and thus an instability in these channels is therefore possible at a finite interaction strength $V^{c,\sigma}_m = -N(0)^{-1}$. For $m > 0$ the instability is of the Pomeranchuk type, i.e., it breaks the rotational symmetry of the Fermi surface.

The notion to treat excitations of interacting electrons in metallic (i.e. gapless) three-dimensional solids as fermionic quasiparticles is an exceptionally successful

concept whose importance hardly can be overestimated. Most metallic system examined experimentally or theoretically exhibit Fermi liquid behavior at sufficiently low temperatures. Even if a system becomes superconducting at exponentially small temperatures or undergoes some other phase transition, the Fermi liquid persists above the transition temperature and serves as a reliable starting point for phenomenological and microscopic theories alike.

In low dimensions few but famous counterexamples to Fermi liquids are known, among them the Luttinger liquid, which can be seen as the one-dimensional analogue of the Fermi liquid, and the fractional Quantum Hall effect in 2D. In these systems the Fermi liquid quasiparticles no longer carry good quantum numbers, and thus different quasiparticles need to replace them. In general, one could also imagine cases where no quasiparticles can be introduced at all, leaving only completely incoherent excitations.

A bordering case occurs when the "sufficiently low" temperature at which Fermi liquid behavior sets in tends to zero. This is exactly what happens in the vicinity of a QCP. Utilizing the Fermi liquid perspective a QCP is thus a specific limit emerging from a normal Fermi liquid. It is then only natural to use the Fermi-liquid state as the starting point for all further calculations near criticality. The simplest variant of this paradigm leads to the Hertz-Millis approach for continuous quantum phase transitions [19–21]. More sophisticated low-energy effective actions like the one we will utilize in the present work also take the Fermi liquid as the initial state but strongly renormalize the self-energy in the course of the calculation to a form which is incompatible with a Fermi liquid [61, 84, 93, 111]. Depending on taste, this usage of Landau quasiparticles outside their usual realm of applicability is called a *singular Fermi liquid*' or *non-Fermi liquid* (NFL). A NFL typically appears in connection with strong scattering which greatly reduces the quasiparticle lifetimes, creating broad peaks instead of sharp resonances in the spectral function and related response functions.

For a successful treatment of fluctuations in the SCM it is elementary to account for the emerging NFL behavior at the critical point.

2.1.1 Hertz-Millis Theory

The Hertz-Millis theory employs the integration over fermionic modes, which is formally exact. Our presentation is based on the reviews by Löhneysen *et al.* [23] and Metzner *et al.* [30] and also the thesis by Thier [132]. First, a Hubbard-Stratonovich transformation is performed for the original system, which introduces the order parameter field and decouples two body interactions, afterwards all integrals over fermionic fields are Gaussian and can be done exactly. The resulting order parameter action is purely bosonic, the Hertz-Millis theory is therefore in essence a way of

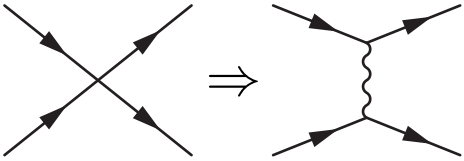

Figure 2.1 Parametrization of the fermion-fermion interaction with a transfer boson in the particle-hole channel. In any perturbative treatment this step introduces a selection bias for the interaction channel associated with the boson.

multidimensional bosonization. While other bosonization methods exist [133], the order parameter action is particularly straightforward to derive and keeps a close connection to the original degrees of freedom.

In the following, we suppress spin indices when possible. Given a fermionic field $\psi_k = \psi(k_0, \mathbf{k})$, let the action consist of a kinetic part and a two-body interaction $V(k, k', q)$,

$$\mathcal{S}[\bar{\psi}, \psi] = \int_k G_0^{-1}(k)\bar{\psi}_k\psi_k + \frac{1}{2}\int_{k,k',q} V(k, k', q)\bar{\psi}_{k'-q/2}\bar{\psi}_{k'+q/2}\psi_{k-q/2}\psi_{k+q/2}. \tag{2.16}$$

Before any explicit manipulations can be carried out, one must specify the interaction channel of interest, i.e., one must decide on the one or several types of bosons to introduce. The restriction to one channel and one boson which we take now is the first major approximation and restricts the form of $V(k, k', q)$ (Fig. 2.1). This selection limits the approach to the treatment of one instability, competing orders cannot be tackled this way [30]. We concentrate on a quantum phase transition with momenta near to $\mathbf{q} = 0$ and factorize the two-body interaction $V(k, k', q)$ into an interaction strength $g(q)$ and a general structure factor $d_\mathbf{k} d_{\mathbf{k}'}$, which could for example take d-wave symmetry. The derivation of the Hertz action can also be done for other channels and symmetries, with only minimal changes in some explicit expressions. Using the weighted density

$$\rho_q = \int_k d_\mathbf{k}\bar{\psi}_{k-q/2}\psi_{k+q/2} \tag{2.17}$$

the interaction is then of the density type

$$\tfrac{1}{2}\int_q g(q)\rho_q\rho_{-q}. \tag{2.18}$$

After the introduction of the order parameter field $\phi_q = \phi(q_0, \mathbf{q})$, this becomes

$$-\tfrac{1}{2}\int_q g^{-1}(q)\phi_q\phi_{-q} - \phi_{-q}\rho_q. \tag{2.19}$$

Integrating out the fermions yields a partition function for the order parameter field,

$$Z = \int \mathcal{D}\phi \det(\mathbf{G}_0^{-1} - \mathbf{V}) \exp\left(\tfrac{1}{2}\int_q g^{-1}(q)\phi_q\phi_{-q}\right), \tag{2.20}$$

where the matrix elements are $(\mathbf{G}_0^{-1})_{kk'} = G_0^{-1}\delta_{kk'}$ and $(\mathbf{V})_{kk'} = d_{(\mathbf{k}+\mathbf{k}')/2}\phi_{k-k'}$. The functional determinant is then evaluated with the tr-log identity $\det(A) = \exp(\mathrm{tr}\,(\log A))$, which brings all order parameter fields into the exponent of the partition function and thus restores the usual form of the partition function as a functional integral over an exponential. A Taylor expansion of the logarithm then leads to the well known order parameter action, which is polynomial in the order parameter field:

$$\begin{aligned}\mathcal{S}[\phi] = &\frac{1}{2}\int_q \phi_q \left(g^{-1}(q) + \Pi_{d,2}(q)\right)\phi_{-q} \\ &+ \sum_{N=3}^{\infty}\frac{(-1)^N}{N}\int_{q_1\ldots q_N}\delta(q_1+\cdots+q_N)\Pi_{d,N}(q_1,\ldots,q_N)\phi_{q_1}\ldots\phi_{q_N}.\end{aligned} \tag{2.21}$$

The $\Pi_{d,N}$ is the *N-point loop* with respect to the structure factor $d_{\mathbf{k}}$ of the interaction and originates from the expansion of the functional determinant. It is given by (see also Fig. 2.2 for a graphical representation)

$$\Pi_{d,N}(q_1,\ldots,q_N) = \int_k \prod_{j=1}^{N} d_{\mathbf{k}-\mathbf{p}_j-\mathbf{q}_j/2} \times G_0(k-p_j), \tag{2.22}$$

where we recognize $G_0(k)$ as the bare fermionic propagator.

Expanding around $\mathbf{q} = 0$, the kinetic part of the action Eq. 2.21 can be calculated explicitly, which yields the inverse bosonic two point function

$$D^{-1}(q) = c_1\mathbf{q}^2 + c_2|q_0|/|\mathbf{q}|^{z-2}, \tag{2.23}$$

where $c_1 > 0$ and $c_2 > 0$ are constants. The kinetic part provides the reference energy scale in a scaling analysis, the frequency and momentum dependence thus determines the dynamics in the bosonized theory. Equation 2.23 enforces a low

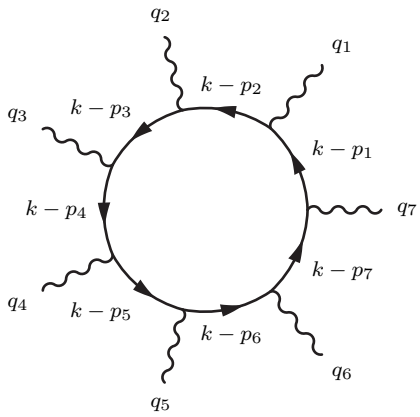

Figure 2.2 The N-point loop consists of a fermionic ring with N momenta and frequencies q_N flowing out. All external momenta add up to zero, k is the free loop momentum and p_i are determined by the q_i via the connection $p_{i+1} - p_i = q_i$.

energy limit where frequencies scale like $|\mathbf{q}|^z$, the exponent z is therefore known as the *dynamical critical exponent* (DCE). The value of z varies depending on the symmetry class of the instability. For an antiferromagnetic transition, which is not an instability in the forward scattering channel, it is $z = 2$ in 2D. A ferromagnet in 3D and in 2D obeys $z = 3$. The nematic instability has $z = 3$ as well (see also Sec. 2.2.2).

Using the order parameter action Eq. 2.21, Hertz proceeded to truncate the action at fourth order in the order parameter field and assumed that the coefficients $\Pi_{d,N}$ are constants for $N > 2$. This is the second major approximation within Hertz-Millis theory, which was at the time derived from a power counting of the effective interactions and their frequency and momentum dependence. The argument is essentially that the effective interactions $\Pi_{d,N}$ are dominated by their local part, which implies that the vertex functions can be evaluated for zero frequency and momentum. We note that in this approximation interactions with N odd are zero as long as one stays in the disordered phase. A renormalization group analysis of the action then yields the scaling properties around the QCP. The fixed point turns out to be Gaussian if dimension d and dynamical exponent z fulfill $d + z > 4$. Under this condition all relevant dynamics is encoded in the collective modes ϕ and a QCP can be fully understood once the single particle excitations of the noncritical system are known. While the QCP bears an irrelevant ϕ^4 interaction if $d + z > 4$ so that the order parameter field is free, for $d + z = 4$ the ϕ^4 term is marginal and introduces logarithmic corrections. A large number of two- and three-dimensional electronic systems naturally fulfill the condition $d + z \geq 4$ so that a QCP in their phase diagram seems accessible for a treatment with the Hertz-Millis approach.

These conclusions have an important caveat. Although the Hertz-Millis theory

seemingly resolves a QCP in the low temperature limit, it does not address under which circumstances a truncation of the order parameter action is valid. The power counting estimate which is necessary to safely discard higher orders requires an intimate knowledge of the effective vertices $\Pi_{d,N}$, and generally these can have a very rich structure. The by far most frequently encountered problem is a non-analytic frequency and momentum dependence of $\Pi_{d,N}$. In this case the zero frequency and momentum limit is ambiguous as it depends on the order in which the limits are taken. As a consequence, different estimates can be made for the same interactions depending on the scaling hypothesis.

Historically, this complication was underestimated for quite some time [23]. Part of the reason is the (un)fortunate coincidence that some of the "usual" limits like first taking frequencies to zero (static limit) or first taking momenta to zero (dynamical limit) are unsuspecting [25, 134]. In many cases, a very precise calculation was done for $\Pi_{d,2}$, including any nonanalytic dependencies. The resulting kinetic energy as the one in Eq. 2.23 clearly shows that the low energy dynamics is nontrivial, and supplies with z the relevant scaling exponent. Due to the complicated frequency and momentum structure, the same level of attention usually was not attributed to the higher order vertices $\Pi_{d,N}$. Nowadays it is generally acknowledged that also for the higher order terms the limit should be taken in a way which respects the dynamical critical exponent z of the Hertz action, as this reflects the physically relevant limit.

A well known example with this complication is the 2d antiferromagnetic QCP [25, 135, 136]. In this case, the resulting order is a spin density wave, the ordering vector is thus $\mathbf{Q} \neq 0$ and the momentum expansions are performed around this $\mathbf{Q}$. Then, the two point function has the form $D^{-1}(q) = (\mathbf{q} - \mathbf{Q})^2 + |q_0|$, i.e., the DCE is $z = 2$. The low energy limit is therefore approached with the scaling

$$(q - Q) \to \lambda(q - Q) \qquad\qquad q_0 \to \lambda^z q_0, \tag{2.24}$$

where we introduced the renormalization scale $\lambda \to 0$. The kinetic energy in the order parameter action Eq. 2.21 is held constant under scaling,

$$\lambda^0 \sim \underbrace{\int_q}_{\lambda^{2+z}} \underbrace{D^{-1}}_{\lambda^2} \underbrace{\phi_q \phi_{-q}}_{\lambda^{-4-z}} \tag{2.25}$$

the engineering dimension of the order parameter field is therefore $[\phi] = -2 - z/2$. If the four-point vertex $\Pi_{d,4}$ in the order parameter action is evaluated at zero frequency and momentum transfer $\mathbf{Q}$ (restriction to local part), it is proportional to

$$\Pi_{d,4} \sim \int_k \frac{1}{(k_0 - \epsilon(\mathbf{k}) + i0^+)^2} \frac{1}{(k_0 - \epsilon(\mathbf{k} + \mathbf{Q}) + i0^+)^2}, \tag{2.26}$$

which can be integrated to zero by residues after the dispersion $\epsilon(\mathbf{k})$ is linearized around the hot spot. In the presence of a finite bandwidth the value of the integral is then completely determined by the high energy cutoff and can be taken as constant in the low-energy theory. The same holds for the other $\Pi_{d,N}$ with $N > 4$. The power counting estimate of the interaction terms in Eq. 2.21 is therefore

$$(N-1)(2+z) + N(-2-\tfrac{z}{2}) = N-4, \tag{2.27}$$

meaning that the interaction contribution from $\Pi_{d,4}$ is marginal and all higher order terms irrelevant. This is nothing else than the standard result by Hertz, which was discussed earlier on general grounds.

Regarding $\Pi_{d,N}$, Abanov and Chubukov [25] estimated a generalization of the integral Eq. 2.26 for finite frequency $q_0 \neq 0$ and momentum $\mathbf{q} \neq \mathbf{Q}$, with the result

$$\Pi_{d,N} \sim \frac{|q_0|}{(q_0 - v_F(q-Q) + i0^+)^{N-2}}. \tag{2.28}$$

In this expression, the engineering dimension is dependent on the order in which the limits are taken. When taking the low energy limit according to the scaling Eq. 2.24, one obtains $[\Pi_{d,N}] = z - (N-2) = 4 - N$, which perfectly cancels the phase space dimension $N-4$ in the interaction contribution. The special momentum and frequency dependence of the effective interactions thus preserves a marginal four-point interaction but introduces infinitely many marginal interactions also for $N > 4$. The LGW action at the antiferromagnetic QCP thus contains infinitely many terms of equal size at least according to power counting, a truncation of the action is a priori unjustified and strong renormalizations of the Gaussian exponents are expected.

It was established more recently by Thier and Metzner [137] that also the order parameter action for the nematic QCP contains infinitely many marginal couplings. The effective interactions (N-point loops) in the nematic case and also the closely related ferromagnetic instability have been investigated by a number of authors [31, 134, 137, 138], here we focus on the role of different scaling limits. If in the calculation of the N-point loop Eq. 2.22 the fermionic dispersion is linearized and the curvature neglected, the Fermi surface decomposes into a collection of independent one-dimensional modes. In this lowest approximation, all higher loop orders vanish trivially and the critical point is purely Gaussian [26, 139]. This changes dramatically once the curvature is retained, which is therefore a relevant perturbation to the theory, a rather general feature of instabilities in the forward scattering channel. This means that the local expansion of the dispersion is necessarily $v_F k_x + k_y^2/(2m)$ instead of $v_F k_x$, therefore the x-momenta and y-momenta have to be scaled differently, leading

to the so called 321-scaling or 321-limit

$$q_0 \to \lambda^3 q_0 \qquad q_x \to \lambda^2 q_x \qquad q_y \to \lambda q_y. \tag{2.29}$$

Neumayr and Metzner [134] analyzed the effective interactions $\Pi_{d,N}$ in great detail based on some exact results of Feldman *et al.* [138]. They reveal a complicated frequency and momentum structure, which exhibits subtle cancellations in various limits. We will refer to some of their results in Sec. 3.1.3, in the present context it is important that all of the limits considered at the time lead to a favorable scaling of the effective interactions in the LGW functional which justifies the Hertz-Millis treatment. Thier and Metzner [137] showed that it is the 321-limit in which the N-point loops do not benefit from any cancellations, but retain a marginal scaling for any vertex order. Their proof involves a painstaking expansion of exact expressions of the N-point loop for free fermions in the 321-limit and can therefore be considered exact for the given scaling. Again, the presence of infinitely many couplings poses a serious problem for Hertz-Millis theory and calls into question the practicability of the entire approach.

In summary, although an integration over the fermionic fields is formally exact, an infinite number of marginal/relevant couplings in the Hertz action might make the ansatz unusable and *a posteriori* invalidate such a step.

2.1.2 Fermi surface and multiple soft modes

Even if the Hertz-Millis theory fails for the SCM, one might still be tempted to somehow utilize the full order parameter action of Eq. 2.21 while avoiding the common pitfalls for power counting and truncations which were discussed in the last section. We will now show that this is still problematic, with the root of the problem being the integrating-out of the fermions itself.

The paradigmatic example is the ferromagnetic instability in a disordered metal in 3D where the electronic motion is diffusive, details can be found in the review by Löhneysen *et al.* [23]. We again take the order parameter action Eq. 2.21 as the starting point. A perturbative calculation of the two-point and four-point functions for small frequencies and momenta yields [140]

$$\Pi_{d,2} \sim c_2 q^2 + c_2' |q| + c_3 \frac{|q_0|}{q^2} \tag{2.30}$$

$$\Pi_{d,4} \sim u_4 + \frac{u_4'}{q^3}. \tag{2.31}$$

We note that for this result the full momentum dependence in $\Pi_{d,4}$ was approximated by one representative momentum q. The leading terms in the kinetic energy are

$|q|$ and $|q_0|/q^2$, which leads to a DCE of $z = 3$. According to Hertz-Millis theory the QCP would therefore be Gaussian [141], but this is incorrect [142–144]: If one utilizes a combined fermion-boson action to study the problem instead of the pure order parameter action, fluctuations contribute logarithmic corrections and thus renormalize the critical exponents, which is impossible at a Gaussian fixed point. The discrepancy originates from the dynamics of the fermions. The Green's function of free fermions is $G(k) = (ik_0 - \mathbf{k}^2/2m - \mu)^{-1}$, which leads to a DCE of $z' = 2$, different from the boson dynamics with $z = 3$. Inserting z' instead of z into the power counting estimate of the order parameter action leads once again to infinitely many marginal couplings, which makes the appearance of logarithmic corrections plausible. In contrast to the previous examples of the antiferromagnet and nematicity in 2D, where the order parameter action on itself hints at a problem, in case of the diffusive ferromagnet it erroneously signals a Gaussian theory.

Very similar problems occur in a clean metal at a ferromagnetic instability. Repeating the same steps as above, one obtains [145]

$$D^{-1}(q) \sim c_2 q^2 - c_2' q^2 \log(1/q) + c_2'' \frac{|q_0|}{q} \tag{2.32}$$

$$\Pi_{d,4}(q) \sim u_4 - u_4' \log(1/q) \tag{2.33}$$

The leading terms are now $-q^2 \log(1/q)$ and $|q_0|/q$, the DCE is $z = 3$. The fermions exhibit a dynamics with $z' = 1$, as a consequence the order parameter action is again Gaussian according to z and completely marginal for z' [24, 141]. For the clean ferromagnet a further complication is introduced by the negative signs in front of c_2' and u_4', which introduce a sign change in the corresponding correlation functions at very small scales. A negative sign in the effective ϕ^4 interaction destroys the criticality and drives the transition to weak first order [146–148]. The sign change in the propagator implies a negative susceptibility for certain momenta, which can drive the system away from a $\mathbf{q} = 0$ instability to one with $\mathbf{q} \neq 0$ [149].

In the wake of the preceding results, also the 2D ferromagnetic QCP was investigated [31, 150–154] and found to be unstable. We will come back to this case in Sec. 4.3.3 in more detail as the low-energy action at criticality is closely related to the one of the nematic QCP.

In all cases, the complications are introduced by the extended phase space of zero modes provided by a Fermi surface. The fermionic quasiparticles contribute additional soft modes to the action with their own DCE and their own momentum scaling towards the Fermi surface. Their infrared behavior is thus dissimilar from the order parameter and is certainly not negligible. The primary insight from Hertz-Millis theory is the fact that it is not even sufficient to include the effects of Landau quasiparticle excitations in terms of effective interactions $\Pi_{d,N}$ in a bosonized theory.

This leads to incorrect results because not only does the fermionic sector strongly renormalize the bosonic sector (corrections from $\Pi_{d,N}$ in the LGW action), but also the other way round (self-energy corrections to the fermionic Green's function). While the former contributions are captured by Hertz-Millis theory, the latter are not. The inclusion of the feedback of order parameter fluctuations on the quasiparticle excitations is only possible in a combined fermion-boson action. Using such actions one usually generates NFL behavior already at one-loop level, with far reaching consequences: The non-Fermi liquidness alters the fermionic DCE, the power counting and thus also the critical dimensions.

To summarize, in a critical metal, the bosonic and the fermionic sector are both gapless but obey different dynamics, therefore we cannot deduce the relevant interaction processes from a LGW functional alone. The incorporation of the intricate interplay of order parameter fluctuations and quasiparticle excitations and their mutual renormalizations is indispensable for a successful description of metallic criticality.

2.2 Low-energy action

The previous section highlighted the many shortcomings of Hertz-Millis theory and its extensions. The major factor to this failure is the integration over fermionic degrees of freedom. The inadequacy of an integration of the fermionic sector becomes immediately obvious when we take a renormalization group mindset [30, 155, 156]. Many body physics is constantly challenged by the vastly different energy scales which can be present within one and the same system. In the cuprates for example, the interaction effects comprise several orders of magnitudes, from the bare on-site repulsion, over the electron hopping amplitudes, magnetic order down to superconductivity. When dealing with such an hierarchy of energy scales, it is detrimental to select one degree of freedom after the other and treat the complete energy range at once. The most likely outcome of such an approach are spurious divergences, as the influence of the integrated degree of freedom is shuffled and scattered over all energy scales of the remaining modes. This is clearly unphysical; a real measurement, which takes place at a specific energy or energy range, probes the system as a whole. One should therefore integrate over modes based on their energy scale, not their species, working from high to low. During this renormalization group flow the effects of higher scales are successively incorporated into the correlation functions, and are thus able to influence the lower scales coherently.

In a critical metal, the hierarchy of energy scales is introduced by the critical fluctuations, which span - by definition - all energies. In recent years, combined fermion-boson low energy effective actions are frequently used to treat metallic

quantum criticality. The most popular representative is the spin-fermion model [157–160], which was introduced for the ferromagnetic QCP. It is similar to the SCM, but contains a spin structure on the vertex. The nematic QCP was treated almost immediately with the SCM action [61, 111]. In very recent literature, the usage of fermion-boson actions has become the de facto standard [114, 118, 161, 162].

Much variance is present in the proposed solutions of critical fermion-boson field theories. One has for example several choices to incorporate the fluctuation feedback, different approximations are possible for the fermionic dispersion, also expansion schemes and integration techniques vary depending on taste and interest [116–118, 161]. In this section, we reconstruct and examine the approach based on RPA-renormalized propagators which is often used for the SCM action. We comment on the various approximations employed in the course of its derivation and compare with alternative approaches.

2.2.1 Fixed point at one loop

In the following we set the temperature to zero. The spinless critical metal (SCM) is the quantum field theory for the low-energy degrees of freedom of a nematic quantum critical system or fermions coupled to a fluctuating $U(1)$ gauge field. Nematic ordering is captured by the order parameter

$$O(q) = \frac{1}{V} \sum_{k,\sigma} d_{\mathbf{k}} \bar{\psi}_{k-\frac{q}{2},\sigma} \psi_{k+\frac{q}{2},\sigma}, \tag{2.34}$$

where $d_{\mathbf{k}}$ is a structure factor which is determined by the type of symmetry breaking. The Pomeranchuk instability is most often considered with a d-wave structure factor. For an inversion symmetric lattice, the structure factor is inversion symmetric in momentum space, i.e., it is not chiral selective. In a lattice system, the order parameter is a scalar, independent of spin and can be defined real in real space.

In the disordered phase, the order parameter correlation function decays exponentially with increasing distance and the order parameter has a zero mean, in the uniformly ordered phase, the order parameter becomes a constant with a finite expectation value. At criticality, the order parameter correlation function decays with a characteristic power law. In momentum space, uniform ordering is proliferated by scattering events with vanishing momentum transfer, the forward scattering limit. The order parameter $O(q)$ is linearly coupled to the field ϕ.

For the other case considered here of fermions coupled to a $U(1)$ gauge field, the boson ϕ is the transverse component of the gauge field in Coulomb gauge. The coupling constant is in this case given by

$$\hat{\mathbf{q}} \cdot \mathbf{v}(\mathbf{k}) = -v(\mathbf{k}) \sin \alpha_{\mathbf{q}}, \tag{2.35}$$

where $\hat{\mathbf{q}}$ is the unit vector in the direction of $\mathbf{q}$ and $\mathbf{v}(\mathbf{k}) = \nabla\varepsilon(\mathbf{k})$. $\alpha_{\mathbf{q}}$ is the angle between $\mathbf{v}(\mathbf{k})$ and the momentum transfer $\mathbf{q}$. At low energy, scattering is restricted to the vicinity of the Fermi surface, so that $v(\mathbf{k})$ is approximately the Fermi velocity $v_F(\mathbf{k})$ and the momentum transfer is predominantly along the Fermi surface so that $\alpha_{\mathbf{q}} \approx \pm\pi/2$. The coupling constant is then independent of $\mathbf{q}$, henceforth denoted $d_{\mathbf{k}}$. In an inversion symmetric system, the structure constant is then skew symmetric, i.e., $d_{\mathbf{k}} = -d_{-\mathbf{k}}$.

We will frequently refer to a generalization of the model where the number of fermion flavors N_f can take any value instead of the physical $N_f = 2$. The kinetic part of the action then scales like

$$\sum_{\sigma} \bar{\psi}_{\sigma} G^{-1} \psi_{\sigma} \sim N_f. \tag{2.36}$$

To preserve the connection with $N_f = 2$, the four-fermion interaction should have the same scaling,

$$\sum_{\sigma\sigma'} V \bar{\psi}_{\sigma} \bar{\psi}_{\sigma'} \psi_{\sigma'} \psi_{\sigma} \sim N_f. \tag{2.37}$$

This implies a scaling of the four-fermion interaction like $\sim N_f^{-1}$, i.e., in the large-N_f limit each vertex becomes small. In the same way, the Yukawa interaction in the fermion-boson description scales as $N_f^{-1/2}$. Alternatively, one can rescale the bosonic field $\phi \to \sqrt{N_f}\phi$ to shift the flavor index to the bosonic propagator.

In summary, we consider a two-dimensional metal with a single band with bandwidth Λ and a generic inversion symmetric Fermi surface without any nesting. The Landau quasiparticles do not interact directly, but only via a massless, real bosonic field ϕ. The generalized action for N_f fermion flavors is then

$$\begin{aligned} S[\psi, \bar{\psi}, \phi] = &\sum_{k,\sigma} \bar{\psi}_{k,\sigma} G^{-1}(k) \psi_{k,\sigma} + \tfrac{1}{2} \sum_{q} D^{-1}(q) \phi_q \phi_{-q} \\ &+ \sum_{q,k,\sigma} d_{\mathbf{k}} \phi_q \bar{\psi}_{k-\frac{q}{2},\sigma} \psi_{k+\frac{q}{2},\sigma}, \end{aligned} \tag{2.38}$$

where the fermionic Green's function has the standard form $G(k) = (ik_0 - \epsilon(\mathbf{k}))^{-1}$ and the bosonic propagator scales like $D(q) \sim N_f^{-1}$. The Yukawa interaction carries a form factor $d_{\mathbf{k}}$, which either fulfils $d_{\mathbf{k}} = d_{-\mathbf{k}}$ for even interaction or $d_{\mathbf{k}} = -d_{-\mathbf{k}}$ for odd interaction. The dispersion $\epsilon(\mathbf{k})$ is zero at the Fermi surface, the explicit function depends of course on the material in question. Focusing on the simplest

case of free fermions, the dispersion is $\epsilon(\mathbf{k}) = \mathbf{k}^2/2m - \mu$, the Fermi momentum is $k_F = \sqrt{2m\mu}$ and the fermionic Green's function is given by

$$G_0^{-1}(k) = i\bar{a}k_0 - \left(\frac{\mathbf{k}^2}{k_F^2} - 1\right)\mu, \tag{2.39}$$

Here we introduce a coefficient $\bar{a} = 1$ for the discussion of the low-energy limit later on. The energy scale is therefore μ and the momentum scale k_F. We choose units so that $k_F = 1$ and $m = 1$ and therefore $\mu = 1/2$. We also select one point on the Fermi surface $\mathbf{k}_F$ as the origin of the coordinate system and orient the x-axis in the direction of the Fermi velocity. The Green's function then takes the form

$$G_0^{-1}(k) = iak_0 - \tfrac{1}{2}(k_x^2 + k_y^2 + 2k_x), \tag{2.40}$$

where $a = \bar{a}/(2\mu)$. Microscopically, the kinetic energy of the order parameter field is given by the inverse coupling $g^{-1}(q)$ (Eq. 2.19, 2.21), which can be expanded around $\mathbf{q} = 0$ up to second order, yielding

$$g^{-1}(q) \approx r^2 + \frac{\mathbf{q}^2}{e_0^2} \tag{2.41}$$

which is the usual Ornstein-Zernike form of the susceptibility. The same correlation function is of course obtained with a derivative expansion of the order parameter field in real space, which could form the starting point of a phenomenological ansatz. At the critical point the correlation length diverges, which means that the bosonic mass r vanishes. The bosonic propagator is then

$$D_0^{-1}(q) = \frac{N_f}{\tilde{e}^2}\mathbf{q}^2, \tag{2.42}$$

where $\tilde{e}^2 = 2e_0^2\mu/k_F^2$. Along the same lines, the Yukawa interaction strength $d_{\mathbf{k}}$ is approximated by a constant $\tilde{g}$. This is sensible as we are interested in the forward scattering limit, which implies that $\mathbf{q} \approx 0$ and as a consequence also $\mathbf{k} \approx const.$, i.e., only a small part of the Fermi surface around the arbitrary expansion point $\mathbf{k}_F$ takes part in a scattering event, where the structure factor $d_{\mathbf{k}}$ has negligible variation. The notion of locality in momentum space which was used for this approximation will be clarified shortly in much more detail (Sec. 2.2.2). We only mention here that this assumption will lead to problems once the dispersion is actually Taylor expanded around $\mathbf{k}_F$, in this case it becomes important to take the antipodal point to $\mathbf{k}_F$ on the Fermi surface, $-\mathbf{k}_F$, also into consideration. Then, also the differentiation of even and odd interaction will reenter the action explicitly.

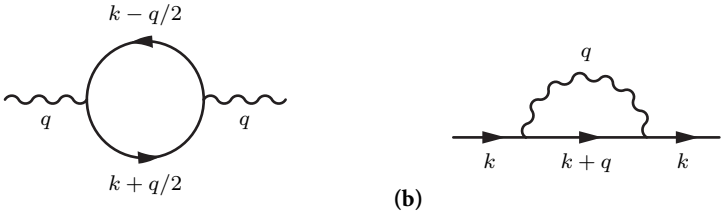

Figure 2.3 The particle-hole bubble (a) and the one-loop self-energy (b).

The action is now

$$S[\psi,\bar{\psi},\phi] = \sum_{k,\sigma} \bar{\psi}_{k,\sigma}(iak_0 - \tfrac{1}{2}(k_x^2 + k_y^2 + 2k_x))\psi_{k,\sigma} + \tfrac{1}{2}\sum_q \frac{N_f \mathbf{q}^2}{\tilde{e}^2}\phi_q\phi_{-q} + \tilde{g}\sum_{q,k,\sigma}\phi_q\bar{\psi}_{k-\frac{q}{2},\sigma}\psi_{k+\frac{q}{2},\sigma}, \tag{2.43}$$

with $\tilde{g} = d_{k_F}/2\mu$. It is obvious that one of both, $\tilde{e}^2$ and $\tilde{g}$ can be absorbed by a redefinition of the order parameter field ϕ. We choose to rescale with $\phi \to \phi/|\tilde{g}|$ to obtain the inverse propagators and the Yukawa interaction

$$G_0^{-1}(k) = iak_0 - \tfrac{1}{2}(k_x^2 + k_y^2 + 2k_x), \tag{2.44}$$

$$D_0^{-1}(q) = \frac{N_f}{e^2}\mathbf{q}^2, \tag{2.45}$$

$$g = \tilde{g}/|\tilde{g}|, \tag{2.46}$$

with $e^2 = \tilde{e}^2|\tilde{g}|^2$.

One can calculate the one-loop corrections in plain perturbation theory, the exact solution for the susceptibility (Fig. 2.3a) was computed a long time ago by Stern [163]:

$$\begin{aligned}\Pi_2(q) &= N_f \int_k G_0(k - \tfrac{q}{2})G_0(k + \tfrac{q}{2}) \\ &= \frac{N_f}{2\pi}\left(\frac{f\left(|\mathbf{q}|/2 - iq_0/|\mathbf{q}|\right) + f\left(|\mathbf{q}|/2 + iq_0/|\mathbf{q}|\right)}{|\mathbf{q}|} - 1\right),\end{aligned} \tag{2.47}$$

with $f(x) = \sqrt{x^2 - 1}$, where the square root has a positive real part. We note that the vertex g does not explicitly enter since always $g^2 = 1$. For small momenta and frequencies, this is approximately

$$\Pi_2(q) = \frac{N_f}{2\pi}\left(\frac{|q_0|}{|\mathbf{q}|} - 1\right). \tag{2.48}$$

The nonanalyticity $|q_0|/|\mathbf{q}|$, which was already mentioned in the study of Hertz-Millis theory (Sec. 2.1.1, see e.g. Eq. 2.23), is a universal feature of forward scattering in a metal, it is even present in 3D [52]. It is the leading contribution to the decay of collective modes, fixing the DCE to $z = 3$, which has strong implications for the effects of order parameter fluctuations. We note that the particle hole bubble Eq. 2.48 also contains a constant part, which introduces a mass gap for the bosons. In a critical field theory such terms could be incorporated in a renormalization group scheme. For a gauge theory, its appearance is more troublesome, since it breaks the gauge invariance of the original action. This is of course not what happens, the static part of the susceptibility is just the density of states at the Fermi surface, which is always exactly cancelled by the diamagnetic term, thus restoring gauge invariance [116].

The fermion self-energy at one loop is given by the Fock diagram (Fig. 2.3b),

$$\Sigma^{(1)}(k) = \int_q G_0(k+q) D_0(q), \tag{2.49}$$

where we again used $g^2 = 1$. In this integral the correlation function $D(q)$ is originally independent of frequency. A term $\sim q_0^2$ could be introduced by continuing the gradient expansion in ϕ, but the large damping of the one-loop correction $|q_0|/|\mathbf{q}|$ completely overpowers this. We therefore employ the random phase approximation (RPA, see also Sec. 2.2.3) to incorporate the one-loop correction into the boson propagator. As a consequence, the imaginary part of the self-energy acquires an anomalous frequency dependence,

$$\begin{aligned} \Sigma^{(1)}(\mathbf{k}=0,k_0) = &\int_q \frac{1}{ia(k_0+q_0) - \frac{1}{2}(q_x^2+q_y^2+2q_x)} \\ &\times \frac{1}{N_f \left(\frac{q_x^2+q_y^2}{e^2} + \frac{|q_0|}{2\pi\sqrt{q_x^2+q_y^2}} \right)} \end{aligned} \tag{2.50}$$

$$\text{Im}\ \Sigma^{(1)}(\mathbf{k}=0,k_0) \sim -\frac{k_0}{|k_0|^{1/3}}. \tag{2.51}$$

Without any approximations in the momentum dependence, the integral can only be accessed numerically (see Fig. 2.4). The result is however conserved within a local expansion of the fermionic dispersion, i.e., $\epsilon(k) = k_x + \frac{1}{2}k_y^2$, giving

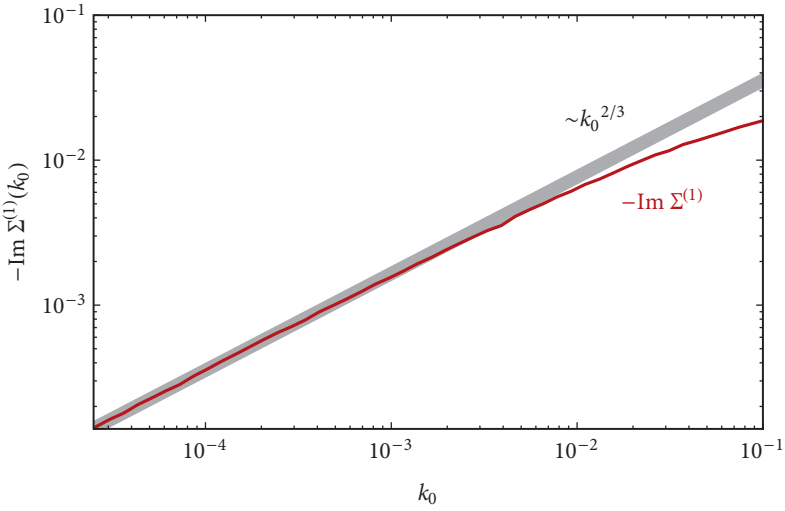

Figure 2.4 Imaginary part of the one-loop self-energy, calculated with the microscopic dispersion of Eq. 2.50 for $N_f = 2$, $e = 1$ and $a = 1$. The limiting power law clearly emerges, although at comparatively small scales.

$$\Sigma^{(1)}(\mathbf{k} = 0, k_0) = \int_q \frac{1}{ia(k_0 + q_0) - \frac{1}{2}q_y^2 - q_x} \frac{1}{\frac{N_f}{e^2}q_y^2 + \frac{N_f|q_0|}{2\pi|q_y|}} \tag{2.52}$$

$$= \int \frac{\mathrm{d}q_y \mathrm{d}q_0}{8N_f\pi^2} \frac{-i}{\frac{q_y^2}{e^2} + \frac{|q_0|}{2\pi|q_y|}} \mathrm{sgn}\,(k_0 + q_0) \tag{2.53}$$

$$= \frac{-i}{\sqrt{3}N_f} \left(\frac{e^2}{2\pi}\right)^{2/3} \frac{k_0}{|k_0|^{1/3}} \equiv -i\kappa\{k_0\}, \tag{2.54}$$

where we have also dropped the q_x^2 in the bosonic propagator. In the last line we introduced $\kappa = e^{4/3}/(\sqrt{3}N_f(2\pi)^{2/3})$ and $\{\omega\} = \mathrm{sgn}\,\omega|\omega|^{2/3}$. While we know that the original integral was strictly convergent, neglecting the various q_x dependencies might lead to a dependence of the integration result on the integration order. This complication and related issues will be discussed in the next section, but we already point out that the nonanalytic term in $\Sigma^{(1)}$ is not affected. From Eq. 2.54 we can also infer that $\Sigma^{(1)}$ does not carry a momentum dependence because the q_x integration completely obliterates the fermionic Green's function in the remaining integral.

The peculiar damping rate with the power $2/3$ was first derived by Lee [110] in context of the $U(1)$ gauge theory with the help of power counting. Similar to the

bosonic self-energy, the $2/3$ overpowers the bare linear frequency dependence in the fermionic propagator. Quasiparticle excitations near the Fermi surface are thus strongly affected by the order parameter fluctuations. We thus obtain a NFL state from the one-loop corrections.

In the very early studies of the $U(1)$ gauge theory, the effects of Gaussian fluctuations were discussed rather implicitly in terms of response functions [164–169], but in the course of only few years, this shifted and the study of the NFL state itself quickly took the centerpiece of attention [27, 33, 39, 112, 170–172].

An important step was the realization by Blok and Monien [170] that the model is strongly coupled. Their argument was based on the renormalized Fermi velocity, which diverges at low energies since the energy scale of excitations decreases slower than linear. Shortly thereafter Polchinski [39] proposed the 321-limit as the correct low-energy scaling and using this insight, identified the boson-mediated four-fermion interaction as the real culprit for the strong coupling by showing that it is RG relevant in the low energy limit. A relevant interaction implies that the dimension in consideration is below the upper critical dimension (UCD) of the field theory.[1]

In a renormalization group calculation the coupling will then flow away from the Gaussian fixed point (weak coupling) to a nontrivial fixed point at strong coupling. Near the strong coupling fixed point the correlation functions and propagators receive corrections to the scaling which can usually be identified with anomalous dimensions. Since the interaction in the SCM is relevant, the emergence of "superleading" corrections which lead to a NFL actually has to be expected. This NFL fixed point was first considered by Nayak and Wilczek [27]. The full scaling analysis of the SCM was done only recently by Lee [115] and Metlitski and Sachdev [114] (see Sec. 2.2.2, 2.2.4). Another subtle point is the form of the corrections. While the nonanalytic fermionic self energy $\sim \omega^{2/3}$ can indeed be interpreted in terms of an anomalous dimension $-1/3$, this is not possible for the ω/k term from the particle-hole bubble. Compared to standard examples of quantum criticality like the ϕ^4-theory the emergence of an anomalous *function* with nonanalytic momentum and frequency dependencies rather than anomalous dimensions might seem alarming, but this should be considered just another consequence of the extended singular manifold which is provided by the Fermi surface.

In the publication of 1994, Polchinski [39] also investigated a self consistent solution of the model via Dyson-Schwinger equations. His solution proceeds in two steps. First, it is rationalized that vertex corrections can be neglected, and the reduced

[1] When a model is above the UCD, the theory is Gaussian, exactly at the UCD logarithmic corrections occur in perturbation theory and below the UCD even stronger power law corrections appear.

Dyson-Schwinger equations are solved based on this assumption. Afterwards, the validity of the approximation is reevaluated in the given solution.

We include the one-loop corrections in the propagators and define the RPA-renormalized quantities

$$D^{-1}(q) = N_f \left(\frac{q_y}{e^2} + \frac{|q_0|}{2\pi |q_y|} \right) \tag{2.55}$$

$$G^{-1}(k) = i\kappa\{k_0\} - \tfrac{1}{2}(k_y^2 + 2k_x). \tag{2.56}$$

In this definition, the irrelevant k_x dependencies have been dropped. The reduced Dyson-Schwinger equations are given by

$$\Pi(q) = N_f \int_k G(k - q/2) G(k + q/2) \tag{2.57}$$

$$\Sigma(k) = \int_q G(k + q) D(q) \tag{2.58}$$

i.e., the internal lines in the one-loop diagrams (Fig. 2.3) are replaced by renormalized propagators. The integrations can be carried out exactly, yielding

$$\begin{aligned}
\Pi(q) &= N_f i \int \frac{\mathrm{d}k_y \mathrm{d}k_0}{(2\pi)^2} \frac{\Theta(k_0 + q_0/2) - \Theta(k_0 - q_0/2)}{i\kappa\left(\{k_0 + q_0/2\} - \{k_0 - q_0/2\}\right) + q_x - k_y q_y} \\
&\quad + q \leftrightarrow -q && (2.59) \\
&= N_f \int \frac{\mathrm{d}k_0}{2\pi} \frac{1}{|q_y|} \left(\Theta(k_0 + q_0/2) - \Theta(k_0 - q_0/2)\right) \operatorname{sgn} q_0 && (2.60) \\
&= \frac{N_f}{2\pi} \frac{|q_0|}{|q_y|} && (2.61) \\
\Sigma(k) &= \int \frac{\mathrm{d}q_y \mathrm{d}q_0}{8 N_f \pi^2} \frac{-i}{\frac{q_y^2}{e^2} + \frac{|q_0|}{2\pi |q_y|}} \operatorname{sgn}(k_0 + q_0) && (2.62) \\
&= -i\kappa\{k_0\}, && (2.63)
\end{aligned}$$

Surprisingly, these are the exact same expressions which were put into the integral equations in the first place. This strange behavior is tied to the favorable momentum dependence of the generic dispersion $\epsilon(\mathbf{k}) = k_x + k_y^2/2$, a topic which will be revisited in Sec. 2.3. To summarize, the one-loop self-energies calculated in Eq. 2.48 and Eq. 2.54 self-consistently solve the reduced Dyson-Schwinger equations.

Equipped with the self-consistent solution, Polchinski then compared the engineering dimensions of the fields for a scaling where the bare propagators are preserved

with a scaling in the 321-limit and found that the fermion-fermion interaction is reduced from relevant to marginal once the self-energy corrections are incorporated and the 321-limit employed. Using the marginality of the bare interaction, he argues that all vertex corrections are finite in the low-energy limit and thus scale at worst like $\mathcal{O}(\omega^0 N_f^{-1})$. For a large enough N_f the vertex corrections are therefore negligible, like it was initially proposed.

At the same time, Altshuler, Ioffe, and Millis [112] did a comparative study of the large-N_f limit and small, finite N_f and concluded that they congruently point towards a stable one-loop fixed point, i.e., higher order corrections are smaller than the leading contributions and cannot change the scaling dimensions. The main focus of their analysis was the magnitude of two-loop diagrams and the general renormalized vertex. As the responsible mechanism they identified a phase space restriction, which places bounds on the internal frequencies.

Also in 1994, Kim *et al.* [113] published a painstaking calculation in perturbation theory up to two-loops, where they proved the absence of any terms more singular than the one-loop corrections. The perturbation theory thus holds at least up to second order, further strengthening the notion of a fixed point which is entirely dominated by the RPA-fluctuations. As an important side result, they demonstrated that only the proper sum of two-loop diagrams including vertex corrections is subleading while single diagrams can indeed produce stronger nonanalyticities.

The combined efforts by Polchinski, Kim *et al.* and Altshuler, Ioffe, and Millis were considered as the "definite solution" of the SCM for more than a decade: The NFL is stable at one-loop, does not receive any corrections at two loop and is seemingly controllable by a large-N_f expansion. Any deviations from the one-loop fixed point at three-loop level or even higher order should therefore be negligible for large enough N_f.

2.2.2 Fermi surface patching

In the derivation of the one-loop fixed point the seemingly innocuous approximation $\epsilon(\mathbf{k}) = k_x + k_y^2/2$ for the dispersion was introduced to make the calculations more manageable. Such an approximation can actually have a great impact on the model with respect to convergence and symmetry properties.

In an isotropic system, the problems for convergence are very straightforward to understand. A propagator usually decays in the UV with a certain power in momentum and frequency, the Green's function for example vanishes according to $\sim k_x^2 + k_y^2$. After locally expanding the dispersion to $k_x + k_y^2/2$, the power counting is worsened to $\sim k_x^{-1}, k_y^{-2}$, the expansion can thus create UV problems. In a lattice system, the dispersion is material dependent and the momenta are confined to the Brillouin zone, possible UV problems of a low-energy theory can then be

formulated in terms of the UV cutoffs which relate the low-energy theory with the microscopic description. The canonical way to determine possible divergences is of course power counting. The main point is now that the power counting estimate is only meaningful if the momentum structure of the integrand is respected. For example, the two dimensional integral

$$\int_0^{\Lambda_y^{1/3}} \mathrm{d}x \int_0^{\Lambda_y} \mathrm{d}y \frac{1}{1+x^3+y} \sim \Lambda_y^{1/3} \tag{2.64}$$

is divergent, but the normal way of power counting in terms of a polar coordinate $r = \sqrt{x^2+y^2}$ would naïvely yield the finite estimate $\int \mathrm{d}r/r^2$. This complication is a consequence of the anisotropies in the propagators, which is easily solved by imposing a scaling which respects these. In the example, this means that we introduce the radius variable r with the help of elliptical coordinates $x \to r\cos\varphi$ and $y \to (r\sin\varphi)^3$. The power counting then directly yields $\int \mathrm{d}r = \Lambda_y^{1/3}$.

The bare propagators of the SCM approach in the UV

$$D_0^{-1}(q) \sim \mathbf{q}^2 \tag{2.65}$$

$$G_0^{-1}(k) \sim ik_0 - (k_x^2 + k_y^2), \tag{2.66}$$

the boson propagator thus suggests a scaling $k_x^2 \sim k_y^2$, while no information about the frequency dependence is contained in D_0. The Green's function seemingly requires a scaling $k_0 \sim k_x^2 \sim k_y^2$. On the other hand, near the Fermi surface the fermions locally follow an anisotropic dispersion $k_x + k_y^2$, which demands $k_x \sim k_y^2$. We are thus in the situation that the theory does not follow a unique scaling law for the bosonic and the fermionic sector. In the same vein, the IR and UV properties of the model are not simply related. Both problems thwart direct power counting. Instead it is necessary to first identify the correct IR scaling, which determines the physically important pieces of the correlation functions. This IR scaling is then also used for the UV limit to determine cutoff scales for the crossover to the high-energy theory.

How can we extract the IR limit with the least amount of assumptions? In the following we use a very thorough derivation which was pioneered by Lee [173]. The following discussion uses a circular Fermi surface for clarity, but the same procedure is possible for a lattice dispersion. Geometrically, the available phase space can be visualized as in Fig. 2.5. The fermionic sector is restricted to a shell of width Λ around the Fermi surface, the bosons have a momentum disk with radius $\tilde{\Lambda}$ available around $\mathbf{q} = 0$. We further impose that always $\Lambda \ll k_F$ and choose the polar coordinate systems (k_r, θ) and (q, φ) for the fermions and bosons respectively. We note that k_r is defined with respect to the Fermi surface, i.e. it can take values between $-\frac{\Lambda}{2}$ and

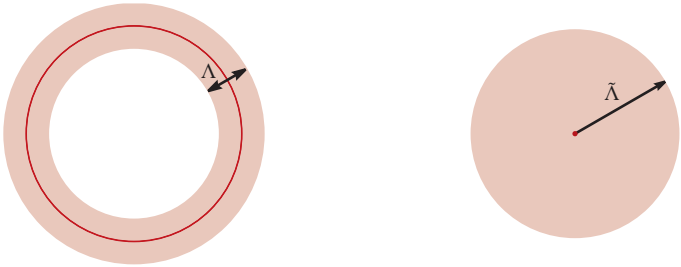

Figure 2.5 Momentum shells of the low energy action. On the left, the momentum shell of thickness Λ around the Fermi surface for fermionic momenta. On the right, the bosonic momentum disk of size $\tilde{\Lambda}$. Dark red marks the location of singularities for the static propagators of both excitations.

$\frac{\Lambda}{2}$. The interacting part of the action is then

$$\begin{aligned}\mathcal{S}_1 = \sum_\sigma \frac{g}{(2\pi)^6} \int_{-\infty}^{\infty} \mathrm{d}\omega \int_{-\Lambda/2}^{\Lambda/2} \mathrm{d}k_r \int_{-\pi}^{\pi} \mathrm{d}\theta \int_{-\infty}^{\infty} \mathrm{d}\nu \int_0^{\tilde{\Lambda}} \mathrm{d}qq \int_{-\pi}^{\pi} \mathrm{d}\varphi \\ \times \Theta(\Lambda/2 - |k_r + q\sin\varphi/2|)\Theta(\Lambda/2 - |k_r - q\sin\varphi/2|)\phi(\nu, q, \theta - \varphi) \\ \times \bar{\psi}_\sigma(\omega + \nu/2, k_r + q\sin\varphi/2, \theta + q\cos\varphi/2k_F) \\ \times \psi_\sigma(\omega - \nu/2, k_r - q\sin\varphi/2, \theta - q\cos\varphi/2k_F), \end{aligned} \tag{2.67}$$

where we wrote the momentum dependences not as indices but brackets for readability. Near the Fermi surface, the dispersion is locally parabolic, so that $\tilde{\Lambda}^2 \sim k_F\Lambda$. Therefore it holds that $k_F \gg \tilde{\Lambda} \gg \Lambda$, i.e., the transmitted q is a lot larger than the extension of the Fermi surface shell. Since the fermions must be scattered from the Fermi surface to another point inside the shell, the momentum transfer is predominantly along the Fermi surface and perpendicular to $\mathbf{k}_F$ (Fig. 2.6). $\mathcal{S}_1$ therefore receives the largest contributions around the Fermi surface points given by $\varphi = 0, \pi$, which corresponds to the Fermi surface patches near to $\mathbf{k}_F$ and its antipode $-\mathbf{k}_F$. One can utilize this and define separate fermionic fields with index $s = \pm 1$ for each semicircle of the Fermi surface. Expanding in φ in both points and resolving the simplified Θ-functions, one obtains

$$\begin{aligned}\mathcal{S}_1 = \sum_{\sigma,s=\pm} \frac{g_s}{(2\pi)^6} \int_{-\infty}^{\infty} \mathrm{d}\omega \int_{-\Lambda/2}^{\Lambda/2} \mathrm{d}k_r \int_{-\pi/2}^{\pi/2} \mathrm{d}\theta \int_{-\infty}^{\infty} \mathrm{d}\nu \int_{-\tilde{\Lambda}}^{\tilde{\Lambda}} \mathrm{d}q|q| \int_{-\Lambda/|q|}^{\Lambda/|q|} \mathrm{d}\varphi \\ \times \phi(\nu, q, \theta - \varphi)\bar{\psi}_{\sigma s}(\omega + \nu/2, k_r + q\varphi/2, \theta + sq/2k_F) \\ \times \psi_{\sigma s}(\omega - \nu/2, k_r - q\varphi/2, \theta - sq/2k_F). \end{aligned} \tag{2.68}$$

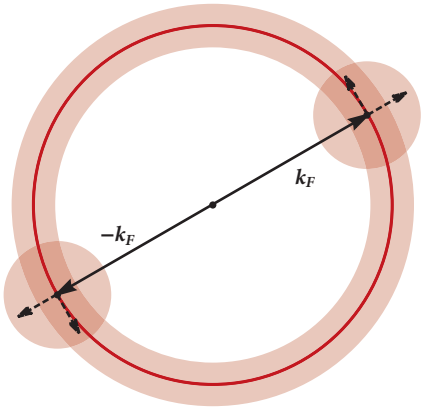

Figure 2.6 Overlay of the fermionic and bosonic momentum shells. Scattering events must respect both phase space restriction. Forward scattering is therefore constrained mostly along the Fermi surface (overlaying region). For a given Fermi momentum $\mathbf{k}_F$, the local neighborhood and the antipodal patch around $-\mathbf{k}_F$ can contribute to the forward scattering.

In this formulation with two Fermi surface patches, the symmetry of the interaction enters explicitly in $g_\pm$. Furthermore, in interaction Eq. 2.68, the two-dimensional nature of the model is implemented via the cutoffs which trace the Fermi surface. As Lee [173] demonstrated explicitly, this construction of the cutoffs is enough to enforce the peculiar dynamics with $z = z' = 3$ at one-loop (cf. Sec. 2.2.1), even if the dispersion is expanded in the lowest possible order $\pm k_r$, which turns the fermions into a set of 1+1 dimensional fields. The curvature of the original Fermi surface is thus a relevant perturbation in the model and an intrinsic feature of the theory.

Implementing the one-loop corrections, the noninteracting part of the action becomes

$$\begin{aligned}\mathcal{S}_0 = &\sum_{\sigma,s=\pm}\int \mathrm{d}\omega \mathrm{d}k_r \mathrm{d}\theta \left(ic_1\{\omega\} - sk_r\right)\bar{\psi}_{\sigma s}(\omega,k_r,\theta)\psi_{\sigma s}(\omega,k_r,\theta)\\ &+\int \mathrm{d}\nu \mathrm{d}q|q|\mathrm{d}\varphi\left(c_2q^2 + c_3\frac{|\nu|}{|q|}\right)\phi^*(\nu,q,\varphi)\phi(\nu,q,\varphi),\end{aligned} \tag{2.69}$$

with some constants c_1, c_2, c_3. Using this action to derive the IR scaling, one arrives at the following prescription:

$$\omega \to \lambda^3 \omega \qquad \nu \to \lambda^3 \nu \tag{2.70}$$

$$k_r \to \lambda^2 k_r \qquad q \to \lambda q \tag{2.71}$$

$$\Lambda \to \lambda^2 \Lambda \qquad \tilde{\Lambda} \to \lambda \tilde{\Lambda}. \tag{2.72}$$

To make the action invariant under the scaling, it is then also necessary to rescale the angular variables according to

$$\theta \to \lambda \theta \qquad \varphi \to \lambda \varphi \tag{2.73}$$

In the rescaled action, this leads to diverging integration boundaries for θ

$$\pm\pi/2 \to \pm\lambda^{-1}\pi/2. \tag{2.74}$$

The anomalous dynamical critical exponent thus introduces a scale dependence of θ. In the IR limit, the integration boundaries tend to infinity, effectively decompactifying the angular variable. Geometrically, two points on the Fermi surface become increasingly decoupled in the low energy limit, so that the quasiparticles lose the ability to probe the Fermi surface as a whole. However, as Lee pointed out, this dynamical decoupling does not lead to a one-dimensional theory, and it is not due to the Fermi surface geometry, but entirely due to quantum fluctuations. A low-energy limit which adheres to the bare scaling properties does not decompactify the angular variables.

While conceptually very appealing, the interaction Eq. 2.68 is unwieldy to use in practical calculation. Instead, we opt to incorporate the two-dimensionality of the model with a better approximation for the dispersion $\epsilon(\mathbf{k}) = \pm k_x + k_y^2/2$, while setting the cutoffs in momenta and frequencies to infinity. This approximation is known as the *two-patch approximation* or *patch construction*. It resembles the implicit approximations which were used in early treatments of the SCM action, with the crucial difference that two points on the Fermi surface are kept ($\mathbf{k}_F$ and $-\mathbf{k}_F$), spoiling the chirality which was present in a local expansion of $\epsilon(\mathbf{k})$.

Having identified the correct low-energy scaling, we can now enumerate the UV properties of the reduced model and identify the neglected irrelevant dependencies. The former is done in Sec. 2.2.4 together with the derivation of the flow equations. For the latter, we observe that the natural cutoff scales within the two-patch regime are given by $\Lambda_x^{1/2} \sim \Lambda_y \sim \Lambda_0^{1/3}$. From the structure of the bare propagators,

$$G_{0,s}^{-1} \sim ik_0 - \left(\frac{k_x^2 + k_y^2}{2} + s k_x \right) \tag{2.75}$$

$$D_0^{-1} \sim \mathbf{q}^2 \tag{2.76}$$

we conclude that the first out-of-patch contributions arise once $\Lambda_x \sim \Lambda_y$ or $\Lambda_0 \sim \Lambda_y$. From a comparison with the patch scaling one can conclude that the irrelevant

momentum terms reappear first in the UV. With respect to the original Fermi surface, the patch cutoffs are not actually diverging momenta or frequencies, but rather a measure for the smallness of the average transmitted momentum or frequency. UV divergences in the two patch approximation are therefore IR divergences in the physical model.

A more subtle issue related to patching is the decompactification of the Fermi surface itself. The angular variable around the Fermi surface is a compact field index like a compact gauge field in standard field theories. The multivalued nature of a compact variable allows for instantonic solutions which are lost when the theory is expanded around one minimum. The two-patch approximation is exactly such an expansion, it is therefore only useful if instantons are irrelevant. Lee [173] studied this question using the scaling theory presented above and concluded that the instanton plasma is most likely irrelevant for any value of N_f. We will encounter similar questions in Sec. 4.3.3 when we discuss the possible deformation of the low-energy theory due to fluctuations between both patches.

Another important aspect of the two-patch approximation is the location of the expansion point on the Fermi surface. In the derivation we used a circular Fermi surface, but in the absence of nesting, the same derivation can be done for a Fermi surface with changing curvature. Metlitski and Sachdev [114] pointed out that the two-patch approximation possesses the desirable property that the actual choice of the expansion point is also irrelevant in the RG sense. For this, they consider a sliding transformation along the expanded Fermi surface which shifts the expansion point by a (dimensionful) angle of θ, transforming the fields according to

$$\phi(q_x, q_y) \to \phi(q_x - \theta q_y, q_y) \tag{2.77}$$

$$\psi_{\sigma s}(q_x, q_y) \to \psi_{\sigma s}(q_x - \theta q_y - s\theta^2/2, q_y + s\theta) \tag{2.78}$$

In local coordinates, the shift displaces the expansion point by (κ_x, κ_y) with the constrained $\kappa_x + \kappa_y^2/2 = 0$. The transformation between the local coordinate systems (k_x, k_y) and (k'_x, k'_y) of the old and new expansion point respectively is then up to $\mathcal{O}(k_x^1)$ and $\mathcal{O}(k_y^2)$

$$k'_x = k_x - \kappa_x + \kappa_y(k_y - \kappa_y) \tag{2.79}$$

$$k'_y = k_y - \kappa_y \tag{2.80}$$

It is $k'_x + {k'}_y^2/2 = k_x + k_y^2/2$, making this transformation a symmetry of the Hamiltonian within the two-patch regime. Using this, Metlitski and Sachdev constrained the forms of the low-energy propagators to

$$G_s(k_x, k_y) = G_s(sk_x + k_y^2/2) \tag{2.81}$$

$$D(q_x, q_y) = D(0, q_y) \tag{2.82}$$

i.e., the curvature of the Fermi surface is stable against renormalization and the boson cannot acquire a q_x dependence. We reiterate that the sliding symmetry is only a symmetry of the two-patch approximation and will be broken at the UV cutoff scales. The symmetry is therefore preserved on the quantum level only if the model does not contain any quantum anomalies. We will address this question in Sec. 4.3.1.

As the last complication we consider the reconstruction of the original model from a patched calculation. Usually, the size of a Fermi surface patch is not explicitly specified. Most authors assume that the patch is rather small so that the original Fermi surface is reconstructed by gluing together a large number of patches. Alternatively, one could use only few patches whose extension is almost the size of the original Fermi surface. In both cases, the gluing procedure necessitates some boundary conditions for the patches. If the patches are large, the boundary conditions restrict the size of the patches based on microscopic parameters like the variation of the curvature along the Fermi surface. In this case scattering events which take place between different patches are irrelevant. On the other hand, large patches introduce a bias in the calculation by specifying a set of preferred points at the center of each patch. This is undesirable. If the patch size is decreased for example in an RG flow and the number of patches becomes large, the bias of the expansion point is reduced, but inter-patch coupling might become important. It is therefore nontrivial to go back from a patched to a full Fermi surface no matter how the patches are implemented. This problem is relevant if the competition of nematicity and superconductivity is of interest: In two dimensions, the particle-particle channel is marginal for a generic electron-electron interaction. If the particle-hole channel now becomes singular at criticality, it enforces the decompactification of the Fermi surface, which renders the critical channel marginal and the particle-particle channel irrelevant. In essence, the particle-particle channel can originally make use of the whole Fermi surface, leading to an enhanced phase space volume which is negated when the Fermi surface is chopped up into patches. The gluing prescription then has the delicate task to properly reverse this step and reinstate the correct scaling of the superconducting channel [121]. In cases like these, it can therefore be beneficial to avoid patching completely [161].

We reiterate that the entire issue of an irrelevant BCS interaction is not tied to the two-patch approximation, but to the scaling at criticality: When the four-fermion interaction is parametrized with a transfer boson and the boson becomes massless at criticality the interaction strength diverges like λ^{-2}. The result is a relevant interaction in this channel which is necessary leading compared to the normal - and still marginal - BCS channel. The NFL behavior then reduces the scaling dimension of the critical channel back to marginal, making the BCS interaction irrelevant in this limit. In the presence of relevant fluctuations such a flow to a nontrivial fixed point is the only possible outcome, ambiguity can only be claimed for the exact nature of the fixed point.

2.2.3 Renormalized perturbation theory

While it was believed for a comparatively long time that the NFL fixed point which is enforced by the one-loop corrections is stable, this is not actually the case [114, 115]. The deviation from the one-loop fixed point was obtained in a perturbative expansion in terms of the renormalized one-loop propagators. In other words, the one-loop fixed point was taken as the starting point and further fluctuations added on top. Before presenting the calculation in Sec. 2.2.5, we briefly discuss this setup and the framework behind it.

The addition of a subset of diagrams to the inverse propagators amounts to a redefinition of the action in terms of effective two-point functions which arise from a partial resummation of infinitely many diagrams of a certain class. The partial resummation employed here is usually known as the *random phase approximation* (RPA), which has a long history [174]. The RPA can be motivated in many ways, most easily with the Dyson equation. The Dyson equation connects the bare and the full propagator via all one-particle irreducible corrections Σ in a recurrence relation:

$$G(k) = G_0(k) + G_0(k)\Sigma(k)G(k) \tag{2.83}$$

$$\Sigma(k) = G_0^{-1}(k) - G^{-1}(k), \tag{2.84}$$

which is the definition of the self-energy $\Sigma(k)$. A similar relation holds for the boson self-energy. Using the Dyson equation, one can immediately see that the lowest nontrivial approximation for the full propagator is given by the lowest order contribution to the self-energy. The RPA is thus perturbative in the self-energy. Conceptually more stringent are the Dyson-Schwinger equations, which formulate integral equations in terms of the renormalized Yukawa interaction Γ,

$$\Sigma(k) = \int_q \Gamma(k, k+q)G(k+q)D(q) \tag{2.85}$$

$$\Pi(q) = N_f \int_k \Gamma(k+q/2, k-q/2)G(k+q/2)G(k-q/2). \tag{2.86}$$

The Dyson-Schwinger equations are the simplest example for a hierarchy of equations which relate the effective interactions of different degrees. The right hand sides are depicted in Fig. 2.7, (a) and (b). The next equation for the Yukawa vertex is drawn schematically in (c). The hierarchy can obviously not be closed without making some approximations for certain higher order vertices. The RPA approximation is in this formulation given by the assumption that the vertex Γ is not significantly renormalized from the bare Yukawa interaction. We have already encountered this kind of argumentation in Sec. 2.2.1 for the derivation of the one-loop fixed point. The main problem is that corrections to Γ do not contain a small parameter for

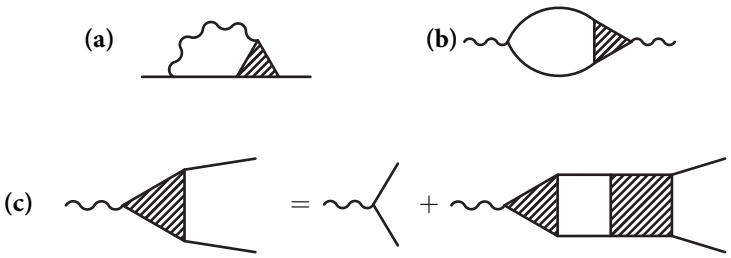

Figure 2.7 Diagrams for the one-particle irreducible parts of the two- and three-point functions. **(a)** defines the fermion self-energy and **(b)** the boson self-energy. In **(c)**, the Yukawa vertex is given.

the physical flavor number $N_f = 2$. The idea is now to improve on the RPA while using the RPA result as the starting point for further calculations. This approach is sometimes called next-to-leading-order RPA [175], or Eliashberg-type theory in reference to the electron-phonon problem [31]. The program is rather straightforward, the calculation proceeds like a normal perturbative expansion, but with RPA-renormalized propagators. As one-loop self-energies are already accounted for, one then disregards all diagrams containing such one-loop self-energy insertions. Clearly, this avoids any double counting of diagrams.

How well is this approach expected to work for the SCM? It is usually argued that RPA resums the "most singular" contributions and thus serves to regularize the theory. In case of the Coulomb interaction in a Fermi liquid, this mechanism is traditionally called screening [176]. This is certainly true for the SCM as the one-loop corrections enforce the 321-limit, reducing the interaction strength from relevant to marginal. On the other hand, the RPA includes only one-loop corrections of the two-point functions and not of the vertex. More seriously, as an infinite sum was used to derive the Dyson equation, the RPA is nonperturbative in the interaction with regards to two-point functions, but not with regards to the Yukawa vertex. This dissonance is problematic because it makes the RPA a non-conserving approximation, i.e., the new expansion will not necessarily respect the symmetries of the original action. The main question is of course whether this violation is of the same order or magnitude as the next-to-leading order calculations which we attempt, i.e., whether one finds a small parameter which makes the influence of the renormalized vertex strictly less than the corresponding self-energy. If such a differentiation were to fail, one would obtain *qualitatively* different results from an inclusion of the renormalized vertex. If

the differentiation works, the vertex corrections can be summed in the usual way order by order in the new perturbative expansion. As we have briefly mentioned in Sec. 2.2.1 and will discuss in detail in Sec. 2.2.6, there is no strict measure under which vertex corrections are small. It therefore remains undetermined how well a perturbation of the one-loop fixed-point is representative of the original action. In the next section we show how this issue can be circumvented at least for the calculation of the critical exponents.

2.2.4 Field-theoretic renormalization group

The field-theoretic renormalization group based on RPA propagators was pioneered by Metlitski and Sachdev [114]. Since we later make contact to some of their explicit results, we mention a slightly different normalization which is used in their calculations. They chose units so that the dispersion is $\varepsilon_s(\mathbf{k}) = sk_x + k_y^2$ and define the bare propagator as

$$\mathcal{G}_{0,s}^{-1} = \varepsilon_s(\mathbf{k}) - iak_0. \tag{2.87}$$

The one-loop renormalized propagators are then

$$D^{-1}(q) = N_f \left(r^2 + \frac{q_y^2}{e^2} + \frac{|q_0|}{4\pi|q_y|} \right) \tag{2.88}$$

$$\mathcal{G}_s^{-1}(k) = (sk_x + k_y^2) - i\bar{\kappa}\{k_0\} \tag{2.89}$$

where $\bar{\kappa} = 2(e^2/4\pi)^{2/3}/\sqrt{3}$.

In the following we will suppress the spin and momentum index in the fermionic fields ψ when possible. We begin with a discussion of the Ward identities. The SCM action closely resembles nonrelativistic QED, not unsurprisingly, this correspondence extends to the formal expressions for symmetries and conservation laws.

It is worth mentioning that the Ward identities follow from different symmetries for even and odd interaction. The low-energy action obeys two $U(1)$-gauge transformations,

$$\psi_s \to e^{i\alpha}\psi_s \qquad \psi_s \to e^{si\alpha}\psi_s \tag{2.90}$$

which correspond to the total conservation of particle number and on each patch respectively. For even interaction, the boson couples to the combination $\bar{\psi}_+\psi_+ - \bar{\psi}_-\psi_-$, which is the x-component of the current associated with the transformation $\psi_s \to e^{i\alpha}\psi_s$. In the same way, for odd interaction the boson couples to $\bar{\psi}_+\psi_+ + \bar{\psi}_-\psi_-$ which is obtained from the second gauge symmetry $\psi_s \to e^{si\alpha}\psi_s$. For the structure of the Ward identities the different origins are immaterial.

We define the currents (it is $a\overleftrightarrow{\partial_y}b = (\partial_y a)b - a(\partial_y b)$)

$$(j_x, j_y, j_0)_\pm = \Big((\bar\psi_+\psi_+ \mp \bar\psi_-\psi_-), -(\bar\psi_+\overleftrightarrow{\partial_y}\psi_+ \pm \bar\psi_-\overleftrightarrow{\partial_y}\psi_-), a(\bar\psi_+\psi_+ \pm \bar\psi_-\psi_-)\Big) \quad (2.91)$$

where the upper sign corresponds to the gauge transformation with $e^{i\alpha}$ and the lower sign to the one with $e^{si\alpha}$. The one particle irreducible polarization function is

$$\Pi_{\mu\nu} = \int \mathrm{d}\tau \mathrm{d}^2\mathbf{x} e^{iq_0\tau - i\mathbf{q}\cdot\mathbf{x}} \langle j_\mu(\mathbf{x},\tau) j_\nu(\mathbf{0},0)\rangle_{1PI}, \quad (2.92)$$

and the one particle irreducible vertex function is

$$\Gamma_\mu = \int \mathrm{d}\tau_1 \mathrm{d}^2\mathbf{x} \mathrm{d}\tau_2 \mathrm{d}^2\mathbf{y} e^{-iq_0\tau_1 + i\mathbf{q}\cdot\mathbf{x}} e^{i(p_0+q_0)\tau_2 - i(\mathbf{p}+\mathbf{q})\cdot\mathbf{y}} \times \langle j_\mu(\mathbf{x},\tau_1)\psi(\mathbf{y},\tau_2)\bar\psi(\mathbf{0},0)\rangle_{1PI}. \quad (2.93)$$

The Ward identities connecting the various two- and three-point functions are then

$$q_x\Pi_{xx}(q) + q_y\Pi_{yx}(q) - iq_0\Pi_{0x}(q) = 0 \quad (2.94)$$

$$q_x\Gamma_x(k,k+q) + q_y\Gamma_y(k,k+q) - iq_0\Gamma_0(k,k+q) = \mathcal{G}^{-1}(k+q) - \mathcal{G}^{-1}(k). \quad (2.95)$$

Due to the 321-scaling in the two-patch regime, a is irrelevant and can be set to zero. We also note that the Ward identities themselves are of limited use as they contain vertices for the y-component of the current. Compared to the one-dimensional case of the Tomonaga-Luttinger model, this prevents a closed solution for the renormalized Green's function [177–179].

As we explained in the previous section, the Ward identities do not actually hold for the RPA-based expansion point. Fortunately, the one-loop self-energies vanish for zero frequency. This means that correlation functions and all relations based on them are the same for bare and RPA-based quantities if evaluated at zero frequencies. To make use of the Ward identities we therefore adopt the constraint to calculate all beyond-RPA corrections for zero frequencies. We emphasize that this does not mean a deviation from the 321-scaling, which is still encoded in the propagators and will also be reflected in the RG.

For the renormalization flow we use the UV cutoff Λ and the IR-renormalization scale λ, where everything is measured in the same units as y-momenta. We note that physically, the IR scale λ is actually determined through the typically transferred y-momenta, in measureable quantities both are therefore indistinguishable and can be exchanged at will. For the derivation of the RG equations, we strictly differentiate

both quantities. In the field-theoretic RG, marginal operators in the action are generalized to flowing functions of λ/Λ. With the help of the Callan-Symanzik equations it is then possible to infer a set of renormalization group equations which parametrize how the marginal operators evolve under a lowering of the scale. As we have seen in Sec. 2.2.2, the local form of the Fermi surface is conserved in the two-patch approximation. The low energy action thus contains six marginal operators, namely three terms in the bosonic propagator (cf. Eq. 2.88), two in the fermionic propagator (Eq. 2.89) and the Yukawa vertex. Among them are both one-loop self-energies, whose scaling is already fixed by the remaining terms. This leaves four renormalization constants. The RG flow will also introduce a shift of the chemical potential, which is a relevant perturbation. It is however possible to absorb this by a momentum shift, eliminating it from the final RG equations.

UV power counting indicates the following UV structure

$$\Pi = K_1 + K_2 r^2 + K_3 q_y^2 + \dots \tag{2.96}$$

$$G = K_4 + K_5 \varepsilon(\mathbf{k}) + \dots \tag{2.97}$$

$$\Gamma = K_6 + \dots \tag{2.98}$$

where the ellipsis indicate any nonanalytic momentum or frequency dependences. Since the nonanalytic terms in the propagators from the RPA vanish for zero frequencies, it is reasonable to assume that the remaining UV structure is analytic. Inserting the power counting estimate in the Ward identities yields

$$K_1 = 0 \quad K_2 = 0 \quad K_5 = K_6. \tag{2.99}$$

This means that no mass renormalization is needed for the boson, and the fermion self-energy and the vertex renormalize in the same way. Due to the Ward identities the number of independent operators is thus only two.

There is some freedom to choose which two constants in Eq. 2.88 and Eq. 2.89 to renormalize. Metlitski and Sachdev chose the amplitude of the fermionic field ψ and e^2, with the relation between bare and renormalized (index r) quantities being

$$\psi = Z_\psi^{1/2} \psi_r \qquad e^2 = Z_e e_r^2. \tag{2.100}$$

The associated anomalous dimensions are

$$\alpha = -\Lambda \frac{\partial}{\partial \Lambda} \log Z_\psi \tag{2.101}$$

$$\beta = \Lambda \frac{\partial}{\partial \Lambda} \log Z_e. \tag{2.102}$$

Correlation functions Γ^{n_f,n_b} of n_f fermions and n_b bosons are renormalized with $Z_\psi^{n_f/2}$. The renormalized correlation functions are the physical observables and thus independent of the cutoff. Taking the total differential yields the renormalization group equations

$$\begin{aligned}\Lambda\frac{\mathrm{d}}{\mathrm{d}\Lambda}\left(Z_\psi^{n_f/2}\Gamma^{n_f,n_b}\right) &= \left(\Lambda\frac{\partial}{\partial\Lambda}+\beta e^2\frac{\partial}{\partial e^2}-\frac{n_f}{2}\alpha\right)\Gamma^{n_f,n_b}(p_x,p_y,p_0,r^2,e^2,\Lambda)\\ &= 0,\end{aligned} \tag{2.103}$$

where the shift of the chemical potential is already canceled. From the one-loop propagators Eq. 2.88 and Eq. 2.89 one can infer the UV-structure of the correlation functions. The global scale dependence is directly given by the number of fields in the correlation function. Additionally, we pull out a factor of $(e^2)^{n_b-1}$ in order to shift the dependence on e^2 to the frequencies, resulting in

$$\Gamma^{n_f,n_b} = \Lambda^{6-2n_f-2n_b}(e^2)^{n_b-1}\widetilde{\Gamma}^{n_f,n_b}\left(\frac{p_x}{\Lambda^2},\frac{p_y}{\Lambda},\frac{p_0e^2}{\Lambda^3},\frac{\Lambda^2e^2r^2}{\lambda^2}\right). \tag{2.104}$$

Inserted into the RG equations we obtain

$$\begin{aligned}\widetilde{\Gamma}^{n_f,n_b}(\lambda^2p_x,\lambda p_y,&\lambda^{3-\beta}p_0,\lambda^{\beta-2}r^2) =\\ &\lambda^{6-\beta-(\alpha/2+2)n_f+(\beta-2)n_b}\widetilde{\Gamma}^{n_f,n_b}(p_x,p_y,p_0,r^2)\end{aligned} \tag{2.105}$$

From the arguments, we can deduce the renormalized scaling which solves the renormalization group equations as

$$p_x \to \lambda^2 p_x \tag{2.106}$$
$$p_y \to \lambda p_y \tag{2.107}$$
$$p_0 \to \lambda^{3-\beta} p_0 \tag{2.108}$$
$$r^2 \to \lambda^{\beta-2} r^2. \tag{2.109}$$

The dynamical critical exponent is thus $z = 3-\beta$. The correlation length is given by $\xi = r^{-\nu}$ with $\nu = (1-\beta/2)^{-1} = 2/(z-1)$. The scaling forms of the correlation functions are

$$D^{-1}(q) = \frac{q_y^{2-\beta}\Lambda^\beta}{e^2} f_1\left(\frac{q_0e^2}{q_y^z\Lambda^\beta}\right) \tag{2.110}$$

$$G_s^{-1}(k) = \Lambda^\alpha|\varepsilon_s(\mathbf{k})|^{1-\alpha/2} f_2\left(\frac{k_0e^2}{|\varepsilon_s(\mathbf{k})|^{\alpha/2}\Lambda^\beta}\right), \tag{2.111}$$

where f_1 and f_2 are analytic functions. The scaling forms correctly recover each momentum and frequency limit, but as usual they do not reproduce the complete functional form of the original correlation functions. By construction, the one-loop self-energies are not renormalized independently. This is not actually a limitation of the RG, but rather a consequence of the coupling of spatial and temporal degrees of freedom at criticality: If we chose to renormalize the one-loop self-energies, a redefinition of the momenta and fields would be enough to redistribute all renormalization constants back to the fermionic field strength and e^2.

We mentioned in the beginning that we need to restrict external frequencies to zero to be able to profit from the Ward identities. The resulting RG is unaffected by this restriction since it concerns the scaling near criticality, where momenta and frequencies are coupled via the DCE. It therefore suffices to calculate corrections as a function of momentum alone with vanishing frequencies, as the frequency dependence is dictated by the RG equations.

Equipped with the RG equations, one can now calculate the critical exponents α and β order by order in a loop expansion. The calculation proceeds according to the normal rules of a perturbative expansion with minimal subtraction [2]: Since the interaction is marginal, diagrams can be at most (multi-)logarithmically divergent. Finite diagrams contain an analytical momentum dependence and do not affect the flow. A logarithm enters the flow equations via

$$Z_\psi = 1 - \frac{\partial \Sigma(\varepsilon_s(\mathbf{k}))}{\partial \varepsilon_s(\mathbf{k})} \tag{2.112}$$

$$Z_e = 1 + \frac{e^2}{2N_f} \frac{\partial^2 \Pi(q_y)}{\partial q_y^2} \tag{2.113}$$

Diagrams with logarithmic singularities always imply a nonanalytic momentum dependence of the correction as the IR cutoff is set by the typically exchanged momenta (cf. Sec. 2.2.2). For each singular correction a counterterm is required in the action to make it finite up to this order. At higher orders, typically singular diagrams with multiple logarithms occur. If the SCM action is renormalizable, these singularities are always reduced to a logarithmic one after subtracting the counterterms, otherwise the theory is not renormalizable.

Prior to this work, calculations were completed up to three loops. One loop is already contained, no corrections are found at two loop and a small contribution to α is found from some logarithmically divergent three-loop diagrams, while β remains zero. In the next section, we give the details of the results at three loop; counterterms at three-loop level and the more general question when and why singular contributions occur is the topic of chapter 3.

2.2.5 Failure of large-N

In Sec. 2.2.2 it was shown that the SCM is a strong coupling problem, a perturbative approach is therefore not justified in terms of the interaction. For many systems one can create a small parameter $1/N_f$ by extending the number of fermion flavors from the physical value $N_f = 2$ to arbitrary large N_f (see for example Sachdev [6]). This large-N_f expansion was also universally employed for the SCM action until it was pointed out by Lee [115] that the theory does not become weakly interacting in the limit $N_f \to \infty$. The origin of this failure can easily be traced back to the fermionic one-loop self-energy of the fermion Green's function. Its prefactor κ is proportional to $1/N_f$ and vanishes in the large-N_f limit, suppressing the frequency dependence in the propagator. While the bare Green's function additionally contains the linear frequency term $\sim iak_0$, this dependence is irrelevant. The propagator will therefore induce additional divergences in some diagrams in the large-N_f limit. Upon taking the limit $N_f \to \infty$, these divergences will emerge as additional positive powers of N_f which enhance the simple estimate based on the number of loops.[2] Lee also developed an enumeration scheme based on the topology of the graph for diagrams which contain fermions from only one patch. This scheme allows to precisely read of the suppression (or lack thereof) of any diagram in the large-N_f limit. As the main result, he proved that there are infinitely many diagrams which contribute at leading order in N_f. In other words, the enhancement by the Green's function is in certain diagrams strong enough to exactly cancel the suppression which would be obtained by naïvely applying the large-N_f limit, but not stronger. We point out that some diagrams are still suppressed. Nevertheless, employing the large-N_f limit does not justify the usual ordering in terms of number of loops. Likewise, the SCM does not become weakly interacting for large N_f. Notably, no terms with higher powers of N_f occur, which means that corrections from one-patch diagrams are at most marginal in powers of N_f.

One year later Metlitski and Sachdev [114] calculated the self-energies up to three loops. At this loop order, diagrams involving fermions from both patches occur for the first time. They discovered that these two-patch diagrams contain a larger enhancement which boosts the three-loop corrections to a higher power in N_f than all previous contributions. The offending diagrams are depicted in Fig. 2.8. According to the RG presented in the last section, the calculation was done while setting external frequencies to zero. Using the shorthand $\delta = k_x + k_y^2$, one obtains

[2] One might wonder whether the problem is related to the perturbation theory around the RPA result. This is not the case, using bare propagators the enhancement is also present, but instead parametrized in powers of a^{-1}, which diverges in the 321-limit.

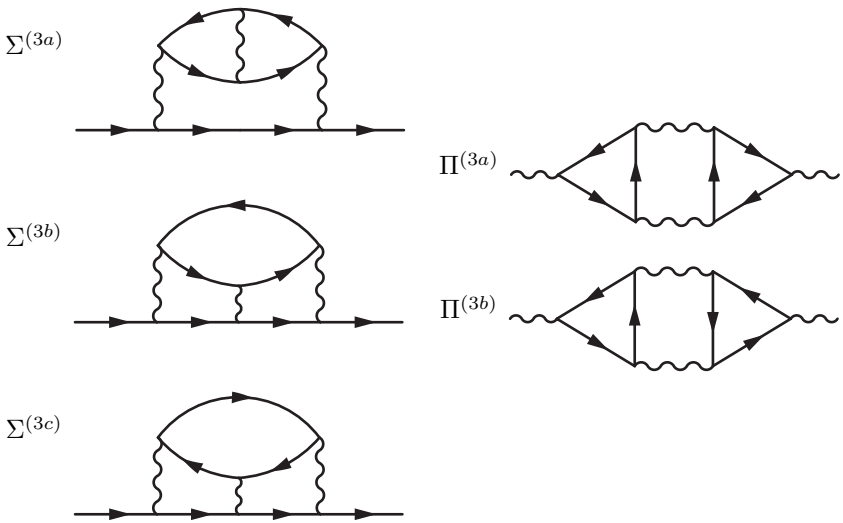

Figure 2.8 Important three-loop corrections which were considered in [114]. The diagrams on the left contribute to the fermion self-energy, the ones on the right (Aslamazov-Larkin diagrams) to the boson self-energy.

in the large-N_f limit

$$\Pi^{(3)}(q_y, 0) = \Pi^{(3a)} + \Pi^{(3b)} = c_{b,3} N_f^{3/2} g_+ g_- \frac{q_y^2}{e^2} \tag{2.114}$$

$$\Sigma^{(3a)}(\delta, 0) = 0 \tag{2.115}$$

$$\Sigma^{(3b)}(\delta, 0) = c_{f,3b} g_+ g_- \delta \log\left(\frac{\Lambda}{\sqrt{|\delta|}}\right) \tag{2.116}$$

$$\Sigma^{(3c)}(\delta, 0) = \Sigma^{(3c)}(0, 0) + c_{f,3c} \frac{\log^3 N_f}{N_f^2} g_+ g_- \delta \log\left(\frac{\Lambda}{\sqrt{|\delta|}}\right), \tag{2.117}$$

where $c_{b,3}$, $c_{f,3c}$ and $c_{f,3c}$ are constants. The inverse boson propagator is of order N_f, the three loop correction $\Pi^{(3)}$ with power $N_f^{3/2}$ is thus superleading with respect to large-N_f. Remarkably, both diagrams $\Pi^{(3a)}$ and $\Pi^{(3b)}$ are actually divergent with Λ^1, but this divergence is canceled upon symmetrization, leaving only a finite term. The three-loop fermion self-energy $\Sigma^{(3)}$ is of order N_f^0, which is the same as

the bare inverse Green's function but larger than the one-loop self-energy, which scales as N_f^{-1}. We conclude that the SCM action does not decouple with increasing N_f, quite on the contrary it develops a new and different strong coupling limit. These complications make an interpretation of results at large-N_f very difficult, at the moment the whole limit is therefore considered as inapplicable to the SCM action [114, 116, 118].

While the three-loop corrections are large for $N_f \to \infty$, all numerical factors $c_{b,3} \approx -0.096$, $c_{f,3b} \approx 0.11$ and $c_{f,3c} = 9/4\pi^2$ are quite small. An evaluation of the diagrams for $N_f = 2$ confirms this, yielding values (including all factors of $N_f = 2$) of -0.045 for $\Pi^{(3)}$ and -0.038 for $\Sigma^{(3c)}$ respectively. Inserting the logarithmic divergence of $\Sigma^{(3)}$ into the RG equations leads to a tiny anomalous dimension $\alpha = 0.068 g_+ g_-$. This numerically small correction has sparked some interest that the theory may be well controlled by other means. Two suggestions, one of them very recent, will be discussed in Sec. 4.2. There, we also present a new control mechanism in the SCM action which follows from the kinematic constraints discussed in chapter 3.

2.2.6 Vertex corrections

For the derivation of the 321-limit, the two-patch approximation and the RG equations we deferred the detailed discussion of vertex corrections. As discussed in Sec. 2.2.1, the original argument for the relative smallness of vertex corrections is based on the large-N_f limit [39, 112]. Since we do not employ this limit, the argumentation is more tricky. One angle of attack is an explicit calculation of some diagrams, the results of which are then extended self-consistently or by power counting. More methodically, one might single out certain vertex corrections which supposedly have the largest effect. In extensions of Eliashberg theory for the electron-phonon problem, this is accomplished with the help of Migdal's theorem. In its modern formulation, Migdal's theorem compares the available phase space of the loop variables, and often boils down to the selection of vertex corrections which contain ladders of boson propagators. The same line of reasoning to separate ladder diagrams from the remaining ones was advocated for the SCM [112, 180]. We remark that in the following discussion we will look at a part of the irreducible vertex to which only fermions from one patch contribute. Working with the plus patch and setting $a = 1$, we obtain from Eq. 2.91 that $\Gamma_x = \Gamma_0$. The renormalized vertex from ladders will therefore be denoted by $\Gamma_{x,||} = \Gamma_{0,||} = \Gamma_{||}$

If only ladder diagrams are important, it is possible to also write down a self-consistency equation for the renormalized vertex $\Gamma_{||}$ which contains the bare inter-

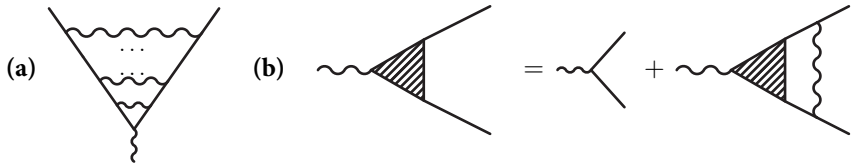

Figure 2.9 (a) Ladder-type vertex corrections. **(b)** Graphical representation of the integral equation for the fully renormalized vertex from ladder insertions.

action and all ladder contributions (Fig. 2.9)

$$\Gamma_{||}(p, p+q) = g + \int_k \Gamma_{||}(p+k, p+k+q)\mathcal{G}(p+k)\mathcal{G}(p+k+q)D(k). \tag{2.118}$$

Chubukov [180] solved this integral equation under the assumption that only frequency dependences of the self-energy and the vertex function matter, with the result

$$\Gamma_{||}(\omega, \omega+\Omega) = 1 + \left(\frac{c_\omega}{\Omega}\right)^{1/3} \left(\left(1 + \frac{\omega}{\Omega}\right)^{2/3} - \left(\frac{\omega}{\Omega}\right)^{2/3} \right). \tag{2.119}$$

For the calculation, the bare interaction was set $g = 1$, c_ω is a constant. By keeping only frequency dependences and setting momenta to zero, he reduced the Ward identity to

$$\Gamma_0(\omega, \omega+\Omega) = 1 + \frac{\Sigma(\omega+\Omega) - \Sigma(\omega)}{-i\Omega}. \tag{2.120}$$

For small frequencies, the result Eq. 2.119 diverges like $\Omega^{-1/3}$, thus fulfilling the reduced Ward identity.

In the 321-limit, the above calculation is not applicable as frequencies and momenta scale exactly such that the different dependences are of the same order of magnitude. Furthermore, the reduced Ward identity of Eq. 2.120 is problematic in the 321-limit as a tends to zero, meaning that the current vertices $\Gamma_{x,y}$ are very likely the leading terms compared to Γ_0. We also note that the vertex renormalization in Eq. 2.119 scales like λ^{-1}, making it irrelevant in the UV. The renormalized vertex Eq. 2.119 therefore describes a limit which is not relevant for the critical theory and should not be employed as the next order improvement beyond RPA. The solution of Eq. 2.118 was originally constructed to restore the Ward identities for one-loop propagators. In Sec. 2.2.4 we argued that Γ_0 does not play any role in the 321-limit

as it is multiplied with an irrelevant operator, one might then wonder how the vertex can produce an $\omega^{2/3}$-term at all to restore the Ward identities. To answer this it is important to keep in mind that there are many other possibilities for the full theory to achieve this as correlation functions can acquire nonanalytic dependences which are not described by anomalous dimensions (cf. Sec. 2.2.1). One could for example imagine a nonanalytical term of size $\{q_0\}/q_x$ in the current vertex Γ_x, which adheres to power counting and restores the Ward identity.

As we show now, in the 321-limit a self-consistent solution of the integral equation Eq. 2.118 is mainly governed by the dependence of the vertex on y-momentum and not on frequency. In the following, the convention Eq. 2.87 for the Green's function is used. The calculation is done for the plus patch, the expressions for the minus patch can easily by obtained by replacing x-momenta by their negative as well as $g_+ \to g_-$. To avoid clutter we therefore suppress the patch index in this section. The one-loop vertex correction is given by

$$\Gamma^{(1)}(p_1, p_2) = g^3 \int_k \mathcal{G}(k - p_1)\mathcal{G}(k - p_2)D(k), \tag{2.121}$$

where $p_2 - p_1$ is the transferred momentum. Performing the integration in k_x by residues, we obtain

$$\begin{aligned}\Gamma^{(1)}(p_1, p_2) = g^3 \int \frac{\mathrm{d}k_0 \mathrm{d}k_y}{(2\pi)^2} i\Big[&p_{1x} - p_{2x} + 2k_y(p_{1y} - p_{2y}) \\ &- (p_{1y}^2 - p_{2y}^2) + i\bar{\kappa}\left(\{k_0 - p_{10}\} - \{k_0 - p_{20}\}\right)\Big]^{-1} \\ &\times \left(\Theta(k_0 - p_{10}) - \Theta(k_0 - p_{20})\right) D(k).\end{aligned} \tag{2.122}$$

Substituting $k_0 \to (p_{20} - p_{10})z + p_{10}$ and $k_y \to \sqrt{\bar{\kappa}}|p_{20} - p_{10}|^{1/3}\mathrm{sgn}\,(p_{20} - p_{10})$, this becomes

$$\begin{aligned}\Gamma^{(1)}(p_1, p_2) = \frac{g^3}{N_f \pi} \int_{-\infty}^{\infty} \mathrm{d}y \int_0^1 \mathrm{d}z \frac{1}{\alpha y^2 + |\frac{z-A}{y}|} \\ \times \frac{i}{B + yC + i(\{z\} - \{z-1\})},\end{aligned} \tag{2.123}$$

with the definitions

$$\alpha = \left(\frac{2}{N_f\sqrt{3}}\right)^{3/2} \tag{2.124}$$

$$A = \frac{p_{10}}{p_{10} - p_{20}} \tag{2.125}$$

$$B = \frac{p_{1x} - p_{2x} - (p_{1y}^2 - p_{2y}^2)}{\bar{\kappa}\{p_{20} - p_{10}\}} \tag{2.126}$$

$$C = \frac{2|p_{2y} - p_{1y}|}{\sqrt{\bar{\kappa}}|p_{20} - p_{10}|^{1/3}}. \tag{2.127}$$

For the overall prefactor $N_f\pi$ and α, the definition of $\bar{\kappa}$ was inserted for clarity. The integral is invariant under a sign change of C, therefore $C > 0$ was chosen, a sign change in B yields the complex conjugate. As z is bounded between zero and one, the integral is largest for $A = 0.5$ compared to any other A. We thus investigate the value of Eq. 2.123 as a function of B and C for values of A between zero and 0.5. The results for the physical flavor number $N_f = 2$ are shown in Fig. 2.10. The one-loop vertex correction is clearly bounded for *any* conceivable momentum and frequency combination. All three coefficients A,B and C are constant in the 321-limit, the vertex correction is thus marginal with respect to the tree level interaction. For large values of the coefficients, the vertex correction decays like $A^{-1/3}$, B^{-2} and C^{-2} respectively. This limit is reached if the transferred frequency $p_{20} - p_{10}$ is much smaller than the remaining variables. If a one-loop vertex correction appears as a subdiagram, the impact might be approximated by substituting a constant vertex with an appropriate strength. Numerically it is

$$|\Gamma^{(1)}(p_1, p_2)| < |g^3|1.04, \tag{2.128}$$

for $N_f = 2$. Since it is $|g| = 1$ in the two patch regime (Sec. 2.2.4), this estimate is too large to be useful for quantitative purposes. The form Eq. 2.123 can also be used to investigate the resummation of vertex corrections. Using the shorthand $\Gamma^{(1)}(A, B, C)$ for the one-loop correction, it becomes obvious that the renormalized vertex is a function x-momenta and frequencies only through the differences $p_{2x} - p_{1x}$ and $p_{20} - p_{10}$, making it independent of the loop variables k_x and k_0. Exploiting this, the ladder-type two-loop correction (diagram (a) in Fig. 2.11) is given by

$$\begin{aligned}\Gamma^{(2)}(A, B, C) = \frac{g^3}{N_f\pi}\int_{-\infty}^{\infty}\mathrm{d}y\int_0^1 \mathrm{d}z\Gamma^{(1)}(A, B + yC, C)\\ \times \frac{1}{\alpha y^2 + |\frac{z-A}{y}|}\frac{i}{B + yC + i(\{z\} - \{z-1\})}.\end{aligned} \tag{2.129}$$

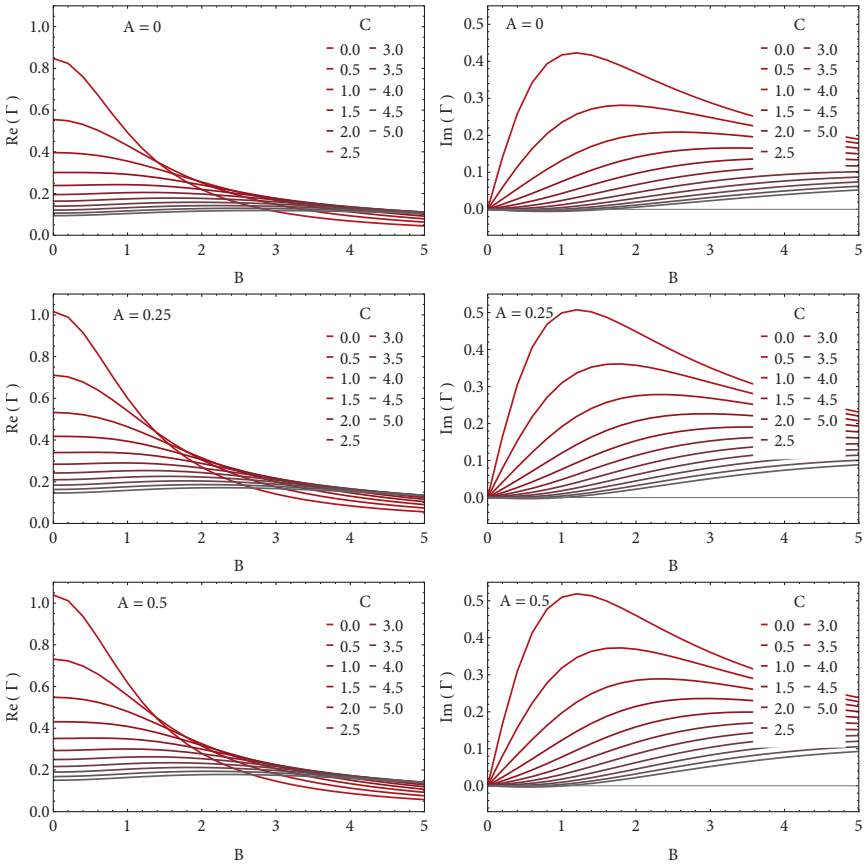

Figure 2.10 The momentum and frequency dependence of the one-loop correction $\Gamma^{(1)}$ to the fermion boson vertex. On the left panel the real part is drawn as a function of B for $A = 0, 0.25, 0.5$ with varying values of C. The right panel shows the corresponding imaginary parts.

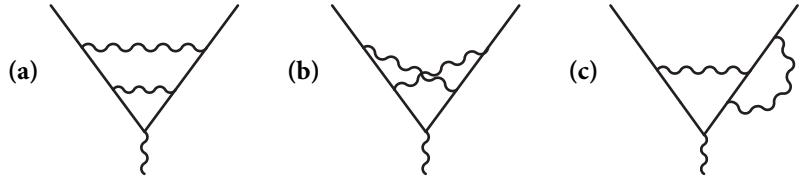

Figure 2.11 Two loop contributions to the vertex. Diagram (a) is a ladder, (b) a crossed diagram and (c) a one-loop vertex with one-loop vertex insertion.

This equation is suitable for a self-consistent evaluation where $\Gamma^{(1)}$ and $(\Gamma^{(2)} + g)$ are promoted to the complete vertex correction $\Gamma_{||}(A, B, C)$ from ladders. We will not pursue this avenue further.

Chubukov [180] argued in favor of a predominant frequency dependence in a recursion relation and obtained a divergence with vanishing frequency like $\Omega^{-1/3}$. This behavior is mimicked in the present formulation if $C \ll 1$, i.e., if the transferred frequency is much larger than the transferred y-momentum cubed. The kernel $\Gamma^{(1)}(A, B, 0)$ is then independent of the loop integral and ladder insertions are multiplicative. As the one-loop correction $\Gamma^{(1)}(A, B, 0)$ is larger than one for small B and $A \approx 0.5$, the resulting geometric sum is divergent for some momentum and frequency combinations. The situation is however different in the 321-limit, which demands both $B \approx 1$ and $C \approx 1$. The absolute values of $\Gamma^{(1)}$ and $\Gamma^{(2)}$ are compared in Fig. 2.12. With each order, the vertex correction becomes increasingly peaked around $B = C = 0$ and decays faster for large B or C.

For the renormalization group flow, one is only interested in singular corrections, finite renormalizations can always be absorbed in a redefinition of constants or fields. Given the fast decay of the higher order vertex corrections for momenta in the 321-limit ($B \approx C \approx 1$), it is natural to assume that the complete sum over ladder insertions does not influence the critical scaling, as it was historically done [39, 112]. The present calculation therefore recovers the qualitative argumentation why the renormalized vertex does not play a role, but without resorting to the large-N_f limit. At the same time there are cases when the ladder sum is not negligible, especially once the regime where $p_{20} - p_{10} \gg (p_{2y} - p_{1y})^3$ is relevant ($B \approx C \approx 0$). From the structure of the vertex corrections one can *not* conclude that this region is very small or vanishes for higher orders (cf. Fig. 2.12). It is therefore not safe to make any assumptions about the importance of vertex corrections for any finite transfer frequency $p_{20} - p_{10}$. For quantitative estimates within the RPA-based perturbation theory it is therefore necessary to restrict the calulation to external frequencies equal zero.

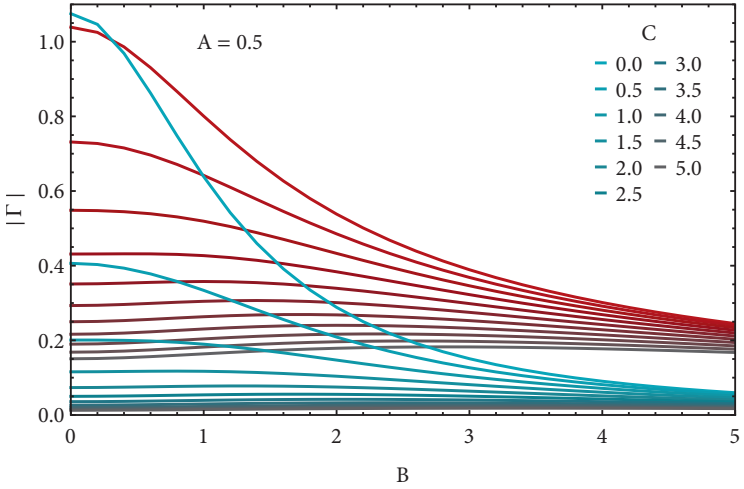

Figure 2.12 Plot of the absolute value of the one-loop (red) and two-loop (blue) contribution to the vertex from ladder diagrams. At two-loop the function has a higher peak value around $B = C = 0$ and decays faster with increasing B and C.

This is consistent with the violation of the Ward identities at finite frequencies (Sec. 2.2.4): The vertex corrections have to be included once the complete frequency and momentum dependence of the self-energies or the vertex is desired. As was explained previously, this information is not necessary to calculate the critical exponents, and it is enough to calculate all corrections for finite external momenta with frequencies equal zero. The use of the one-loop renormalized propagators is therefore a suitable starting point for a discussion of a metal at criticality, but it is insufficient for a calculation of the frequency and momentum dependent forms of the correlation functions.

In Sec. 3.4.2 it will be discussed whether vertex correction subdiagrams (vertex insertions) pose a problem at higher loop order. Based on power counting improvements from symmetrized fermion loops we show that the opposite is the case: It is actually beneficial to not resum vertex corrections from the outset as vertex insertions form an important subset of a larger group of diagrams which should always be treated together to avoid spurious divergences. More precisely, it will turn out that contractions of a fermion loop with a number of boson lines which run between different parts of the fermion loop should always be considered in a symmetrized manner. With regards to the two-loop vertex correction this means for example that

all diagrams depicted in Fig. 2.11 are equally important not necessarily in amplitude but with regards to the scaling their combination produces. At a high enough loop order it is furthermore necessary to account for two-fermion-two-boson terms and even higher order irreducible terms. For this reason partial vertex resummations are not recommmendable for the SCM.

2.3 Contour integration and chiral fermions

In Sec. 2.2 we saw how the two-patch approximation emerged as the low-energy theory for the SCM action and derived the field theoretic RG around the one-loop fixed point. In the course of the derivation we made use of the linearized dispersion perpendicular to the Fermi surface in several places to easily calculate integrals by a contour integration. This approach is not free of pitfalls and can potentially fail due to boundary terms which are omitted. We clarify these issues now and list how they can be avoided.

A striking result of the three-loop calculation presented in Sec. 2.2.5 was the absence of any singular corrections from one-patch diagrams. It was already suggested by Polchinski [39] that no logarithms occur due to the chiral nature of a local expansion. Altshuler, Ioffe, and Millis [112] also noted a strong restriction of internal loop variables in their calculation and concluded that they are responsible for the smallness of higher order corrections.

Below, we present a simple proof how such kinematic constraints restrict all one-patch diagrams, rendering them finite. For this, we use ideas from the work of Lee [115], who first proved the absence of singular contributions for planar diagrams.

In 2014, Sur and Lee [181] independently published a much more elaborate proof to the same effect, also extending the absence of singular corrections to all one-patch diagrams.

2.3.1 Integration by residues

To illustrate the possible pitfalls related to the integration by residues within the two-patch approximation, we recall the one-loop boson self-energy. In Sec. 2.2.1 we performed a contour integration in x-momentum and then in y-momentum. The result was (Eq. 2.61)

$$\Pi(q) = \sum_{s=\pm} N_f \int_k G_s(k - q/2) G_s(k + q/2) = N_f \frac{|q_0|}{2\pi |q_y|}. \tag{2.130}$$

This calculation is missing a constant part, the correct result should be $N_f(|q_0/q_y| - 1)/2\pi$. The origin of this discrepancy is the removal of the UV cutoff in the integra-

tion. In the presence of integration boundaries due to the finite size of the Fermi surface patch, the result would be different. As it was already pointed out in [116], it is therefore mandatory to impose cutoffs on the loop variables when patching the Fermi surface. Still, carrying around the integration boundaries or comparable regulators is cumbersome, also at least the nonanalytic part is correctly captured in Eq. 2.130.

To deal with these kinds of issues in the critical scaling theory, one can appeal to the criterion of universality of a quantity [2, 18]. Universal quantities are not affected by the short range properties of the model, i.e., they are the same for any regularization or cutoff scheme. It is well known that only universal quantities are reliably reproduced by the critical scaling theory, which is designed to capture the scale independent power laws at criticality, while purposefully neglecting any short-range properties of the physical system. As we discussed in Sec. 2.2.1, the constant part of the particle-hole bubble is related to the density of states, which is nonuniversal. The absence of the constant term within the two-patch approximation and with infinite cutoffs is therefore no surprise. The nonanalytic term $|q_0/q_y|$ on the other hand is independent of microscopic properties of the model and is thus universal. We therefore conclude that the removal of UV cutoffs is generally harmless for the determination of the critical exponents. From the same fact we can also conclude that the order of integration does not play a role: Exchanging two integrals is the same as exchanging in which order the cutoffs are taken to infinity. Since the cutoffs can be removed before integrating, the order is commutable and thus immaterial. In the following we always chose the order x-momenta, y-momenta and last frequencies for integrations. This way, we can make maximal use of contour integrals.

Everything said so far is only true in the absence of *quantum anomalies*. A quantum anomaly is easiest explained within the path integral formulation of the partition function [2, 182]. The anomaly appears if a symmetry of the action is not a symmetry of the measure of the partition function, which deforms the classically preserved symmetry. In diagrammatics this manifests as divergences which can only be regulated by permanently breaking the symmetry.

It is usually not mentioned that the particle-hole bubble with bare propagators could in the absence of regulators also be evaluated in a different route (stated here for the plus patch). We decompose

$$\int_k G_0(k-q/2)G_0(k+q/2) \tag{2.131}$$

$$= \int_k \frac{1}{iq_0 - q_x - k_y q_y} \left(G_0(k-q/2) - G_0(k+q/2)\right) \tag{2.132}$$

and then shift the frequency integration by $\pm q_0/2$ in each term, yielding

$$= \int \frac{\mathrm{d}k_y \mathrm{d}k_0}{(2\pi)^3} \frac{1}{iq_0 - q_x - k_y q_y} \times \left(\int \mathrm{d}k_x G_0(\mathbf{k} - \mathbf{q}/2, k_0) - \int \mathrm{d}k_x G_0(\mathbf{k} + \mathbf{q}/2, k_0) \right) \tag{2.133}$$

$$= i \int \frac{\mathrm{d}k_x \mathrm{d}k_y}{8\pi^2} (\operatorname{sgn} k_0 - \operatorname{sgn} k_0) \tag{2.134}$$

$$= 0. \tag{2.135}$$

This is obviously bogus, as dropping the boundary terms in the x-integration is disallowed after the shift, showing that the success of contour integrations depends on the additional restriction that no variable shifts are undertaken. Such an oddity is actually very similar to the chiral anomaly in the Luttinger liquid. In this one-dimensional electron liquid, the equally linearized dispersion seemingly allows to do the same "trick" in the calculation of the particle-hole bubble, also annihilating an otherwise vital term [183]. We are therefore led to the conclusion that the nonanalytic term $|q_0/q_y|$ is within the two-patch approximation a quantum anomaly, but not for the full dispersion.

To be safe against this kind of error, we impose in the following the rule that an integration variable cannot be shifted as long as the integration is unbounded.

2.3.2 One-patch diagrams

The unrenormalized Green's function in the two-patch approximation is given by $G_s^{-1}(k) = iak_0 - (sk_x + k_y^2/2)$ where $s = \pm 1$ depending on which patch the fermion resides. In diagrams which contain fermions only from one patch all Green's functions carry the same sign for s. As the boson propagator is entirely independent of x-momentum, it is always possible to perform all integrations in x-momenta in a diagram by residues. This property can be utilized in a particularly transparent way when setting all external frequencies to zero. In this case, all propagators take the following form

$$G^{-1}(k + \dots) = i(k_0 + u) - (sk_x + v), \tag{2.136}$$

where u and v indicates terms which result from the additional variables which run through the fermion line. Most importantly, u only contains loop frequencies from the remaining integrations. Taking the residue in k_x in the upper half plane will then

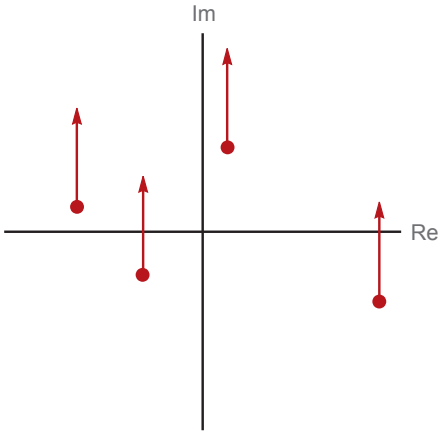

Figure 2.13 Graphical representation of the UV-cutoff in one-patch diagrams. A residue integration in x-momentum will only lead to a finite result if not all poles lie on the same half plane below or above the imaginary axis. With increasing loop frequency, all poles will move in the same direction, eventually leading to a zero result.

result in

$$\int \frac{\mathrm{d}k_x}{2\pi} \prod_i \frac{1}{i(k_0+u_i)-(sk_x+v_i)} \tag{2.137}$$

$$= i \sum_i \prod_{j\neq i} \frac{\Theta(s(k_0+u_i))}{i(u_j-u_i)-(v_j-v_i)}. \tag{2.138}$$

This means that each x-integration annihilates the corresponding frequency term in each propagator in which it was present. The last x-integration then acts on propagators which contain (in the absence of finite external frequencies) only the corresponding (and last) frequency variable as the imaginary part. For this last residue the poles are then all on the same half plane below or above the real axis, rendering the entire integral zero. This mechanism works completely independent of the topology of the diagram.

When the external frequencies are not zero, the last x-integration will no longer be zero as long as the internal frequency is smaller than some combination of external frequencies (Fig. 2.13). While the exact cutoff depends on the specific diagram in question, the scale of the cutoff is set by external variables which means that it carries the IR-scaling. When using one-loop renormalized propagators the exact

cancellation of the frequency variables in the imaginary parts does no longer hold. An arbitrary one-patch diagram is therefore not necessarily exactly zero for zero external frequencies. The scaling argument on the other hand is still valid as the last x-integration yields zero as soon as the internal frequency is sufficiently larger than some combination of external frequencies. The exact magnitude of this cutoff is again undetermined, but it carries the scale of the external frequencies. In the 321-limit, frequencies scale like λ^3, which is enough to render all one-patch diagrams UV-finite.

On the other hand, if a diagram involves fermions from both Fermi surface patches, Green's functions with either $s = +1$ or $s = -1$ will be present. A contour integration which includes fermionic propagators from both patches will then lead to an addition of the corresponding frequency variable in the denominators instead of a subtraction. The last x-integration is then no longer bound by external frequencies, thereby removing the IR-cutoff. As a consequence, singular contributions may appear in these two-patch diagrams.

3 Symmetrized N-point fermion loops

In Sec. 2.1.1 we have seen how symmetrized fermion loops arise naturally as effective N-point density interactions for the bosonized action. Historically, many intricate properties are known about symmetrized N-point fermion loops, which have also been used to improve the naïve power counting estimates in the order parameter action. In the present fermion-boson approach the N-point loops appear explicitly at higher loop orders. Reviewing the calculations up to three loops (Secs. 2.2.3,2.2.5, 2.3.2), it became obvious that diagrams are only singular if they contain fermions from both Fermi surface patches. For two and three-point functions this result implies that singular diagrams necessarily contain at least one N-point loop. Motivated by the explicit results from Thier and Metzner [137] and Metlitski and Sachdev [114], we search for a formulation of the N-point loop which offers insight into the momentum and frequency structure and reveals the odd disparity between bosonic and fermionic self-energies. Such a formulation can indeed be found by combining contour integration and a generalization of a reduction formula for N-point loops of free fermions. As a result we obtain two simple rules which allow us to classify which self-energy and vertex corrections are singular within the field theoretic RG which was presented in Sec. 2.2.4.

3.1 N-point loop in the 321-limit

Throughout the calculation we will use a labeling scheme of external momenta which automatically incorporates momentum conservation: Each external leg carries the momentum $q_i = p_{i+1} - p_i$ with $q_N = p_1 - p_N$, which implies $\sum_i q_i = 0$. The labeling with p_i contains one surplus momentum label which we can fix arbitrarily. We therefore impose the further constraint that each of the p_i have to be chosen such that all p_i scale the same as the q_i, ensuring that the forward scattering limit of the variables q_i is realized in the same way for p_i.

The N-point loops can then be stated as

$$\Pi_{g,N}(q_1,\ldots,q_N) = N_f \sum_{s=\pm} \int_k \prod_{i=1}^{N} g_s G_s(k-p_i) \tag{3.1}$$

Using the p_i-labels, the external momenta thus enter the loop propagators in a simple and symmetric way. In the following we suppress the index g in $\Pi_{g,N}$. When using the bare fermion Green's function, we set the coefficient a of the frequency dependence $a = 1$. We further use a notation of the N-point loop where the arguments are not $q_1,\ldots,q_N$, but $p_1,\ldots,p_N$. In general this is done with the definition

$$\Pi_N(q_1,\ldots,q_N) = N_f I_N(p_1,\ldots,p_N). \tag{3.2}$$

Within the two-patch approximation and when talking about an N-point loop on only one patch, we use the notation $I_{N,+}$ and $I_{N,-}$.

3.1.1 Reduction formula for free fermions

Assuming free fermions with a quadratic dispersion and a coupling constant $g = 1$ on the entire Fermi surface, the N-point loop can be expressed as a sum of three-point loops with rational coefficients [134, 138, 184]

$$I_N(p_1,\ldots,p_N) = \sum_{1\le i<j<k\le N} \left(\prod_{\nu\neq i,j,k} f_{\nu,ijk} \right) I_3(p_i,p_j,p_k). \tag{3.3}$$

We note that no patching is present in this formulation and no special low energy limit is assumed. The three-point loop is given by

$$I_3(p_1,p_2,p_3) = \int_k \prod_{i=1,2,3} G(k-p_i), \tag{3.4}$$

and the coefficients are

$$\begin{aligned} f^{-1}_{\nu,ijk} &= \tfrac{1}{2}(\mathbf{p}_i - \mathbf{p}_\nu) + i(p_{i0} + p_{\nu 0}) \\ &\quad + \left(\left(\tfrac{1}{2}(\mathbf{p}_k - \mathbf{p}_i) + i(p_{k0} + p_{i0})\right) \frac{\det(\mathbf{p}_j - \mathbf{p}_i, \mathbf{p}_\nu - \mathbf{p}_i)}{\det(\mathbf{p}_j - \mathbf{p}_i, \mathbf{p}_k - \mathbf{p}_i)} + j \leftrightarrow k \right). \end{aligned} \tag{3.5}$$

The determinant is defined as

$$\det(\mathbf{p_1}, \mathbf{p_2}) = \begin{vmatrix} p_{1x} & p_{2x} \\ p_{1y} & p_{2y} \end{vmatrix} \tag{3.6}$$

While the three-point loop can be cast into a form where only one contour integration along a complex path remains, the result is not particularly insightful for the present discussion and will not be further pursued here.

3.1.2 Direct integration in the 321-limit

We begin with the 3-point loop, for which explicit results in the 321-limit were derived by Thier and Metzner [137], starting from the expression Eq. 3.4 for free fermions. Their result for even coupling was

$$I_3(p_1, p_2, p_3) = \frac{1}{2\pi} \sum_{(ijk)^{\mathrm{P}}} \frac{p_{j0} - p_{i0}}{D_{ijk} + c_{ij} F_{ijk}}, \tag{3.7}$$

where $(ijk)^{\mathrm{P}}$ denotes cyclic permutations and with

$$D_{ijk} = (p_{ky} - p_{jy}) p_{ix} + cycl., \tag{3.8}$$

$$F_{ijk} = \tfrac{1}{2}(p_{jy} - p_{iy})(p_{ky} - p_{jy})(p_{iy} - p_{ky}) \tag{3.9}$$

$$c_{ij} = \begin{cases} 1 & \text{for} \quad \operatorname{sgn}(p_{j0} - p_{i0}) = \operatorname{sgn}(p_{jy} - p_{iy}) \\ -1 & \text{else.} \end{cases} \tag{3.10}$$

Remarkably, the 3-point loop is a purely rational function of momenta and real. We also point out that I_3 vanishes if $c_{12} = c_{23} = c_{31}$. With the help of the reduction formula of Eq. 3.3, one can immediately conclude that also the N-point loop is a rational function of frequency and momenta.

In the 321-limit, the external bosonic legs in a diagram have increasingly (anti-)parallel momenta with decreasing λ. For the moment we look at the case of non-collinear external momenta, then all denominators of the propagators are dissimilar. Since we use the two patch approximation, it is necessary to specify whether the fermion line in the N-point loop is from the plus or minus patch and ultimately sum over both patches. In the remainder of this section we work with the plus patch. The inverse of the bare fermion Green's function is linear in k_0 and k_x. In Sec. 2.3.1, we argued that non-analytic and singular contributions are unaffected by the order of integration. This will be used here, integrating first in k_x, then k_y and finally k_0. This way, the simple poles in k_x give way to an easy contour integration, leading

to denominators linear in k_y, which allows to repeat the procedure. Following this course, we obtain

$$\begin{aligned}
\frac{I_{3,+}}{g_+^3} &= -i\int \frac{\mathrm{d}k_0\mathrm{d}k_y}{(2\pi)^2}\sum_i \Theta(k_0-p_{i0}) \\
&\quad\times\prod_{j\neq i}(p_{jx}-p_{ix}+\tfrac{1}{2}(p_{iy}^2-p_{jy}^2)+(p_{jy}-p_{iy})k_y+i(p_{i0}-p_{j0}))^{-1} \\
&= \int\frac{\mathrm{d}k_0}{2\pi}\sum_{(ijk)^{\mathrm{P}}}\Theta(k_0-p_{i0})\Theta\left(\frac{p_{j0}-p_{i0}}{p_{jy}-p_{iy}}\right)\frac{1}{p_{jy}-p_{iy}} \\
&\quad\times\Bigg[(p_{kx}-p_{ix})+\tfrac{1}{2}(p_{iy}^2-p_{ky}^2)+i(p_{i0}-p_{k0}) \\
&\quad+\frac{p_{ky}-p_{iy}}{p_{jy}-p_{iy}}(-(p_{jx}-p_{ix})-\tfrac{1}{2}(p_{iy}^2-p_{jy}^2)-i(p_{i0}-p_{j0}))\Bigg]^{-1} \qquad (3.11) \\
&= \int\frac{\mathrm{d}k_0}{2\pi}\sum_{(ijk)^{\mathrm{P}}}\Theta(k_0-p_{i0})\Theta\left(\frac{p_{j0}-p_{i0}}{p_{jy}-p_{iy}}\right)\frac{1}{D_{ijk}+F_{ijk}+i\Omega_{ijk}} \qquad (3.12) \\
&= \int\frac{\mathrm{d}k_0}{2\pi}\sum_i\sum_{j>i}(\Theta(k_0-p_{i0})-\Theta(k_0-p_{j0})) \\
&\quad\times\Theta\left(\frac{p_{j0}-p_{i0}}{p_{jy}-p_{iy}}\right)\frac{1}{D_{ijk}+F_{ijk}+i\Omega_{ijk}} \qquad (3.13)
\end{aligned}$$

with the same D_{ijk} and F_{ijk} as beforehand and an additional frequency term

$$-\Omega_{ijk} = p_{i0}(p_{ky}-p_{jy})+cycl. \qquad (3.14)$$

The denominator is cyclic in (i,j,k), but changes sign under anticyclic permutations. The summation over elements with $j>i$ and $j<i$ is thus related by the exchange $i\leftrightarrow j$, but have opposite sign, allowing to sum only over $j>i$ in Eq. 3.13. The integration over k_0 is restricted to the interval $[p_{i0},p_{j0}]$. Performing the last integration leaves

$$\frac{2\pi I_{3,+}}{g_+^3} = \sum_{i,j>i}\Theta\left(\frac{p_{j0}-p_{i0}}{p_{jy}-p_{iy}}\right)\frac{p_{j0}-p_{i0}}{D_{ijk}+F_{ijk}+i\Omega_{ijk}} \qquad (3.15)$$

The three-point loop is thus zero if all three Heaviside-Θ are zero or one. A nonzero value is only obtained if $(p_{i0}-p_{j0})(p_{iy}-p_{jy})$ has not the same sign for all (i,j), in perfect agreement with Eq. 3.10.

To confirm that the results for I_3 are indeed completely identical for both integration routes we have to add the minus patch. Furthermore, we note that $D_{ijk} \sim F_{ijk} \sim \lambda^3$, but $\Omega_{ijk} \sim \lambda^4$, therefore the frequency dependence in the denominator is subleading. Discarding Ω_{ijk} and inserting the different possibilities for the signs of the Θ functions in the patch summed version of Eq. 3.15 and for the c_{ij} in Eq. 3.10, one can then confirm the equality. We postpone the details of the summation over patches, which are better discussed in conjunction with the symmetrization of N-point loops in Sec. 3.1.3.

The original derivation of I_3 in the 321-limit from the expression for free fermions is quite long[1] and the result does not reveal the signs of the imaginary parts, something which would become important for subsequent integrations. On the other hand, the use of two contour integrations within the two-patch approximations is very transparent, so that we can easily keep track of the imaginary parts. Repeating the above steps for more than three bosonic legs, a not symmetrized N-point loop on the plus patch can be stated immediately as

$$\frac{2\pi I_{N,+}}{g_+^N} = \sum_{i,j>i} \Theta\left(\frac{p_{j0}-p_{i0}}{p_{jy}-p_{iy}}\right)(p_{j0}-p_{i0})(p_{jy}-p_{iy})^{N-3} \times \prod_{k\neq i,j}\left(\frac{1}{D_{ijk}+F_{ijk}+i\Omega_{ijk}}\right). \tag{3.16}$$

We point out that one now obtains a product of several denominators. Also, for the three-point loop it was possible to write the summation as a cyclic sum (Eq. 3.7), which is not true for $N > 3$. The combination of Θ functions can be rewritten in a more transparent way. It is generally $\Theta(xy) = \Theta(x)\Theta(y) + \Theta(-x)\Theta(-y)$. Using the shorthand $(\![x]\!)$ for the ramp function to indicate that the value is x for $x > 0$ and zero otherwise, we can write

$$\Theta\left(\frac{p_{j0}-p_{i0}}{p_{jy}-p_{iy}}\right)(p_{j0}-p_{i0})(p_{jy}-p_{iy})^{N-3} = (\![p_{j0}-p_{i0}]\!)(\![p_{jy}-p_{iy}]\!)^{N-3} + (-1)^N(\![p_{i0}-p_{j0}]\!)(\![p_{iy}-p_{jy}]\!)^{N-3}. \tag{3.17}$$

Geometrically, in the plane spanned by p_{jy} and p_{j0}, one summand in Eq. 3.16 is nonzero only in the first and third quadrant of a coordinate system with shifted

[1] For a complete presentation we refer to Stefan Thier's diploma thesis [132]

origin at (p_{iy}, p_{i0}). We further condense the notation, introducing

$$\theta_{ij}^N = \Theta\left(\frac{p_{j0}-p_{i0}}{p_{jy}-p_{iy}}\right)(p_{j0}-p_{i0})(p_{jy}-p_{iy})^{N-3} \tag{3.18}$$

$$J_{ijk}^{++} = \frac{1}{D_{ijk}+F_{ijk}+i\Omega_{ijk}}, \tag{3.19}$$

which leads to

$$I_{N,+} = \frac{g_+^N}{2\pi}\sum_{i,j>i}\theta_{ij}^N\prod_{k\neq i,j}J_{ijk}^{++} \tag{3.20}$$

The derivation of Eq. 3.20 assumed distinct p_i. As already noted in [132], configurations where this is not fulfilled are a set of measure zero at a given scale λ. Equal propagators thus only pose a problem for explicit calculations as Eq. 3.20 is ill-defined when directly inserting the p_i. Although a contour integration of the N-point-loops with two or even more equal p_i can be done, this is particularly cumbersome. As a workaround it is possible to offset the momentum in one propagator. Then, upon using Eq. 3.20 one must take the zero limit in this offset momentum.

The most frequent case where two equal propagators occur is a fermion loop where two adjacent external legs have the same momentum entering and exiting. For example, upon joining two adjacent legs in the N-point loop one forms a one-loop self-energy correction to one fermion propagator in the $N-2$-point loop. Fortunately, the expansion around the RPA result already removes these kinds of diagrams, like it was explained in Sec. 2.2.3. In this work, the only cases where the complication with two equal propagators occurs are therefore corrections to the boson self-energy, where the external momentum enters and leaves at adjacent legs (Sec. 3.4.1).

The contour integration in k_x and k_y respectively which was employed to compute the N-point loop can also be used for loops consisting of RPA-renormalized propagators containing the NFL term from $\Sigma^{(1)}$. Instead of Eq. 3.13 we obtain for the N-point loop

$$\begin{aligned}\widetilde{I}_{N,+} = g_+^N\int\frac{\mathrm{d}k_0}{2\pi}\sum_{i,j>i}&\left(\Theta(\{k_0-p_{i0}\})-\Theta(\{k_0-p_{j0}\})\right)\\ &\times\Theta\left(\frac{\{k_0-p_{j0}\}-\{k_0-p_{i0}\}}{p_{iy}-p_{jy}}\right)(p_{jy}-p_{iy})^{N-3}\\ &\times\prod_{k\neq i,j}\frac{1}{D_{ijk}+F_{ijk}+i\widetilde{\Omega}_{ijk}(k_0)},\end{aligned} \tag{3.21}$$

with the new

$$\widetilde{\Omega}_{ijk}(k_0) = \kappa\{k_0 - p_{i0}\}(p_{ky} - p_{jy}) + cycl. \tag{3.22}$$

Unlike beforehand, the dependence on k_0 in the denominator does not cancel, which made the integration so simple for bare propagators. The dependence on k_0 inside the Θ functions still cancels, since it holds that

$$\{k_0 - p_{j0}\} - \{k_0 - p_{i0}\} > 0 \quad \Leftrightarrow \quad p_{i0} - p_{j0} > 0. \tag{3.23}$$

Using $\widetilde{J}^{++}_{ijk}(k_0) = (D_{ijk} + F_{ijk} + i\widetilde{\Omega}_{ijk}(k_0))^{-1}$, it is thus

$$\widetilde{I}_{N,+} = g_+^N \sum_{i,j>i} \int_{p_{i0}}^{p_{j0}} \frac{\mathrm{d}k_0}{2\pi} \Theta\left(\frac{p_{j0} - p_{i0}}{p_{jy} - p_{iy}}\right) (p_{jy} - p_{iy})^{N-3} \prod_{k\neq i,j} \widetilde{J}^{++}_{ijk}(k_0). \tag{3.24}$$

3.1.3 Symmetries and power counting

The discussion about symmetries is done for the bare expressions for clarity, all conclusions hold for the renormalized variants as well. The effective interactions in the bosonized action are symmetric under any permutation P of the external legs. The symmetrized N-point loops Π_N^S are defined by

$$\Pi_N^S(q_1, \ldots, q_N) = \sum_P \Pi_N(q_{P1}, \ldots, q_{PN}), \tag{3.25}$$

where the summation runs over all permutations of the external legs $(q_1, \ldots, q_N)$, but excluding cycles.

Within the two-patch scheme, we must also sum over both patches. The corresponding N-point loops where the fermions in the loop originate from either of the two patches are dissimilar as the curvature of the Fermi surface is nonzero around $\mathbf{k}_F$ and $-\mathbf{k}_F$. Together, the symmetrized vertex contains $2(N-1)!$ N-point loops which are related by one or several permutations of external legs and/or a switch to the opposite Fermi surface patch. The permutation $(q_1, \ldots, q_N) \to (q_N, \ldots, q_1)$ can alternatively be seen as the inversion of the loop direction. We want to separate this permutation from the other for its importance. The three operations are achieved with combinations of the following prescriptions:

$$I_N(p_1, \ldots, p_N) \to I_N(-p_1, \ldots, -p_N) \quad \text{Inversion} \tag{3.26}$$

$$I_N(p_1, p_2, \ldots, p_\alpha, p_{\alpha+1}, \ldots, p_N) \to I_N(p_1, p_3 - q_1, \ldots, p_{\alpha+1} - q_1, p_{\alpha+1}, \ldots, p_N) \quad \text{Permutation} \tag{3.27}$$

$$(p_{ix}, p_{iy}, p_{i0}) \to (-p_{ix}, p_{iy}, p_{i0}) \quad \text{Refl. } \mathbf{k}_F \to -\mathbf{k}_F \tag{3.28}$$

The permutation shifts one external leg q_1 up to q_α, with each momentum in between declining one position, e.g. taking q_1 and q_5, the order 123456789 turns into 234516789. The use of this permutation as essential building block for all permutations is taken from [134]. The switch to the other Fermi surface patch reverses the direction of the Fermi velocity and the curvature in a local coordinate system, so that all momenta (but no frequencies) have to be reversed. Since k_y enters quadratically in the dispersion, only the sign change of k_x is relevant, leading to the replacement rule $(k_x, k_y, k_0) \to (-k_x, k_y, k_0)$.

How a symmetrization operation affects the N-point loop can most easily seen in Eq. 3.20. Under inversion θ_{ij}^N receives a sign $(-1)^N$, likewise

$$\frac{1}{D_{ijk} + F_{ijk} + i\Omega_{ijk}} \overset{Inv.}{\to} \frac{1}{D_{ijk} - F_{ijk} + i\Omega_{ijk}} \tag{3.29}$$

$$J_{ijk}^{++} \overset{Inv.}{\to} J_{ijk}^{-+}, \tag{3.30}$$

because D_{ijk} and Ω_{ijk} contain even products of p_i, while F_{ijk} is odd. Thus

$$I_{N,+} \overset{Inv.}{\to} (-1)^N \frac{g_+^N}{2\pi} \sum_{i,j>i} \theta_{ij}^N \prod_{k\neq i,j} J_{ijk}^{-+}. \tag{3.31}$$

Switching to the other Fermi surface patch will not affect θ_{ij}^N since it contains no p_{ix}, but it will lead to an minus sign in front of D_{ijk} and replace g_+ by g_-. Therefore, the switch will result in

$$J_{ijk}^{++} \overset{Ref.}{\to} -J_{ijk}^{--}, \tag{3.32}$$

which completes the set of simple symmetrization operations

$$I_{N,+} = \frac{g_+^N}{2\pi} \sum_{i,j>i} \theta_{ij}^N \prod_{k\neq i,j} J_{ijk}^{++} \qquad \text{+ patch} \tag{3.33}$$

$$I_{N,+}^{\text{Inv}} = \frac{(-g_+)^N}{2\pi} \sum_{i,j>i} \theta_{ij}^N \prod_{k\neq i,j} J_{ijk}^{-+} \qquad \text{+ patch, Inv.} \tag{3.34}$$

$$I_{N,-} = \frac{(-g_-)^N}{2\pi} \sum_{i,j>i} \theta_{ij}^N \prod_{k\neq i,j} J_{ijk}^{--} \qquad \text{- patch} \tag{3.35}$$

$$I_{N,-}^{\text{Inv}} = \frac{g_-^N}{2\pi} \sum_{i,j>i} \theta_{ij}^N \prod_{k\neq i,j} J_{ijk}^{+-} \qquad \text{- patch, Inv.} \tag{3.36}$$

We can immediately refer from this list that the combination of $I_{N,+}$ and $I^{\text{Inv}}_{N,-}$ will result in a purely real quantity for even coupling and if N is even also for odd coupling. Effective bosonic vertices with an odd number of external legs are purely imaginary for odd coupling. The same holds for the combination of $I_{N,-}$ and $I^{\text{Inv}}_{N,+}$, and thus also for the fully symmetrized N-point loop. We reiterate that the use of a linearized dispersion makes it necessary to consider both Fermi surface patches "by hand" since the linearized dispersion does not fulfill $\varepsilon(\mathbf{k}) = \varepsilon(-\mathbf{k})$. It is therefore recommended to consider at least a combination of $I_{N,+}$ and $I^{\text{Inv}}_{N,-}$ or equivalent combinations together. I^S_3 is special as the four simple operations of inversion and patch summation fully symmetrize the vertex, yielding

$$I^S_3 = \frac{g_+^3}{2\pi}\left(\sum_{i,j>i}\theta^3_{ij}\right)\left(J^{++}_{123} - J^{-+}_{123} + \ell(J^{+-}_{123} - J^{--}_{123})\right) \tag{3.37}$$

where ℓ is $+1(-1)$ for even (odd) coupling.

Generic permutations cannot be stated in a simple and elegant manner without referencing explicitly to each single momentum which enters the loop. Fortunately a very general result about possible cancellations in the symmetrized N-point loops containing free fermions was obtained already in the work of Neumayr and Metzner [134], which concerns the factors $f_{\nu,ijk}$ in the reduction formula of the N-point loop. As shown in Sec. 3.1.2 a free electron dispersion results in the very same low energy approximation as a generic dispersion. We will therefore apply the factorization theorem which they derived, but here within the 321-limit. We consider only the case of bare propagators.

The reduction formula Eq. 3.3 contains a number of rational factors $f_{\nu,ijk} \sim \lambda^{-2}$ and the three-point loop $I_3(p_i, p_j, p_k) \sim \lambda^0$. A full symmetrization of the N-point loop affects both f and I_3. The factorization is achieved with regards to the product of $f_{\nu,ijk}$ where i, j, k are fixed. Upon summing over a certain subset of permutations $\tilde{P}$ of the external momenta, the scaling can be improved. Defining $\mathbf{p}^\perp = (-p_y, p_x)$ and introducing functions h_ρ ($\widetilde{\ }$ denotes momenta subject to permutation)

$$\begin{aligned} h_\rho = (\mathbf{p}_j + \widetilde{\mathbf{q}}_\rho - \mathbf{p}_i)\left(\frac{\frac{1}{2}(\mathbf{p}_k^2 - \mathbf{p}_i^2) + i(p_{k0} - p_{i0})}{\det(\mathbf{p}_j - \mathbf{p}_i, \mathbf{p}_k - \mathbf{p}_i)}(\mathbf{p}_j - \mathbf{p}_i)^\perp + j \leftrightarrow k\right) \\ + \tfrac{1}{2}(\mathbf{p}_i^2 - (\mathbf{p}_j + \widetilde{\mathbf{q}}_\rho)^2) + i(p_{i0} - (p_{j0} + \widetilde{q}_{\rho 0})), \end{aligned} \tag{3.38}$$

it is possible to recast the sum over permutations of products of $f_{\nu,ijk}$ with i, j, k fixed into a product like

$$\sum_{\tilde{P}}\prod_{\nu=1}^{M} f_{\nu,\tilde{P}} = \prod_{\nu=1}^{M}\frac{\widetilde{\mathbf{q}}'_\nu \widetilde{\mathbf{q}}''_\nu}{h'_\nu h''_\nu}. \tag{3.39}$$

The transformation to the right hand side works according to an involved algorithm. The result contains different combinations of external momenta $\widetilde{\mathbf{q}}'$, $\widetilde{\mathbf{q}}''$ and different h' and h'' in each factor. The new h' and h'' are derived from the simpler h_ρ and carry the same scaling. As an example, in the dynamical limit momenta scale like $\mathbf{q} \to \lambda' \mathbf{q}$ where the scale $\lambda' \to 0$, while frequencies are kept fixed. In this case, the scaling estimate for the left hand side is seemingly λ'^0, while the right hand side is of order λ'^{2M}. On the other hand, under 321-scaling $h_\rho \sim \lambda^2$, so that we obtain a scaling with λ^{-2M} both before and after symmetrizing.

The factorization theorem therefore does not reveal any cancellations in the sum over all permutations when using 321-scaling, as opposed to the other limits. This is in accord with the finding of Thier [132], who noted the absence of cancellations upon symmetrization for I_3 and, numerically, also for $N > 3$.

We now turn to the scaling analysis of N-point loops. As already mentioned, straightforward power counting can only be applied if the propagators are homogeneous functions of the scale (Sec. 2.2.2). The following estimates are therefore only valid for the one loop fixed point and for a finite value of fermion flavors N_f. Power counting of diagrams with bare fermionic propagators is complicated by the nonhomogeneity of G_0 in the 321-limit, the same holds for a large-N_f expansion (2.2.5). In a diagram, a propagator contributes a λ^{-2}, and a loop integral $\lambda^{1+2+3} = \lambda^6$. An arbitrary diagram containing n loops, p internal propagators, v vertices and e external legs both bosonic or fermionic obeys the relations [115, 185]

$$n + v = p + 1 \tag{3.40}$$

$$3v - 2p = e \tag{3.41}$$

If the integrand is homogeneous upon scaling and all integrals are individually finite, the diagram will therefore scale in the 321-limit with the exponent

$$6n - 2p = 6 - 2e. \tag{3.42}$$

The N-point loop thus scales as λ^{6-2N}. At this point it is worthwhile to briefly reflect on the meaning of such exponents. In Sec. 2.1.1 we discussed how the scaling λ^{6-2N} of the N-point loops leads to the conclusion that the effective interactions in the bosonized theory scale exactly like the kinetic energy. The effective interactions are therefore not irrelevant in the forward scattering limit, neither do they diverge, but they are marginal. We stress that this analysis concerns the *action*. Now we are instead interested in the scaling dimension of single diagrams. If a diagram has a negative power in λ, the diagram diverges upon approaching the forward scattering limit, it is thus singular in the infrared (IR). At the same time the negative power tells us that the loop integrals will converge in the ultraviolet (UV). The same is

true vice versa and for a scaling like λ^0, the diagram can produce logarithms.[2] The important point is now that the scaling in the IR is exactly what we want to capture with the RG treatment in the first place. If a diagram has IR divergences, which are nothing else than poles for certain momenta and frequencies, these divergences do not carry any new information about the system, but they rather have the exact same scaling imprinted with which we constructed the effective action. A UV divergence on the other hand carries information about the influence of high energy modes onto the dynamics of the model in the IR. When searching for singular contributions which renormalize the model and produce anomalous dimensions, we are therefore interested solely in UV divergent diagrams. One example of such a diagram which renormalizes the scaling was already discussed in Sec. 2.2.5 with the logarithmically divergent three-loop correction to the fermion self-energy. For the renormalized perturbation theory we know that by construction only two-point ($e = 2$) and three-point ($e = 3$) diagrams can potentially diverge in the UV, with a power of 2 and 0 (logarithmically) respectively (Sec. 2.2.4). This is reproduced in Eq. 3.42. The SCM contains a marginal interaction in the 321-limit, this means that all corrections to the tree level result, i.e., in our case all corrections to the one loop fixed point, should be at most logarithmic. If this is the case, the power counting estimate must be no larger than 0 for all diagrams, meaning that bosonic self-energy corrections are overestimated. This kind of disparity between the simple power counting and the true degree of divergence appears frequently in field theories and can be resolved by exploiting symmetries in the corresponding correlation functions [185]. In the present case the resolution is less obvious since the expansion is done around the one-loop result. In particular, one cannot assume a priori that the correspondence between marginality and logarithms is preserved. If it indeed holds, this is a good sign that the renormalization group can be utilized. The issue was partially addressed by Metlitski and Sachdev [114], who argued that the leading momentum dependence of the fermionic self-energy corrections should diverge at most logarithmically to match with vertex corrections in the corresponding Ward identities. If a divergence was actually stronger than logarithmic, this would break the RG ansatz and point towards processes which originate outside the two-patch region.

3.2 Improved power counting I

We prove that all bosonic self-energies are of power zero and only logarithmic correction can occur. This is an important sign that the decompactification of the Fermi surface into patches captures the essential physics at the QCP.

[2] We point out that power counting can overestimate the degree of divergence, the particle-hole bubble for example scales like λ^2 but is not singular in the UV.

3.2.1 Classification from Ward identities

The Ward identity connecting the fermion Green's function and the irreducible charge and current vertices was given in Eq. 2.95. For zero momentum transfer ($q \to 0$) and also $p_y, p_0 = 0$ this simplifies to

$$g + \partial_{p_x} \Sigma(p_x) = \Gamma_x(p_x, p_x). \tag{3.43}$$

Analyzing the Ward identity order by order in a loop expansion of the left and right hand side, one can relate two- and three-point functions on a diagrammatic level.

In full generality, Ward identities are derived on a functional level from the gauge invariance of the generating functional of connected Green's functions [186]. For our purpose it suffices to use the information that the irreducible vertex is related to the amputated connected Green's function by a *functional* derivate with respect to the order parameter field. Diagrammatically speaking, the Ward identity relates a self-energy diagram to all vertex diagrams which can be produced by attaching one boson leg in the self-energy diagram.

Using the knowledge that there is only one singular self-energy contribution up to three loops, the Ward identity for *all* singular diagrams reads up to three loops

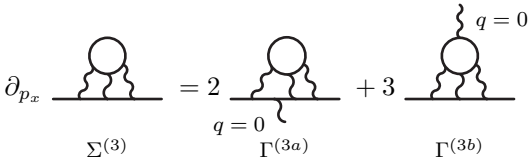

(3.44)

where the closed fermion loops in the diagrams are to be taken as fully symmetrized. The vertex has two contributions, $\Gamma^{(3a)}$, where the boson line is attached to the fermion line which connects to the in- and outgoing momentum, and $\Gamma^{(3b)}$, where the boson is attached to the closed fermion loop. On the other hand, in the momentum space formulation in Eq. 3.43, the derivative ∂_{p_x} will only act on propagators which contain the external momentum. It is now natural to chain the momentum p only through the propagators of the open fermion line, so that $\Gamma^{(3b)}$ is never generated. Other choices for the distribution of internal momenta will not change this result, as labellings which run p_x through the closed fermion loop instead of the open fermion line will never cover all propagators of the fermion loop and thus never produce all diagrams which are necessary to symmetrize the fermion loop completely. The statement that $\Gamma^{(3b)}$ is not generated is therefore not arbitrary, as a formulation which removes $\Gamma^{(3a)}$ from the equation will not generate $\Gamma^{(3b)}$, but another object which does not conform to the present classification.

This consideration thus only leaves one option, $\Gamma^{(3b)}$ must vanish for $q = 0$. In fact, since the Ward identity Eq. 3.43 is actually a relation for the limit $q \to 0$,

$\Gamma^{(3b)}$ vanishes smoothly. In view of the different choices to distribute p_x, one can furthermore conjecture that the finiteness of $\Gamma^{(3b)}$ is related to the presence of a symmetrized N-point loop with one external boson leg. This is indeed the case and will be proven in the next section.

3.2.2 One small external momentum

We consider a symmetrized N-point loop where one external leg has a vanishing momentum q_N.

The symmetrized N-point loop comprises all permutations of $N-1$ legs, since cycles are indistinguishable. We now assume that one boson line has momentum zero. In the extreme case of vanishing momentum two fermion lines in the loop become identical. The permutations over $N-1$ legs then also contain the assignments where the doubled fermion line is cycled through all indices. For example, the symmetrized 4-point loop consists of six diagrams where the ingoing momenta q_1, q_2, q_3, q_4 are permuted with respect to three of the four momenta. Without loss of generality, we can chose q_4 as vanishing and sum the three permutations which are cyclic in q_1, q_2, q_3. The sum is given by

$$\begin{aligned}\int_k & G_s(k-p_1)G_s(k-p_2)G_s(k-p_3) \\ & \times \left[G_s(k-p_1)+G_s(k-p_2)+G_s(k-p_3)\right], \end{aligned} \tag{3.45}$$

where we used that $q_4 = 0 = p_1 - p_4$. The cycle obviously allows to write the integrand as a derivative,

$$s\int_k \frac{\partial}{\partial k_x}\left[G_s(k-p_1)G_s(k-p_2)G_s(k-p_3)\right]. \tag{3.46}$$

Since the integration in k_x just leaves $G_s(k-p_1)G_s(k-p_2)G_s(k-p_3)$ evaluated at the lower and upper cutoff in k_x, which goes to infinity, the integral is zero. We conclude that the 4-point loop vanishes in leading order if one leg has a vanishing momentum. This result does not depend on the scaling. The extension to arbitrary N is straightforward, the selection of all cyclic permutations of $N-1$ legs while one leg with zero momentum is kept separate, will cancel exactly.

We can use this insight to refine the power counting estimate of diagrams where an N-point loop contains at least one external bosonic leg q_N. The Taylor expansion in q_N will be zero at zeroth order and the UV-divergence of the diagram is then

dominated by the first order term. In the forward scattering limit the first order terms and their scaling are

$$\begin{aligned}\Pi(q_1,\ldots,q_{N-1},q_N) = &\underbrace{q_{Nx}}_{\lambda^2}\underbrace{\partial_{q_{Nx}}\Pi(q_1,\ldots,q_{N-1},q_N)|_{q_N=0}}_{\lambda^{4-2N}} + \\ &\underbrace{q_{Ny}}_{\lambda}\underbrace{\partial_{q_{Ny}}\Pi(q_1,\ldots,q_{N-1},q_N)|_{q_N=0}}_{\lambda^{5-2N}} + \\ &\underbrace{q_{N0}}_{\lambda^3}\underbrace{\partial_{q_{N0}}\Pi(q_1,\ldots,q_{N-1},q_N)|_{q_N=0}}_{\lambda^{3-2N}} + \ldots \end{aligned} \tag{3.47}$$

Of course the total scaling is unaffected, but the UV convergence of the loop integrals is improved by at least one power as q_N is an external momentum and not integrated over. What happens if Π_N is non-analytic around $q_N = 0$? In this case the Taylor expansion is not defined, something which is signaled by IR divergences in the first order terms. Since the Ward identity enforces a smooth limit

$$\lim_{q_N\to 0}\Pi(q_1,\ldots,q_{N-1},q_N) = 0, \tag{3.48}$$

a divergence of the Taylor coefficients is not expected to restore the original power of divergence. We numerically checked that the Taylor coefficient of q_{Ny} is finite up to $N = 7$, with the other terms being subleading.

Using analyticity and the invariance under $q_i \to -q_i$ one can conclude that symmetrized loops vanish even quadratically, if a vanishing momentum q enters and leaves the same loop at two distinct vertices, provided that the other momenta remain finite. Due to momentum conservation this is possible only for $N \geq 4$. Hence, the UV scaling of symmetrized loops for $N-2$ large momenta and two fixed external momenta q and $-q$ is reduced by a factor Λ^{-2}.

One can now apply the power counting improvement to the two- and three-point functions. Potentially singular vertex corrections contain one or more N-point loops, thus a contribution is singular only if the external boson line is not attached to any of these. Potentially singular self-energy corrections to the boson self-energy contain at least two N-point loops and never any open fermion lines, so both external boson legs are attached to a closed fermion loop, making the maximum UV divergence logarithmic. For the fermionic self-energy the power counting estimate is not changed. As Metlitski and Sachdev [114] already established, a scaling like $\sim C_2 + C_3(p_x + p_y^2)$ is expected due to the local stability of the Fermi surface curvature. The trivial constant C_2 can be absorbed in a shift of the chemical potential, the next order terms are of order λ^2 and thus imply that the fermion self-energy is at most logarithmically divergent.

In summary, the improvement in power counting which we obtained from the Ward identities excludes any power law divergences and supports the ansatz for the renormalization group equations with two flowing couplings. The improved power counting I is also important if the critical exponents are calculated with a minimal subtraction scheme, because it reduces the number of singular diagrams and consequently also the number of counterterms necessary to cancel the former.

3.3 Improved power counting II

We prove that the presence of an N-point loop in a diagram where no more than two boson legs from the N-point loop are internal lines of the diagram leads to a nonsingular correction.

3.3.1 Cyclic formulation of N-point loops

Albeit cancellations which change the scaling of the interaction are generally absent, kinematic constraints can be found in all N-point loops. In the following we work again with the plus patch but drop the patch index and also the interaction constant g for clarity.

Recalling the reduction formula Eq. 3.3 for free fermions

$$I_N(p_1,\ldots,p_N) = \sum_{1\leq i<j<k\leq N} I_3(p_i,p_j,p_k) \prod_{\nu\neq i,j,k} f_{\nu,ijk}, \tag{3.49}$$

it seems possible to cast the N-point loops $\widetilde{I}_N$ for the RPA propagators also in this form, since each occurring frequency in the denominator can be accounted for by explicitly replacing the frequency dependence

$$\widetilde{\Omega}_{ijk}(k_0) \overset{\kappa\{..\}\leftrightarrow(..)^1}{\longleftrightarrow} \Omega_{ijk}, \tag{3.50}$$

thus shifting between bare and renormalized quantities without affecting the structure of the N-point loop. Using this replacement rule, the putative coefficients $\widetilde{f}_{\nu,ijk}$ can be guessed by first rederiving the reduction formula in the 321-limit for one patch. Writing out $f_{\nu,ijk}$ as given in Eq. 3.5 and trying a number of different possibilities, we find

$$f^{-1}_{\nu,ijk} = \frac{D_{ijk}J^{-1}_{ij\nu} - D_{ij\nu}J^{-1}_{ijk}}{D_{ijk}(p_{jy}-p_{iy})}. \tag{3.51}$$

This relation expresses $f_{\nu,ijk}$ with building blocks of I_3, which seems quite remarkable when we consider that the original reduction formula had very different expressions for $f_{\nu,ijk}$ and I_3. On the other hand, I_N is a rational function in the 321-limit, so it can be expected that the different parts in the reduction formula are algebraically related. The original reduction formula applied for free fermions and is of importance since the I_N cannot be explicitly integrated. Here the situation is better as a lot of properties of I_N are known. For example, the N-point loop contains $N-2$ factors of J_{ijk} whereas I_3 contains exactly one J_{ijk}. The reduction formula should thus follow from a decomposition rule for products of J_{ijk}. To test this, we write

$$\begin{aligned} J_{ijk}J_{ij\nu} &= J_{ijk}J_{ij\nu}\frac{D_{ijk}J_{ijk}-D_{ij\nu}J_{ij\nu}}{D_{ijk}J_{ijk}-D_{ij\nu}J_{ij\nu}} \\ &= J_{ijk}J_{ij\nu}\left(\frac{D_{ijk}J_{ijk}}{D_{ijk}J_{ijk}-D_{ij\nu}J_{ij\nu}}+\frac{D_{ij\nu}J_{ij\nu}}{D_{ij\nu}J_{ij\nu}-D_{ijk}J_{ijk}}\right) \\ &= J_{ijk}\frac{D_{ijk}}{D_{ijk}J_{ij\nu}^{-1}-D_{ij\nu}J_{ijk}^{-1}}+J_{ij\nu}\frac{D_{ij\nu}}{D_{ij\nu}J_{ijk}^{-1}-D_{ijk}J_{ij\nu}^{-1}}, \end{aligned} \tag{3.52}$$

therefore

$$(p_{jy}-p_{iy})J_{ijk}J_{ij\nu} = f_{\nu,ijk}J_{ijk}+f_{k,ij\nu}J_{ij\nu}. \tag{3.53}$$

We stress the tautological nature of this decomposition since each $f_{\nu,ijk}$ still contains J's. $f_{\nu,ijk}$ is invariant under any permutation of the indices i, j and k, which can be seen by writing out f explicitly. Along the same line, one can rearrange the product $D_{ijk}f_{\nu,ijk}^{-1}$ into determinants, which are of course completely antisymmetric under permutations,

$$D_{ijk}f_{\nu,ijk}^{-1}(k_0) = \tfrac{1}{2}\begin{vmatrix} p_{ix} & p_{jx} & p_{kx} & p_{\nu x} \\ p_{iy} & p_{jy} & p_{ky} & p_{\nu y} \\ p_{iy}^2 & p_{jy}^2 & p_{ky}^2 & p_{\nu y}^2 \\ 1 & 1 & 1 & 1 \end{vmatrix} - i\begin{vmatrix} p_{ix} & p_{jx} & p_{kx} & p_{\nu x} \\ p_{iy} & p_{jy} & p_{ky} & p_{\nu y} \\ k_{i0} & k_{j0} & k_{k0} & k_{\nu 0} \\ 1 & 1 & 1 & 1 \end{vmatrix}. \tag{3.54}$$

Since D_{ijk} is antisymmetric under permutations of (i,j,k), $f_{\nu,ijk}$ is symmetric. We can repeat the decomposition for products of three and more J_{ijk}. The result in terms of $f_{\nu,ijk}$ is nonunique and depends on the order in which pairs of J were replaced by the right hand side of Eq. 3.53. Comparing all possible ways to perform the composition, it is easy to see that there is always a route which leaves only one

instance of an particular J. For example, the product with three J can be decomposed into either

$$(p_{jy}-p_{iy})^3 J_{ijk_1}J_{ijk_2}J_{ijk_3} = f_{k_2,ijk_1}f_{k_3,ijk_1}J_{ijk_1} + f_{k_1,ijk_2}f_{k_3,ijk_2}J_{ijk_2} + (f_{k_1,ijk_2}f_{k_2,ijk_3} + f_{k_2,ijk_1}f_{k_1,ijk_3})J_{ijk_3} \quad (3.55)$$

or

$$= f_{k_2,ijk_1}f_{k_3,ijk_1}J_{ijk_1} + (f_{k_1,ijk_3}f_{k_3,ijk_2} + f_{k_3,ijk_1}f_{k_1,ijk_2})J_{ijk_2} + f_{k_1,ijk_3}f_{k_2,ijk_3}J_{ijk_3} \quad (3.56)$$

and since both must be identical, we know that equally

$$(p_{jy}-p_{iy})^3 J_{ijk_1}J_{ijk_2}J_{ijk_3} = f_{k_2,ijk_1}f_{k_3,ijk_1}J_{ijk_1} + f_{k_1,ijk_2}f_{k_3,ijk_2}J_{ijk_2} + f_{k_1,ijk_3}f_{k_2,ijk_3}J_{ijk_3}. \quad (3.57)$$

The emergent identity

$$f_{k_1,ijk_2}f_{k_2,ijk_3} + f_{k_2,ijk_1}f_{k_1,ijk_3} = f_{k_1,ijk_3}f_{k_2,ijk_3} \quad (3.58)$$

can be proven by inserting the definition of f and comparing terms. This generalizes to higher order products by induction. The decomposition of a product of J's results therefore in

$$(p_{jy}-p_{iy})^{N-3}\prod_{k\neq i,j} J_{ijk} = \sum_{k\neq i,j}\left(\prod_{\nu\neq i,j,k} f_{\nu,ijk}\right)J_{ijk}. \quad (3.59)$$

Using the properties of Θ_{ij}, J_{ijk} and $f_{\nu,ijk}$ under permutation, we can rearrange the summation in I_N,

$$\begin{aligned}
&\sum_{i,j>i}\theta_{ij}^N \prod_{k\neq i,j} J_{ijk} \\
&= \sum_{i,j>i,k\neq i,j} \theta_{ij}^3 J_{ijk}\prod_{\nu\neq i,j,k} f_{\nu,ijk} \\
&= \sum_{i,j>i,k>j}\left(\theta_{ij}^3 J_{ijk}\prod_{\nu\neq i,j,k} f_{\nu,ijk} + \theta_{ik}^3 J_{ikj}\prod_{\nu\neq i,k,j} f_{\nu,ikj} + \theta_{kj}^3 J_{kji}\prod_{\nu\neq k,j,i} f_{\nu,kji}\right) \\
&= \sum_{i,j>i,k>j}(\theta_{ij}^3+\theta_{jk}^3+\theta_{ki}^3)J_{ijk}\prod_{\nu\neq i,j,k} f_{\nu,ijk}, \qquad (3.60)
\end{aligned}$$

where three terms are obtained because a restriction of $k>j$ drops two terms, one which corresponds to an interchange of $k\leftrightarrow j$, and the other $k\leftrightarrow i$. Please note

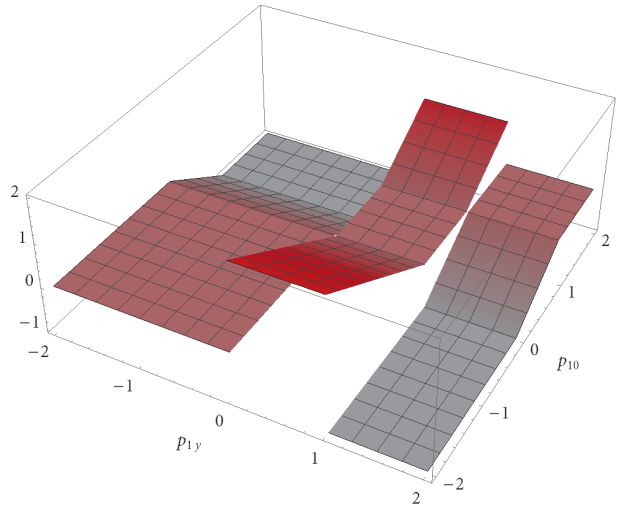

Figure 3.1 Plot of the function Eq. 3.61 with the choice of $p_1 = (p_{1x}, p_{1y}, p_{10})$, $p_2 = (p_{2x}, 0, 0)$ and $p_3 = (p_{3x}, 1, 1)$.

that $(\theta^3_{ij} + \theta^3_{jk} + \theta^3_{ki})J_{ijk}$ can be trivially converted into I_3. Equation 3.60 proves that the reduction formula Eq. 3.49 for I_N is in the 321-limit a purely algebraic rearrangement.

We briefly comment on the significance of the reduction formula for our purposes. In the 321-limit, $I_3(p_i, p_j, p_k)$ is proportional to the peculiar combination of Θ functions

$$\theta^3_{ij} + \theta^3_{jk} + \theta^3_{ki}, \tag{3.61}$$

which is generically of order p_{i0}, but is zero if $\operatorname{sgn}(p_{j0} - p_{i0}) = \operatorname{sgn}(p_{jy} - p_{iy})$ or $\operatorname{sgn}(p_{j0} - p_{i0}) = -\operatorname{sgn}(p_{jy} - p_{iy})$ for all three combinations (i, j), (j, k) and (k, i). Additionally, whenever both $p_{iy} > \max(p_{jy}, p_{ky})$ and $p_{i0} > \max(p_{j0}, p_{k0})$ or $p_{iy} < \min(p_{jy}, p_{ky})$ and $p_{i0} < \min(p_{j0}, p_{k0})$, the proportionality to p_{i0} cancels in Eq. 3.61. This is visualized in Fig. 3.1, where Eq. 3.61 is plotted in the plane spanned by one (p_y, p_0).

As a consequence of the reduction formula, I_N inherits these kinematic constraints from I_3, at least for each momentum triple (i, j, k). The kinematic constraint acts globally once it applies for all possible momentum triples. For example, once a momentum-frequency pair (p_{iy}, p_{i0}) fulfills the condition

$$p_{iy} > \max(\dots, p_{ky}, \dots)_{k \neq i} \wedge p_{i0} > \max(\dots, p_{k0}, \dots)_{k \neq i}, \tag{3.62}$$

the UV convergence is improved. The conditions for the other three limits follow analogously. To summarize, diagrams involving N-point loops have some kinematic constraint for $p_y, p_0 \to \pm\infty$ even for two-patch diagrams. Up to now the precise effect of the constraint on power counting cannot be evaluated, especially since the derivation only applies for free fermions.

The generalization to a NFL is straightforward. Equation 3.53 implies Eq. 3.49 but does not make use of the detailed nature of J_{ijk}, therefore one can immediately state the identity

$$(p_{jy} - p_{iy})\widetilde{J}_{ijk}(k_0)\widetilde{J}_{ij\nu}(k_0) = \widetilde{f}_{\nu,ijk}(k_0)\widetilde{J}_{ijk}(k_0) + \widetilde{f}_{k,ij\nu}(k_0)\widetilde{J}_{ij\nu}(k_0), \quad (3.63)$$

with the definition

$$\widetilde{f}^{-1}_{\nu,ijk}(k_0) = \frac{D_{ijk}\widetilde{J}^{-1}_{ij\nu}(k_0) - D_{ij\nu}\widetilde{J}^{-1}_{ijk}(k_0)}{D_{ijk}(p_{jy} - p_{iy})}. \quad (3.64)$$

where $\widetilde{\Omega}$ and therefore also $\widetilde{J}$ and $\widetilde{f}$ carry a k_0 dependence. After repeating the same steps as beforehand, a close equivalent of the reduction formula is obtained

$$\begin{aligned} I_N = \sum_{i<j<k} \Bigg[& \int_{p_{i0}}^{p_{j0}} \frac{\mathrm{d}k_0}{2\pi} \Theta\left(\frac{p_{j0} - p_{i0}}{p_{jy} - p_{iy}}\right) \left(\prod_{\nu\neq i,j,k} f_{\nu,ijk}(k_0)\right) \widetilde{J}_{ijk}(k_0) \\ & + \int_{p_{j0}}^{p_{k0}} \frac{\mathrm{d}k_0}{2\pi} \Theta\left(\frac{p_{k0} - p_{j0}}{p_{ky} - p_{jy}}\right) \left(\prod_{\nu\neq i,j,k} f_{\nu,ijk}(k_0)\right) \widetilde{J}_{ijk}(k_0) \\ & + \int_{p_{k0}}^{p_{i0}} \frac{\mathrm{d}k_0}{2\pi} \Theta\left(\frac{p_{i0} - p_{k0}}{p_{iy} - p_{ky}}\right) \left(\prod_{\nu\neq i,j,k} f_{\nu,ijk}(k_0)\right) \widetilde{J}_{ijk}(k_0) \Bigg]. \end{aligned} \quad (3.65)$$

Once again, if all three Θ functions have the same sign, the integrations cancel completely, in any case where the i-th momentum (in fact p_{iy} and p_{i0}) is large, the first and last Θ function will have same signs and the p_{i0} integration boundary drops out, only leaving the j, k frequencies. This is the same behavior like the one we demonstrated with free fermions, although a reduction into a sum of I_3 is no longer possible.

3.3.2 One large momentum variable

In Sec. 2.3.2 it was elaborated how the external frequency acts as a small cutoff on loop frequencies in one-patch diagrams, reducing the leading power by three and

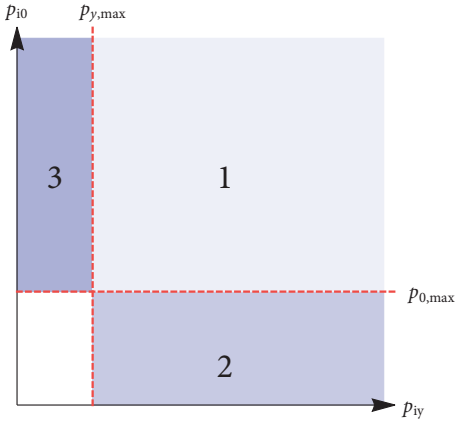

Figure 3.2 Integration regions in the first quadrant of the plane spanned by a y-momentum p_{iy} and the corresponding frequency p_{i0}. $p_{y,max}$ and $p_{0,max}$ are the maximal values of the other momenta and frequencies with index $k \neq i$ (cf. Eq. 3.62). In the remaining quadrants, corresponding regions can be identified.

rendering all diagrams finite. The generalized reduction formula Eq. 3.65 shows that two patch diagrams which contain an N-point loop still exhibit kinematic constraints in the form of cyclic sums, which are however considerably weaker.

First, we investigate constellations where all possible momentum triples (p_i, p_j, p_k) lead to the kind of behavior which we discussed in connection with Eq. 3.61. The condition for this to be true was already formulated in Eq. 3.62: Both the y-momentum and the frequency of the same ingoing variable p_i must be larger or more negative than all the other respective loop variables. The situation in the (p_{iy}, p_{i0})-plane was illustrated in Fig. 3.1, for the moment we take both $p_{iy} > 0$ and $p_{i0} > 0$ and name the regions as shown in Fig. 3.2. The other cases can be treated analogously. We consider the case that all other momenta (p_{ky}, p_{k0}) (where $k \neq i$) are fixed by an IR scale. Region 1, where p_{iy} and p_{i0} are larger than all other p_{ky} and p_{k0} is subject to a reduction of the original power counting by a power of three due to the cancellation of one power of p_{i0} in the cyclic sum (Eq. 3.65). Region 2 is constrained by the condition that $p_{i0} < \max(\dots, p_{k0}, \dots)_{k \neq i}$, with an analogous condition for region 3. In the 321-limit a small momentum cutoff in p_y reduces the original power counting estimate by one power, a cutoff in p_0 by a power of three. Thus, if the other loop variables were constrained by a small momentum instead of the usual UV cutoff, the additional reduction of power counting due to the appearance of the different integration regions 1-3 is at least of power one.

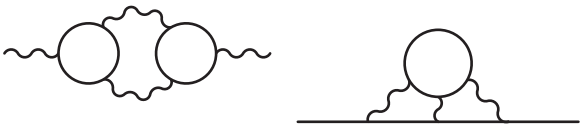

Figure 3.3 Two-patch diagrams for the self-energies at three loops, drawn with symmetrized N-point loops (cf. Fig. 2.8 in Sec. 2.2.5). The left diagram (Aslamazov-Larkin diagram) leads to a finite correction of the propagator of order parameter fluctuations, the right diagram yields a logarithmic correction for the electron propagator.

This result readily explains the odd behavior of the three-loop self-energies (Fig. 3.3). The diagrams in consideration contain only three-point loops, for which the mechanism is very transparent: The three-point loop has two independent momenta, therefore it suffices to have one external momentum running through the loop to limit the regions in Fig. 3.2 by an IR scale. The described behavior can be observed in the Aslamazov-Larkin diagram, where the unsymmetrized terms diverge exactly linearly. Upon symmetrization, an additional reduction by Λ^2 is provided by the improved power counting I, which was discussed in the previous section. The combined three-loop contibution to the boson self-energy is therefore finite. In contrast to the Aslamazov-Larkin diagram, the three loop correction to the fermion self-energy contains a three-point loop where both independent momenta running through the loop are unrestricted (Fig. 3.3). Then no IR scale is present in the momenta and the kinematic constraint does not impact the power counting estimate, because the limits of regions 2 and 3 can be extended indefinitely. This explains why no cancellation is present for the fermion self-energy at three loops, as two independent bosonic loop momenta (and no external momentum) run through the three-point loop. In previous works, the differences between fermions and bosons were taken as an indication of a more general cancellation mechanism which might render corrections to the boson self-energy finite, while not affecting fermionic ones [114]. This is not the case, the difference between both diagrams is in regards to the connectivity of closed fermion loops and not in regards to the type of self-energy.

We now analyze the asymptotic behavior of an N-point loop traversed by a single large momentum. More precisely, we assume that two of the external momenta, say q' and $q'' \approx -q'$ are large and almost antiparallel, while all the other momenta are kept finite, that is, relatively small. This implies that the momenta p_i fall in two groups, where momenta within a group are close together, while the distance between momenta in different groups is large (see Fig. 3.4). Choosing $p_1 = 0$, the momenta in the group containing p_1 are all close to zero, that is, relatively small.

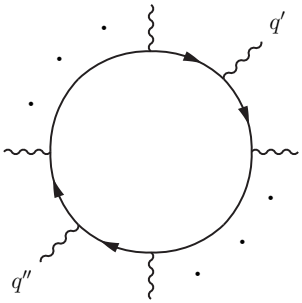

Figure 3.4 N-point loop with two large momenta q' and $q'' \approx -q'$. Momenta p_i on the bold lines are large, those on thin lines (relatively) small.

Using the generalized reduction formula (Eq. 3.65), we can show that the frequency integrations are effectively restricted to small intervals, although the differences $p_{i0} - p_{j0}$ may be large. To this end, let us fix some i, j, k and write out the cyclic sum:

$$\int_{p_{i0}}^{p_{j0}} \frac{dk_0}{2\pi} \Theta\Big(\frac{p_{j0} - p_{i0}}{p_{jy} - p_{iy}}\Big) g(k_0) + \int_{p_{j0}}^{p_{k0}} \frac{dk_0}{2\pi} \Theta\Big(\frac{p_{k0} - p_{j0}}{p_{ky} - p_{jy}}\Big) g(k_0) + \int_{p_{k0}}^{p_{i0}} \frac{dk_0}{2\pi} \Theta\Big(\frac{p_{i0} - p_{k0}}{p_{iy} - p_{ky}}\Big) g(k_0)\,, \tag{3.66}$$

where $g(k_0) = \Big[\prod_{\nu \neq i,j,k} f_{\nu,ijk}(k_0)\Big] \widetilde{J}_{ijk}(k_0)$. Note that the latter function is invariant under cyclic permutations of i, j, k.

If p_i, p_j, p_k are in the same group of small or large momenta, all frequency integrations in Eq. 3.66 are obviously limited to small intervals. Now assume that they are in two distinct groups, say p_i is large and the others are small. The argument of the first and third step function in Eq. 3.66 is then dominated by p_i, leaving $\Theta(p_{i0}/p_{iy})$ in both cases, and the whole expression can be simplified to

$$\int_{p_{k0}}^{p_{j0}} \frac{dk_0}{2\pi} \Theta\Big(\frac{p_{i0}}{p_{iy}}\Big) g(k_0) + \int_{p_{j0}}^{p_{k0}} \frac{dk_0}{2\pi} \Theta\Big(\frac{p_{k0} - p_{j0}}{p_{ky} - p_{jy}}\Big) g(k_0)\,. \tag{3.67}$$

The frequency integration is thus effectively restricted to the small interval between p_{j0} and p_{k0}. The large contributions from integrations from p_{i0} to p_{j0} and from p_{k0} to p_{i0} cancel in the cyclic sum.

In naïve power-counting for the N-point loop, the frequency integration yields a factor Λ^3. In the specific limit discussed above, the ultraviolet asymptotics is thus reduced by that factor. For the above argument it was important that both q_0' and q_y' are large. The x-component did not matter. If only q_0' is assumed to be large, the k_0-integration does extend over a large interval, yielding a factor Λ^3, but only as long as q_y' is of the order of the other y-components. One thus obtains an effective restriction of q_y' as discussed already for the 3-point loop beforehand.

3.4 Classification of singularities

In the previous sections two power counting improvements for symmetrized N-point loops were derived. The first states that an N-point loop which has one or two external legs will have its UV scaling improved by a power of one or two respectively. The second states that an N-point loop has its UV scaling improved by a power of one if no more than two legs are part of another loop in the diagram.

For the moment, diagrams are always assumed to be grouped into classes which are fully symmetrized with respect to all N-point loops. Applying the rules to two- and three-point diagrams then yields the following power counting rules:

Rule 1 Corrections to the boson self-energy are singular if the diagram contains at least two N-point loops from either patch, all with at least three internal legs.

Rule 2 Fermion self-energy corrections are singular if the diagram contains at least one N-point loop with at least three internal legs which is from the opposite patch compared to the open fermion line.

Rule 3 Corrections to the irreducible fermion-boson vertex are singular if they contain at least one N-point loop from the opposite patch compared to the open fermion line, with at least three internal legs, and if the external boson leg is not connected to the N-point loop.

These rules are actually easy to fulfill, except for the lowest orders, where it is impossible to construct enough internal boson legs. The absence of corrections beyond one loop is thus not the result of a hidden symmetry or a general mechanism, but rather accidental. Singular corrections first turn up at three loops for the fermion self-energy and the vertex and at four loop for the boson self-energy.

3.4.1 Singular diagrams at four loops

With the new improvements in power counting, it is possible to classify corrections based on the connectivity of closed fermion loops. We neither include diagrams containing only one fermion line because they are finite, nor do we include diagrams containing self-energy insertions, which are already accounted for in the expansion

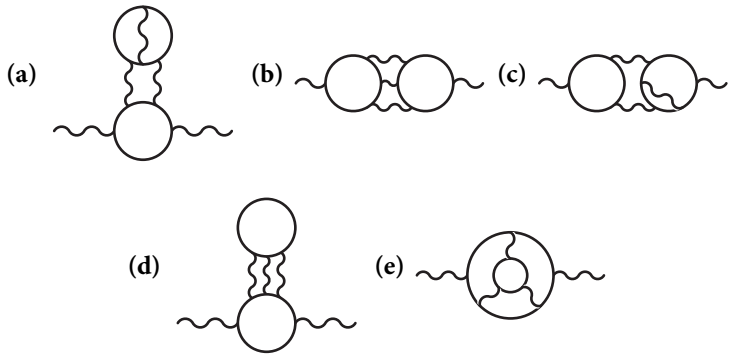

Figure 3.5 Contributions to the boson self-energy at four loops where fermions from both patches appear. Each diagram represents a whole class of diagrams, the remaining ones can be obtained by permuting the attachment points of the boson lines to the N-point loops. Diagrams (d) and (e) belong to the same class once the five-point loop is symmetrized.

around the one-loop result. Furthermore, whenever a closed fermion loop occurs, it is implied that the loop is symmetrized with respect to the external legs. Subtleties of this symmetrization will be considered in the next section.

At four loop, this leads to four classes of diagrams for the bosonic self-energy (Fig. 3.5). For clarity, we draw one of the classes in two different ways, creating diagrams (d) and (e). Diagrams (a-b) contain an even number of vertices on both fermion loops, and since each loop originates from another patch, they carry a factor $g_+^4 g_-^4 = g_+^8$. (c-e) likewise contain an odd number of vertices, which leads to a factor of $g_+^5 g_-^3 = g_+^8$ for even interaction and $g_+^5 g_-^3 = -g_+^8$ for odd interaction. (a-b) and (c-e) therefore belong to different groups with respect to the interaction, a distinction which does not appear at three loops as there is only one class diagrams for the boson self-energy corrections which contains fermions from both patches, the Aslamazov-Larkin diagram. Diagram (a) is zero since it contains a vanishing subdiagram [114], diagram (c) fulfills the condition for improved power counting II as it contains a three-point loop with exactly two internal legs, making it finite. Diagrams (b), (d) and (e) are singular. We point out that (d) contains diagrams with two adjacent external legs, for which the explicit expressions for the N-point loops cannot be applied directly (cf. Sec. 3.1.2).

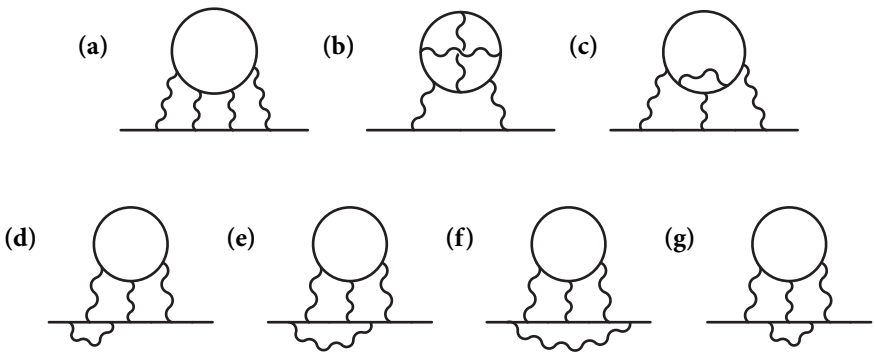

Figure 3.6 Contributions to the fermion self-energy at four loops where fermions from both patches appear. Each diagram represents a whole class of diagrams, the remaining ones can be obtained by permuting the attachment points of the boson lines to the N-point loops.

The four-loop corrections to the fermion self-energy are shown in Fig. 3.6. Diagrams (a) and (b) are even with respect to vertices from both patches so that they share the same sign for even and odd interaction. For diagrams (c-g) the numbers of vertices from each patch is odd, resulting in the factor $g_+^3 g_-^5 = g_+^5 g_-^3 = \pm g_+^8$. All diagrams are singular according to the power counting rules.

3.4.2 Contractions of the N-point loop

The preceding considerations regarding symmetrized N-point loops always assumed a full symmetrization over all external legs. This leads to a contradiction once contractions between two legs attached to the N-point loop appear, since all permutations also include cases where the legs are adjacent, so that a one-loop self-energy (Fock diagram) is produced. Such insertions are disallowed because they lead to double counting. To ensure the consistency of the NFL starting point, it is therefore necessary to exclude such contractions.

A self-energy insertion can be integrated exactly (cf. Sec. 2.2.1), with the result $\Sigma^{(1)}(p) = -i\kappa\{p_0\}$. In an N-point loop, this insertion is possible for each internal fermion line, leading to

$$I_{N,\Sigma}(p_1,\ldots,p_N) = \int_k \prod_{i=1}^{N} G(k-p_i) \sum_{j=1}^{N} G(k-p_j)(-i\kappa\{p_{j0}\}). \tag{3.68}$$

Since the same form $\Sigma^{(1)}$ appears in the numerator and in the denominator of the fermion propagators, $I_{N,\Sigma}$ can be written as a derivative with respect to κ,

$$I_{N,\Sigma}(p_1,\ldots,p_N) = \kappa \int_k \frac{\partial}{\partial\kappa} \prod_{i=1}^{N} G(k-p_i). \tag{3.69}$$

The integration is finite except for some poles for certain combinations of external momenta, which we exclude, exchanging the integral and the derivative is then allowed. This leaves the simple relation $I_{N,\Sigma} = \kappa\partial_\kappa I_N$ Upon contracting a fermion loop with $N+2$ legs, the subset which contains all possible self-energy insertions therefore has the same properties as a loop with N legs. This is especially true for symmetrization and the associated power counting improvements, which carry over directly.

When discussing contractions of an N-point loop with itself, it is thus possible to completely separate contractions which lead to self-energy insertions from the rest. When using the NFL-propagators, the disregard of self-energy insertions is mandatory to avoid double-counting. As we showed, omitting these diagrams does not affect the symmetry properties of higher loop orders so that the one-loop fixed point presents a consistent starting point and the renormalization group equations remain unaffected.

The other contractions of the N-point loop can no longer be resolved exactly, making it difficult to precisely estimate their effect. Again, some contractions will resemble the insertion of a one-loop vertex correction $\Gamma^{(1)}$ (Fig. 3.7). The full momentum and frequency dependence of $\Gamma^{(1)}$ was explored in Sec. 2.2.6, the correction is bounded and rapidly decays for a vanishing transfer frequency. Most importantly, $\Gamma^{(1)}(k,k+q)$ is independent of the fermionic variables k_x and k_0. As a function of k_y, it is peaked at $k_y = 0$ in the low momentum regime and decays in the large momentum regime. We can therefore make an (inexact) upper estimate of the integral by setting $k_y = 0$ in $\Gamma^{(1)}$, which results in

$$\begin{aligned} I_{N,\Gamma}(p_1,\ldots,p_N) &= \int_k \prod_{i=1}^{N} G(k-p_i) \left(\sum_{j=1}^{N} \Gamma^{(1)}(k-p_j, k-p_{j+1}) \right) \\ &\lesssim c_1 N \int_k \prod_{i=1}^{N} G(k-p_i), \end{aligned} \tag{3.70}$$

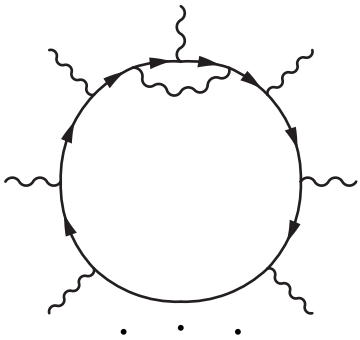

Figure 3.7 A fermion loop with a contraction which is equivalent to the insertion of a one-loop vertex correction.

with c_1 being a constant. This means the vertex correction can approximately be factored out if the dependence on the y-momentum is negligible. Since the power counting improvements depend on the behavior of the N-point loop for $|p_0| \gg |p_y^3|$, we can speculate that vertex corrections do not affect the singularity estimates and can simply be ignored in a classification of diagrams.

On the other hand, the improved power counting II (Sec. 3.3) can only be applied if the N-point loop contains no more than two internal legs, so that the above conclusion is questionable. The crucial question is whether the creation of a box in momentum space whose size is constrained by external variables is possible. The derivation of the power counting improvement used two ingredients to achieve this, the first is the reduction of available phase space by the Θ-function constraint, the second is the presence of IR cutoffs for the remaining regions. As contractions of the N-point loop also constitute integrals within one patch, frequency integrations are still controlled by the external frequencies, thus setting an IR cutoff. The main problem is then an unrestricted y-momentum, which would allow to increase the size of the integration "box" indefinitely (cf. Sec. 3.3.1). At least for the vertex correction $\Gamma^{(1)}$ we already know that this does not actually happen. In the momentum dominated regime (large C), $\Gamma^{(1)}$ decays rapidly as a function of both, the fermionic y-momentum and the transfer y-momentum. The vertex fulfills the full power counting estimate (i.e. a constant) therefore only for a limited range of y-momenta. This is a result of the restriction on frequencies, which ensures that the large momentum regime in the bosonic propagator is reached for a fixed scale set by external variables. In other

words, due to the rapidly decaying boson propagator in the limit of $|p_y|^3 \gg |p_0|$, the frequency cutoff also becomes a momentum cutoff. The insertion of vertex corrections in a fermion loop can thus be treated hierarchically, by constructing a cutoff in terms of external bosonic legs for each loop variable one after the other. As a consequence, the contracted legs pose no problem, and diagrams with vertex insertions have the same singularity properties as the simple N-point loop.

It seems likely that the same line of reasoning is also successful for other contractions of the N-point loop, be it single or multiple. If all contractions could be treated hierarchically, loop integrals including only fermions from one patch would never affect the singularity properties of a diagram. Unfortunately, proving this is difficult. The argumentation for the vertex relied on the (numerically motivated) insight that the vertex correction decays fast enough. The generalization of this result is not straightforward, since it requires some knowledge of the integration in y-momentum. Especially for multiple boson lines in an N-point loop, it becomes very hard to keep track of internal vs. external cutoffs and to find an optimal hierarchical scheme to sort the integrations by.

Nevertheless, the simplistic reasoning that a frequency cutoff entails a y-momentum cutoff due to the presence of a boson line in the loop is well in line with the previous observations: Upon symmetrization of the N-point loop different types of contractions get thrown together, among them self-energy insertions and vertex corrections. In the symmetrized sum, there is no indication, neither numerically nor analytically, that the summands carry unequal singularity properties. Since some types of contractions (namely self-energy and vertex insertions) have no influence on the scaling it is probable that the remaining types are equally unimportant for the scaling estimate.

To summarize, it is always possible to disregard self-energy insertions and it is recommendable to include vertex corrections order by order in the loop expansion to correctly symmetrize contractions of the N-point loops. A resummation of vertex corrections with ladders, on the other hand, is undesirable as it does not respect fermion loop symmetrization and is therefore likely to produce spurious divergences (cf. Sec. 2.2.6).

3.4.3 Fermion boson ladders

In any diagram, an internal boson line can either be attached to one fermion line, or to two. Regarding N-point loops, the former case leads to contractions of a loop with $N+2, N+4, \ldots$ legs. The latter attachment connects different fermion lines, and can thus lead to cross-patch loop integrals. In Sec. 3.4.1, we showed which diagrams lead to singular contributions at four loop, and we found that the first singular diagrams always contain fermion-boson ladders with at least three rungs

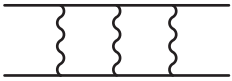

Figure 3.8 The common building block in singular diagrams. The fermions must reside on dissimilar patches.

as a common feature (Fig. 3.8). More precisely, due to the symmetrization of the N-point loop which we always imply for all diagrams, this statement comprises not only fermion-boson ladders, but also all crossed variants which can be obtained by crossing boson lines. In view of the previous section about contracted N-point loops (Sec. 3.4.2), the requirement of (crossed) ladders for a diagram to be singular could only be accidental, with other singular diagrams which do not contain a ladder-type element appearing at higher orders. The first example for such a diagram was class (b) in Fig. 3.6, a contribution to the four-loop correction of the fermion self-energy.

Even if such non-ladder diagrams are singular, due to the reduced phase space in diagrams with many one-patch integrations, and given the higher order in which the first non-ladder diagrams might occur, the primary mechanism to provide singular corrections and produce nonzero anomalous exponents are fermion-boson ladders. This has two interesting physical implications. Firstly, uncrossed ladders contribute the leading renormalization to the four-fermion interaction [187]. As we have seen in Sec. 2.2.2, the generic four-fermion interaction is irrelevant in the 321-limit, but it makes its re-entrance here as building block of singular diagrams. Secondly, from the symmetrization of the N-point loops we know that the various fermion-boson ladders including crossed ladders are equally important. Since this comprises both the particle-particle ladder and the particle-hole ladder and everything in between, we conclude that both ladder types are actually equally important to the low-energy dynamics. This is in line with very recent results which showed an influence of nematic criticality on superconducting correlations [120]. However, we stress that such a far reaching conclusion can not be drawn here just by the appearance of different ladder types. The statement we can positively make is that any field-theoretic approach should probably include not only uncrossed ladders, but also crossed ones. This can quickly make the calculation very difficult. For the same reason many self-consistent approaches are probably insufficient to capture the critical dynamics.

4 Boson self-energy at four loops

While the improved power counting exposed the one-loop fixed point and its exponents as an accident of kinematic constraints at low loop order, the instability of the fixed point and the renewed flow of the exponents cannot be proven from these general arguments. As was observed previously and is also predicted by the power counting, the fermionic field strength renormalization sets in at three loops. The renormalization of e^2 and thus the DCE is predicted to first appear at four loops. We confirm this prediction now with an explicit calculation in Sec. 4.1. Unexpectedly, we find a divergence with a power of a logarithm, which cannot be absorbed in the scaling ansatz. Another interesting aspect are the kinematic constraints which were derived as a byproduct of the improved power counting. In Sec. 4.2 we use these to explain the smallness of fluctuation corrections found so far in the next-to-leading order RPA expansion. In Sec. 4.3 we finally discuss the consequences of the divergence which was found at four loop.

4.1 Calculation of the AL-type contribution

At four loops, there are four classes of diagrams for the boson self-energy, two of which can be singular (Sec. 3.4.1). Of these, one class ((a) and (b) in Fig. 4.1) contains divergent subdiagrams, shown in Fig. 4.1, (d) and (e). The class of diagrams (c) contains no divergent subdiagram due to the power counting improvements discussed in the previous chapter. Since (c) contains an even number of vertices of each Fermi surface patch while (a) and (b) contain an odd number, their sum for even and odd coupling will be dissimilar. As long as $\Pi^{(4a)} + \Pi^{(4b)}$ or $\Pi^{(4c)}$ or both are singular the sum can thus not be finite for both even as well as odd coupling. For this reason it suffices to find a singular contribution from class $\Pi^{(4c)}$ in order to prove that $z = 3$ is not stable. We calculate the contribution from class (c) which is the four-loop analogue to the Aslamazov-Larkin contribution at three loops.

4.1.1 Analytical results

In the following we will always use Λ_y as the unit by which we measure the UV cutoff scale and drop the index y. All diagrams for class (c) are written out in Fig. 4.2.

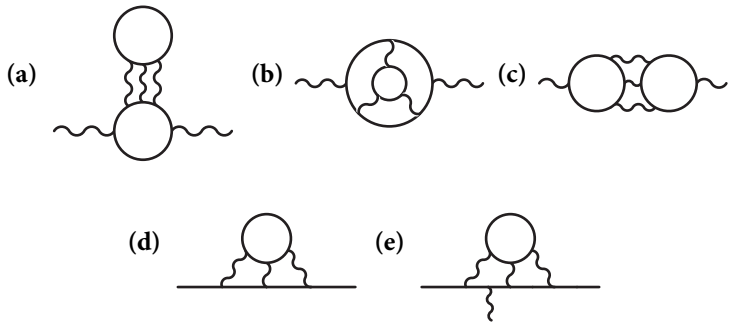

Figure 4.1 (a-c) Singular contributions to the boson self-energy at four loops. (d) Singular self-energy correction at three loop which appears as a divergent subdiagram in (a). (e) singular vertex correction which appears in (b).

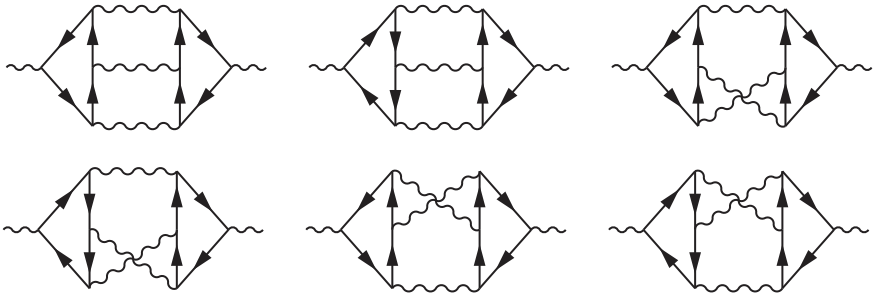

Figure 4.2 All six variants of the four loop correction to the boson self-energy.

Using symmetrized loops, the expression is

$$\begin{aligned}\Pi^{(4c)}(q) = -\int_{l_1,l_2} & D(l_1+\tfrac{q}{2})D(l_2-l_1)D(\tfrac{q}{2}-l_2) \\ & \times \Pi^S_{4,-}(\tfrac{q}{2}-l_2, l_2-l_1, l_1+\tfrac{q}{2}, -q) \\ & \times \Pi_{4,+}(q, -\tfrac{q}{2}-l_1, l_1-l_2, l_2-\tfrac{q}{2})) \\ & + q \leftrightarrow -q. \end{aligned} \tag{4.1}$$

Here, $\Pi^S_{4,-}$ denotes the symmetrized N-point loop according to Eq. 3.25. We point out that due to the topology of the diagram $\Pi^{(4c)}$ there are only six distinct contributions, which in sum symmetrize only one of both N-point loops. The power

counting improvements discussed previously for symmetrized N-point loops are therefore only recovered after carrying out all integrals. Alternatively, one can replace $\Pi_{4,+} \to \frac{1}{6}\Pi^S_{4,+}$ in Eq. 4.1. The external momentum is $q = (q_x, q_y, 0)$. Since the external frequency is zero, the replacement of all loop frequencies by its negative produces the conjugate, showing that $\Pi^{(4c)}$ is real. In the same way we conclude that the integral is invariant under $(q_x, q_y, 0) \to (-q_x, -q_y, 0)$, which means that the respective choice which N-point loop is on the plus and on the minus patch can be accounted for by a factor of 2 instead of summing over q and $-q$ in Eq. 4.1. In the notation of transfer momenta, the four-point loops are given by

$$\begin{aligned} N_f^{-1}\Pi^S_{4,-}(\tfrac{q}{2}-l_2, l_2-l_1, l_1+\tfrac{q}{2}, -q) = \widetilde{I}_{4,-}(-\tfrac{q}{2}, l_1, l_2, \tfrac{q}{2}) \\ + \widetilde{I}_{4,-}(\tfrac{q}{2}, l_2, l_1, -\tfrac{q}{2}) \\ + \widetilde{I}_{4,-}(-\tfrac{q}{2}, l_1, l_1-l_2+\tfrac{q}{2}, \tfrac{q}{2}) \\ + \widetilde{I}_{4,-}(\tfrac{q}{2}, l_1-l_2+\tfrac{q}{2}, l_1, -\tfrac{q}{2}) \\ + \widetilde{I}_{4,-}(-\tfrac{q}{2}, l_2-l_1-\tfrac{q}{2}, l_2, \tfrac{q}{2}) \\ + \widetilde{I}_{4,-}(\tfrac{q}{2}, l_2, l_2-l_1-\tfrac{q}{2}, -\tfrac{q}{2}) \end{aligned} \tag{4.2}$$

$$N_f^{-1}\Pi_{4,+}(q, -\tfrac{q}{2}-l_1, l_1-l_2, l_2-\tfrac{q}{2}) = \widetilde{I}_{4,+}(-\tfrac{q}{2}, l_2, l_1, \tfrac{q}{2}). \tag{4.3}$$

In the following the convention of Sec. 2.2.4 is used where $\mathcal{G}_s^{-1}(k) = sk_x + k_y^2 - i\bar{\kappa}k_0/|k_0|^{1/3}$. The N-point loop (cf. eq. 3.20) is then slightly modified to

$$\begin{aligned} \widetilde{I}_{N,+} = \frac{(-g_+)^N}{2} \sum_{i,j>i} \int_{p_{i0}}^{p_{j0}} \frac{\mathrm{d}k_0}{2\pi} \\ \times \Theta\left(\frac{p_{j0}-p_{i0}}{p_{jy}-p_{iy}}\right)(p_{jy}-p_{iy})^{N-3} \prod_{k\neq i,j} \widetilde{J}^{++}_{ijk}(k_0) \end{aligned} \tag{4.4}$$

$$\widetilde{J}^{++}_{ijk}(k_0) = \frac{1}{D_{ijk} + 2F_{ijk} + i\widetilde{\Omega}_{ijk}(k_0)} \tag{4.5}$$

$$\widetilde{\Omega}_{ijk}(k_0) = \bar{\kappa}\{k_0 - p_{i0}\}(p_{ky} - p_{jy}) + cycl. \tag{4.6}$$

We shift $k_0 \to t(p_{j0} - p_{i0}) + p_{i0}$ inside the sum and obtain

$$\widetilde{I}_{N,+} = \frac{(-g_+)^N}{2} \int_0^1 \frac{\mathrm{d}t}{2\pi} \sum_{i,j>i} \theta_{ij}^N \prod_{k\neq i,j} \widetilde{J}^{++}_{ijk}(t(p_{j0}-p_{i0}) + p_{i0}), \tag{4.7}$$

which is more convenient for numerical integration. At this point only a few more simplifications are possible, most importantly no obvious expansion or limit is

available, because one must preserve the intricate cancellation properties of the N-point loops. With some effort it is still possible to perform the residues in l_{1x} and l_{2x}, after which q_x drops out, we thus set $q_x = 0$ directly. The integrand then only depends on q_y.

The universal scaling is recovered in the limit $q_y \to 0$. In anticipation of a logarithmic divergence, it is often useful to expand the integrand around $q_y = 0$ and decompose the integration into a surface integral and a radial integral with radius variable r. Looking at Eq. 4.1, an expansion will include derivatives of the four-point loops and also of the renormalized boson propagators. The expanded four-point loops read as

$$\Pi_{4,+}(q_y) = F_{0,+} + q_y F_{1,+} + \frac{q_y^2}{2} F_{2,+} + \mathcal{O}(q_y^3) \tag{4.8}$$

$$\Pi^S_{4,-}(q_y) = F^S_{0,-} + q_y F^S_{1,-} + \frac{q_y^2}{2} F^S_{2,-} + \mathcal{O}(q_y^3) \tag{4.9}$$

where higher order terms are neglected as they produce UV-finite contributions. It was shown in Sec. 3.2 that the symmetrization of Π_4 entails that its zeroth order term F_0^S is zero. Furthermore, as a first derivative with respect to q_y, $F_{1,+}$ and $F^S_{1,-}$ are antisymmetric in y-momenta, rendering products with even functions equal zero. With the expansion of the boson propagator

$$D(\tfrac{q}{2} + l) = D(l) + q_y D_1(l) + \mathcal{O}(q_y^2), \tag{4.10}$$

this leaves the following combinations up to second order in q_y in the integrand:

$$\begin{aligned} &q_y^2 F_{0,+} F^S_{1,-} \left[D_1(l_1) D(l_2 - l_1) D(l_2) + D(l_1) D(l_2 - l_1) D_1(l_2)\right] \\ &\quad + q_y^2 F_{1,+} F^S_{1,-} D(l_1) D(l_2 - l_1) D(l_2) + \frac{q_y^2}{2} F_{0,+} F^S_{2,-} D(l_1) D(l_2 - l_1) D(l_2). \end{aligned} \tag{4.11}$$

In the following we assume that the fermionic frequency integration in the 4-point loops was performed, and evaluate all terms in a symmetrical fashion in the remaining loop variables. Then, the first term in eq. 4.11 vanishes under the symmetrization $l_1 \leftrightarrow l_2$, the second vanishes if we choose for the unsymmetrized N-point loop $\Pi_{4,+}$ the standard labeling of momenta $(q, -\frac{q}{2} - l_1, l_1 - l_2, l_2 - \frac{q}{2})$, which entails $F_{1,+} = 0$. The last term is generally nonzero. To calculate $F^S_{2,-}$, we take the second derivative of the N-point loops in the formulation of Eq. 4.7. As a consequence we have to deal with Θ-functions and their derivatives. Any δ-functions appear from derivatives of the term θ^N_{ij}, which vanishes smoothly in the submanifold where $p_{i0} = p_{j0}$. The δ-functions do therefore not contribute to the leading order.

As the expanded expression scales homogeneously with the radius variable r for a properly chosen surface shell (cf. discussion in Sec. 2.2.2), the scale can be factored out. We introduce stretched spherical integration variables $l_{i0} = r^3\tilde{l}_{i0}$, $l_{ix} = r^2\tilde{l}_{ix}$, and $l_{iy} = r\tilde{l}_{iy}$, where r runs from 0 to Λ and tilde variables are constrained to a unit sphere. Scaling out the r-dependence, one obtains

$$\Pi^{(4c)}(q_y) = \frac{q_y^2}{e^2}\int_{|q_y|}^{\Lambda}\frac{\mathrm{d}r}{r}\int_{\Omega}\bar{F}(\Omega), \tag{4.12}$$

where $\bar{F}$ is proportional to $F_{0,+}F^S_{2,-}D(\tilde{l}_1)D(\tilde{l}_2-\tilde{l}_1)D(\tilde{l}_2)$. A logarithmic divergence is then signaled by a nonzero but finite result of the surface integral over Ω.

In order to make the presence of a nonzero logarithmic correction evident independently of numerical results, we simplified the second order term $F_{0,+}F^S_{2,-}$ by replacing the non-Fermi liquid form of the frequencies with their bare, linear dependence. This step destroys the 321-scaling and is therefore only useful to decide whether the integral returns a nonzero value, not to estimate the actual value. For this, it is important to note that the linear frequency dependence enhances the symmetry and is therefore only prone to a false positive towards a zero result, not the other way round. After some rearrangements, one obtains a greatly simplified expression for $\bar{F}$ (neglecting all numerical factors and dropping tildes)

$$\begin{aligned}&[l_{10}\Theta(l_{10}l_{1y}) + (l_{20}-l_{10})\Theta((l_{20}-l_{10})(l_{2y}-l_{1y})) - l_{20}\Theta(l_{20}l_{2y})]^2\\ &\quad\times A^{-2}BD(l_1)D(l_2-l_1)D(l_2)(l_{1y}-l_{2y})^2\end{aligned} \tag{4.13}$$

where A and B are defined as

$$A = l_{1x}l_{2y} - l_{2x}l_{1y} + l_{1y}l_{2y}^2 - l_{1y}^2l_{2y} + i(l_{10}l_{2y} - l_{20}l_{1y}) \tag{4.14}$$

$$\begin{aligned}B = &\left[\frac{l_{2x}l_{1y}^2 + l_{1x}l_{2y}^2 + 2l_{1y}^2l_{2y}^2 - i(l_{20}l_{1y}^2 + l_{10}l_{2y}^2)}{(-l_{1x}l_{2y} + l_{2x}l_{1y} - l_{1y}l_{2y}^2 + l_{1y}^2l_{2y} + i(l_{10}l_{2y} - l_{20}l_{1y}))^4}\right]\\ &- \left[\frac{l_{2x}l_{1y}^2 + l_{1x}l_{2y}^2 - 2l_{1y}^2l_{2y}^2 - i(l_{20}l_{1y}^2 + l_{10}l_{2y}^2)}{(-l_{1x}l_{2y} + l_{2x}l_{1y} + l_{1y}l_{2y}^2 - l_{1y}^2l_{2y} + i(l_{10}l_{2y} - l_{20}l_{1y}))^4}\right].\end{aligned} \tag{4.15}$$

We further simplify the denominators to leading order in the y-momenta, which leaves the real part

$$\begin{aligned}&[l_{10}\Theta(l_{10}l_{1y}) + (l_{20}-l_{10})\Theta((l_{20}-l_{10})(l_{2y}-l_{1y})) - l_{20}\Theta(l_{20}l_{2y})]^2\\ &\quad\times 4l_{1y}^2l_{2y}^2(l_{1y}-l_{2y})^2\frac{(l_{2x}l_{1y} - l_{1x}l_{2y})^2 - (l_{20}l_{1y} - l_{10}l_{2y})^2}{[(l_{2x}l_{1y} - l_{1x}l_{2y})^2 + (l_{20}l_{1y} - l_{10}l_{2y})^2]^4}\\ &\quad\times D(l_1)D(l_2-l_1)D(l_2).\end{aligned} \tag{4.16}$$

This can be decomposed into a nonnegative and nonpositive term, which do not cancel each other as x-momenta and frequencies are not interchangeable. This shows analytically that the exponent is nonzero, as expected. Surprisingly, a numerical integration shows that the surface integral of Eq. 4.12 is neither zero nor finite but diverges. One alarming signal for this kind of behavior is already visible from the simplified expression for bare propagators in Eq. 4.13: Since both x-momenta l_{1x} and l_{2x} only appear in the combination $l_{2x}l_{1y} - l_{1x}l_{2y}$, a contour integration in one of both x-momenta will entirely obliterate the other x-momentum, making the subsequent integration divergent. We note that the nature of this divergence is of course not indicative of the corresponding divergence in the 321-limit, but it makes the observation of a divergent coefficient of the logarithm quite reasonable.

From these considerations we conclude that the singularity is very likely stronger than logarithmic. As a power-law divergence is excluded by the power counting, it should amount to a power of a logarithm. Within the Taylor expansion around $q_y = 0$ it is not possible to detect the exact form of the divergence, because the Taylor coefficient is infinite and has to be regularized. The precise form of this regularization determines the type of divergence. The physical regulator is the nonzero q_y, which just means that it is best to take the original expression for $\Pi^{(4c)}(q_y \neq 0)$ and not to expand at all.

4.1.2 Numerical treatment

The four-point loop contains six terms in the sum over all i, j, one of which is zero due to $q_0 = 0$. The product $\Pi_{4,+}\Pi_{4,-}^{\text{sym}}$ then contains $5 \times (5 \times 6) = 150$ terms, each of which consists of four J_{ijk}. This means that all manipulations have to be automatized. To this end, we employed the computer algebra capabilities of *Wolfram Mathematica 10* and exported the results for an integration with an adaptive routine from the *CUBA* package [188]. The numerical treatment of $\Pi^{(4c)}(q)$ is quite difficult. We document in the following how the integration can be performed successfully.

From the discussion of one-patch diagrams Sec. 2.3 one can conclude that no regulator is needed for the fermionic frequencies which are contained in each four-point loop. The boson propagators on the other hand require a regularization. This can be realized with a hard UV-cutoff Λ on the loop variables l_1 and l_2. The behavior of the integral at the UV-cutoff scale then determines the nature of the divergence. Using this, the parametrization of the integration with a radius variable and a surface shell discussed in the last section is only slightly altered. We again introduce $l_{i0} = r^3\tilde{l}_{i0}$, $l_{ix} = r^2\tilde{l}_{ix}$, and $l_{iy} = r\tilde{l}_{iy}$, where r runs from 0 to Λ, and the tilde-variables

are confined to a unit sphere. The integral can then be written in the form

$$\Pi^{(4c)}(q_y) = \frac{q_y^2}{e^2} \int_0^\Lambda \frac{dr}{r} \int \mathrm{d}\Omega \, F(\Omega, q_y/r). \tag{4.17}$$

A logarithmic divergence is then signaled by a nonzero result of the surface integral over Ω for $|q_y| \ll r$, and the coefficient of the divergence is given by

$$C^{(4c)} = \lim_{\tilde{q}_y \to 0} \int d\Omega \, F(\Omega, \tilde{q}_y). \tag{4.18}$$

We note that is principially possible to perform the residues in l_{1x} and l_{2x}, thus reducing the number of numerical integrations, but this creates more problems than it solves. The first problem is the distinct treatment of bosonic x-momenta, which have to be taken as unrestricted when using a contour integration. Secondly, taking the residues produces several thousand terms, making the subsequent integration quite slow. Additionally, large cancellations happen upon symmetrizing the N-point loop, which need to be resolved numerically. Sporadic tests reveal that the increased number of terms can indeed exacerbate floating point errors. Another point is the convergence speed towards the UV-asymptotics. We know from the structure of the symmetrized N-point loop that the improved power counting is only realized if the internal momenta are *sufficiently* larger than the external ones (Sec. 3.3.1). The precise scale needed to observe this onset is hard to determine and also dependent on the momentum and frequency constellation in consideration. At least in the present case, the scale where the UV-asymptotics sets in increases considerably and consistently after taking the residues. A detailed example for this is given in Fig. 4.3. We also note that the pointwise UV dependence of $\Pi^{(4c)}$ is indeed worsened by one power after taking the residues, which is reminiscent of the analysis of the bare terms. However, one has to keep in mind that the pointwise dependence does not account for the further reduction of phase space which is present due to the additional Θ-functions after the additional contour integrations. Lastly, also the integration in the fermionic frequencies t of the N-point loops (cf. Eq. 4.7) is delicate due to large cancellations (Fig. 4.4). After the contour integrations in l_{1x} and l_{2x}, the frequency integrals of both N-point loops do no longer factorize, so that a two-dimensional integration or at least two chained one-dimensional integrations have to be used. In conclusion, the analytical integration of l_{1x} and l_{2x} is not helpful.

Considering the annihilation of the remaining dependence on x-momentum which we reported in the last section for bare propagators, it would be interesting to compare the results with and without doing the last two residues even if the numerical errors are larger for the former case. This is still not possible as the universal scaling sets in for too large values of r, where the integration of the contour integrated expressions is already unreliable.

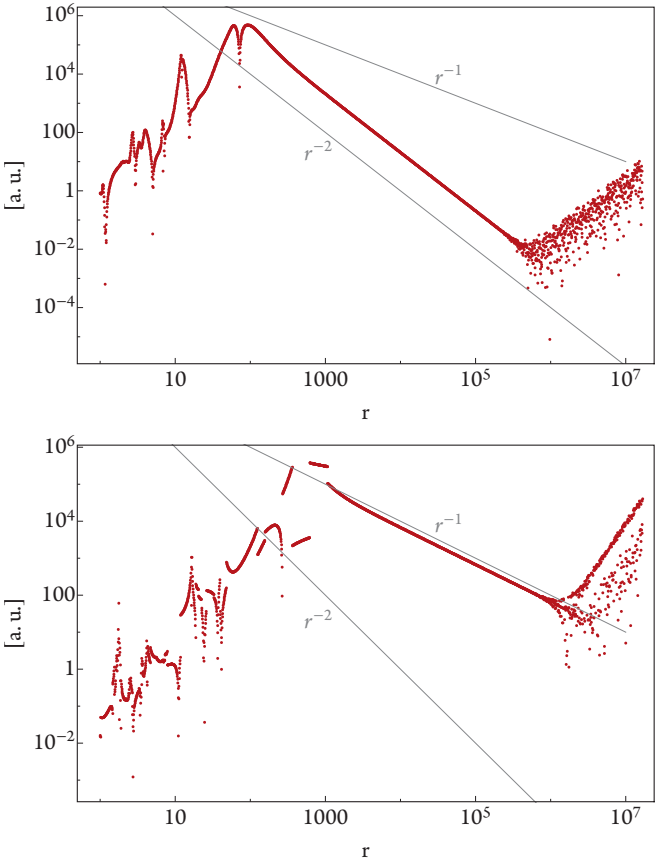

Figure 4.3 Upper panel: Scaling of the absolute value of the fermionic part of $\Pi^{(4c)}$ as a function of $\tilde{q}_y = 1/r$ with the fixed loop frequencies $(l_{1x}, l_{1y}, l_{10}) = (0.58, 0.64, 0.45)$, $(l_{2x}, l_{2y}, l_{20}) = (0.32, -0.17, 0.21)$ and the fermionic frequencies $t_1 = 0.46$ and $t_2 = 0.71$. The improved power counting predicts a decay with r^{-2} for large r. The values are chosen to exemplify the onset of universal scaling for relatively large $r \sim 10^2$. At around $r \sim 10^6$, the finite numerical precision becomes a problem. Lower panel: Same as above, but after the contour integrations in l_{1x} and l_{2x}. The function then displays a slower decay with r^{-1} with an onset of universal scaling at $r \sim 10^3$. We note that the loss of precision sets in at roughly the same scale $r \sim 10^6$ as before.

As the momentum shell in the space spanned by l_1 and l_2 we choose elliptical coordinates with

$$l_{1x} = \operatorname{sgn} l_{1x} \left(r \sin\phi_1 \sin\phi_2 \sin\phi_3 \sin\phi_4 \sin\phi_5\right)^2 \tag{4.19}$$
$$l_{1y} = r \sin\phi_1 \sin\phi_2 \sin\phi_3 \sin\phi_4 \cos\phi_5 \tag{4.20}$$
$$l_{1z} = \left(r \sin\phi_1 \sin\phi_2 \sin\phi_3 \cos\phi_4\right)^3 \tag{4.21}$$
$$l_{2x} = \operatorname{sgn} l_{2x} \left(r \sin\phi_1 \sin\phi_2 \cos\phi_3\right)^2 \tag{4.22}$$
$$l_{2y} = r \sin\phi_1 \cos\phi_2 \tag{4.23}$$
$$l_{2z} = \left(r \cos\phi_1\right)^3, \tag{4.24}$$

where ϕ_5 goes from 0 to 2π and all other angles from 0 to π. The Jacobi determinant is

$$\begin{aligned} &36 r^{11} \operatorname{sgn}\left(\cos\phi_3\right) \operatorname{sgn}\left(\sin\phi_5\right) \cos^2\phi_1 \cos\phi_2 \cos^2\phi_4 \\ &\quad \times \sin^8\phi_1 \sin^7\phi_2 \sin^5\phi_3 \sin^2\phi_4 \sin\phi_5. \end{aligned} \tag{4.25}$$

This momentum shell respects the 321-limit and allows the formulation of a surface integral as in Eq. 4.17. The precise form of the momentum shell is of course not important, but other shapes, e.g. a hypercube, are no easier to implement due to the high dimensionality of the integration.

The complete integrand contains a very high number of poles, and is subject to a substantial sign problem. According to Eq. 4.7, the integration over the rescaled fermionic frequency t in an N-point loop is restricted to the interval $[0, 1]$. A typical plot of the N-point loop in this interval is depicted in Fig. 4.4. We point out that the N-point loop is independent of t for bare fermion propagators (Eq. 3.20). Due to the NFL self-energy this is no longer true for the RPA-renormalized propagators, but upon integration sizable cancellations can happen. The best performance can therefore be accomplished when the fermionic frequency integrals are performed first for each four-point loop separately. Furthermore, we integrate the sum of the contributions of t and $1 - t$ over the interval $[0, 0.5]$. To reduce possible numerical problems, we also symmetrized the second four-point loop in Eq. 4.1.

For the poles in the propagators it is necessary to introduce an IR cutoff or alternatively to use some kind of singularity handler. A comparison of several integration routines and different choices of cutoffs reveals no particular benefit of more advanced singularity handling, so that it suffices to only use a protection against overflows.

The remaining integration in the five angles ϕ_1 to ϕ_5 of the momentum shell Ω was done with a multidimensional integration method. The integration routines offered by the package *CUBA* [188] are especially aimed at integrating Feynman diagrams and offer a number of settings to adjust the integration for the desired purpose.

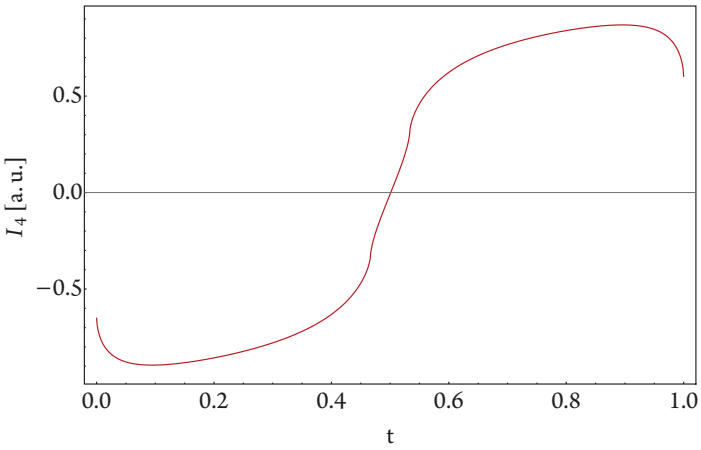

Figure 4.4 Plot of the real part of the symmetrized four point loop as a function of the rescaled fermionic loop frequency t. The other variables were chosen as $q_y = 0.1$ and l_1 and l_2 as in Fig. 4.3. In the example depicted here, the integration over t yields -0.0090.

By comparing the integration results for different routines one can therefore make sure that the integration has converged independently of the error margin which is reported by the routines themselves. Depending on the value of r in Eq. 4.17 the number of required integrand evaluations is between 10^7 to 10^8, where the number increases as $1/r$ approaches zero. The fastest convergence was achieved with the adaptive QMC integrator *Vegas*.

The main result is shown in Fig. 4.5. As expected, $C^{(4c)}$ does not saturate. We can also read off the type of divergence by making a double-log plot with $\log(r)$ as the abscissa. The surface integral increases with the fourth power of the logarithm. This means that $\Pi^{(4c)}$ develops a multilogarithmic divergence $q_y^2 \log^5(\Lambda/q_y)$. We also note that the universal scaling sets in relatively late for $r \sim \exp(4)$. As we have discussed beforehand, the improved power counting from symmetrized N-point loops is not preserved numerically at all scales. While we do not find examples where the floating point errors destroy the symmetrization properties of the N-point loops below $r \sim 10^6$ (cf. Fig. 4.3), one cannot take this as granted. It is therefore imperative to exclude any possible numerical problems in the integration. To make sure that the additional divergence is physical and not an artifact, we therefore performed several additional tests of the physical content of $\Pi^{(4c)}$.

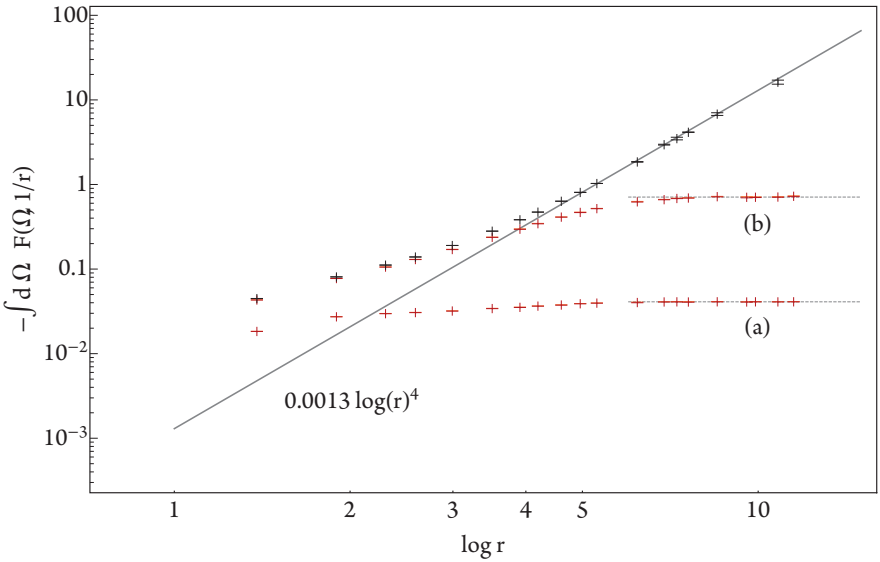

Figure 4.5 Surface integral $\int \mathrm{d}\Omega F(\Omega, q_y/r)$ for $q_y = 1$ as a function of r. The upper data points (black crosses) were computed with the q_x-independent boson propagator $D(q)$ as obtained from the RPA. The lower points (red crosses) were obtained with an additional term proportional to $(q_x/q_y)^2$ with a coefficient $1/e^2$ (a) and $0.01/e^2$ (b) in the denominator of $D(q)$. The error bars as estimated by the integration routine are displayed by the upper and lower bars in the crosses. For all but the largest r they remain invisibly small.

As a first step we verified that the integral is dominated by contributions where $l_{2x}l_{1y} - l_{1x}l_{2y} \approx 0$. By removing regions where

$$|l_{2x}l_{1y} - l_{1x}l_{2y}|^2 + |\{l_{20}\}l_{1y} - \{l_{10}\}l_{2y}|^2 < b^2 \tag{4.26}$$

one can show that the growth of the function is stopped once $1/r$ becomes smaller than b (Fig. 4.6). This confirms that the origin of the divergence of $C^{(4c)}$ is due to the special determinant-like combination $(l_{2x}l_{1y} - l_{1x}l_{2y})$ in which the x-momenta appear. In other words, the odd behavior originates from the pole structure of the fermion Green's function.

Since the x-dependence vanishes after a contour integration in l_{1x} or l_{2x} when the bare propagators are expanded around $q_y = 0$, it is tempting to disturb this speciality of the expressions by adding some marginal terms containing the x-momentum

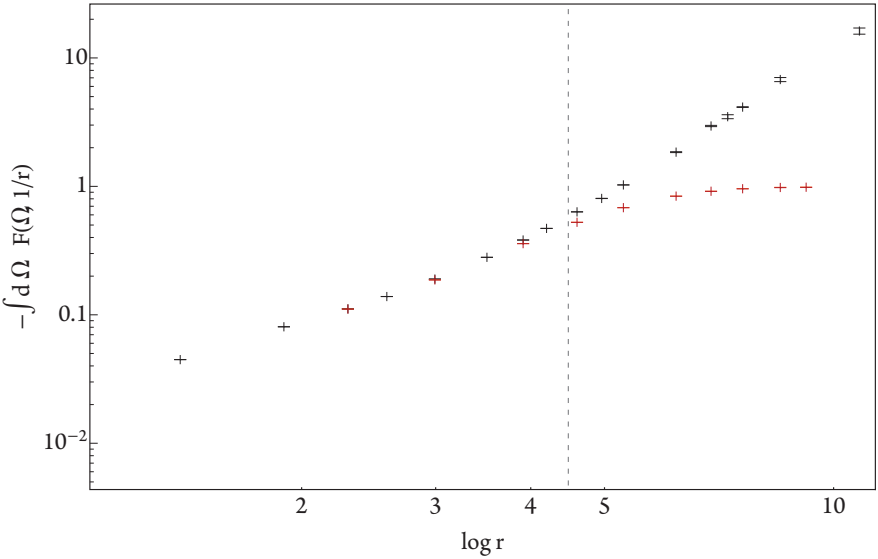

Figure 4.6 Surface integral $\int d\Omega F(\Omega, q_y/r)$ for $q_y = 1$ as a function of r. For this calculation (red crosses), integration regions are excluded where the condition Eq. 4.26 with $b = 0.01$ is fulfilled. The dashed gray line indicates $r = 100$. The function clearly saturates in the limit of large r, which means that $C^{(4c)}$ is finite. The black crosses are the unregulated values.

to the inverse propagators. Since the calculation of $\Pi^{(4c)}$ relies on the analytical manipulation of the four-point loop, we choose to not alter the fermion propagator at all but add a term in the boson propagator. A suitable marginal term which fulfills the 321-scaling is q_x^2/q_y^2, the form of which can be seen more or less in analogy to the anomalous frequency dependence $|q_0/q_y|$ from the particle-hole bubble. We reiterate that any dependence on x-momentum in the boson propagator is disallowed within the two-patch approximation as it breaks the emergent sliding symmetry (cf. Sec. 2.2.2). The numerical results for two values $1/e^2$ and $0.01/e^2$ of the coefficient of q_x^2/q_y^2 are shown in Fig. 4.5. Once again, $C^{(4c)}$ is rendered finite and the multiple logarithm disappears. In analogy to the previous discussion, one can conclude that the additional divergence is produced by the pole structure of the boson propagators. The presented tests probe the poles within the integration region on physical grounds. Numerical errors would affect the entire integration region and would not be influenced by a change of the boson propagators. We can therefore exclude numerical errors as the culprit of the additional divergence.

In summary, the class of four-loop diagrams $\Pi^{(4c)}$ is singular with a fifth power of the logarithm. The function obtained numerically is

$$\Pi^{(4c)}(q_y) = -c^{(4c)} \frac{q_y^2}{e^2} \log^5 \frac{\Lambda}{q_y}, \tag{4.27}$$

with $c^{(4c)} = 2.6 \cdot 10^{-4}$. The origin of the high power of the logarithm is a degeneracy with respect to the x-momentum variables.

4.2 Size of fluctuation corrections

While the singularity of $\Pi^{(4c)}$ is stronger than originally expected, the numerical coefficient is very small. This is in line with previous calculations of fluctuation effects. For the anomalous dimension α of the fermionic field strength for example the obtained values are parametrically small for many approaches.

4.2.1 Alternative expansion schemes

In Sec. 2.2.5 we highlighted the shortcomings of the usual large-N_f expansion. After the discovery that the SCM action cannot be controlled by a large number of fermion flavors, a number of alternatives were suggested. Mross *et al.* [116] generalized not only N_f but also the dynamical critical exponent z_b of the boson field. A controlled expansion is then possible as long as

$$z_b - 2 \sim 1/N_f. \tag{4.28}$$

The extrapolation of their results to $N_f = 2$ and $z_b = 3$ yields the anomalous dimension $\alpha = 0.6$. A value of $\alpha = 0.3$ was found in a study using a functional renormalization group approach by Drukier *et al.* [117].[1] More recently, another approach was presented by Dalidovich and Lee [118]. Using a Fermi surface with an arbitrary number of co-dimensions, they promoted the model to general dimension and established that the upper critical dimension is $d_{uc} = 5/2$. This means that an ϵ-expansion is possible, where $\epsilon = 1/2$ yields the two-dimensional case.[2] Including the one-loop boson self-energy via RPA, the perturbative calculation in $5/2 - \epsilon$

[1] The authors also found a correction to the fermion dynamical critical exponent, which they interpret as a possible artifact of the employed approximations.

[2] We point out that there are also some subtleties present in this expansion which in the worst case makes it necessary to compute diagrams up to loop order $2n$ to obtain results up to $\mathcal{O}(\epsilon^n)$.

dimensions is straightforward, but tedious. Their results up to two loops can be summarized in the propagators

$$D(k) = \frac{1}{k_y^2} f\left(\frac{|\mathbf{K}|^{1/z}}{k_y^2}\right) \tag{4.29}$$

$$G_s(k) = \frac{1}{|sk_x + k_y^2|^{1-0.15\epsilon^2}} g\left(\frac{|\mathbf{K}|^{1/z}}{sk_x + k_y^2}\right), \tag{4.30}$$

where f and g are analytic functions and $\mathbf{K} = (k_x, k_y, k_0)$. The DCE is not renormalized from $z = 3$. This rather different type of expansion thus leads to a anomalous dimension for Z_ψ of $\alpha = 0.075$. We stress that none of these works included corrections to the boson self-energy which are singular according to the improved power counting rules which we derived, it is thus expected and reassuring that $z = 3$ is not renormalized.

In the following, we present a simple argument why the numerical factors in the corrections which have been computed so far are comparatively small, at least a lot smaller than what could be expected for a theory at three and four loops for an interaction strength of order one.

4.2.2 Kinematic reduction

We reiterate that the perturbative expansion around the one-loop fixed point (cf. Sec. 2.2.3) is special in several aspects: After the inclusion of one-loop self-energy corrections in the propagators, the overall number of diagrams is significantly reduced as one-loop self-energy insertions are already taken into account. Additionally, all one-patch diagrams are finite due to the NFL fixed point and the associated 321-scaling (Sec. 2.3.2). Thanks to the improved power counting rules derived in chapter 3, the number of singular diagrams is further decreased by the special requirements which apply to the N-point loops. As a consequence, even at four loop level the total number of diagrams is comparatively small.

Independent of this combinatorial benefit, the few singular diagrams additionally carry the various phase space restriction which were discussed in Sec. 3.3. We can utilize these insights to calculate which fraction of the entire phase space contributes to the singular part of a diagram in the presence of N-point loops. To this end, we consider the N-point loop $I_N(p_1, \dots, p_N)$ and concentrate on the case where all y-momenta and frequencies are positive. Without loss of generality we can choose $p_N = 0$. The singular contributions then originate from the regions where (Eqs. 3.62)

$$(p_{iy} < \max(\dots, p_{ky}, \dots)_{k\neq i} \vee\ p_{i0} < \max(\dots, p_{k0}, \dots)_{k\neq i})\,. \tag{4.31}$$

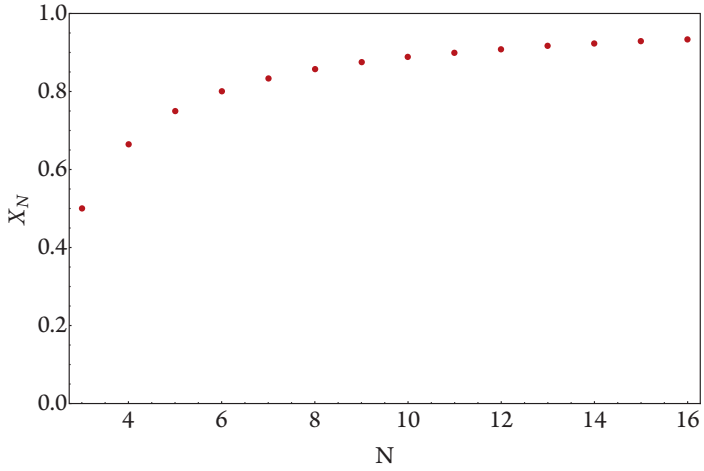

Figure 4.7 Plot of the volume fraction X_N for different N with $\Lambda = 1$.

Analogous conditions follow for the other cases with different signs. If all boson legs of an N-point loop are part of other loops in the diagram, one can determine the relevant phase space fraction by the integral

$$X_N = \Lambda^{-6(N-1)} \prod_{i=1}^{N-1} \left(\int_0^{\Lambda^2} \mathrm{d}p_{ix} \int_0^{\Lambda} \mathrm{d}p_{iy} \int_0^{\Lambda^3} \mathrm{d}p_{i0} \right) f(p_1, \ldots, p_{N-1}) \quad (4.32)$$

where the function f is equal one in the region defined by Eq. 4.31 and zero otherwise. The fraction X_N is plotted for $N \geq 3$ in Fig. 4.7. For $N = 3$ and $N = 4$ the volume fraction is comparatively small, with increasing N it increases and quickly approaches $X_N = 1$ for $N \to \infty$.

Since the one-loop fixed point propagators are homogeneous functions under the 321-scaling, the volume fraction X_N is indicative for the suppression in diagrams containing an N-point loop with not too large N. On the other hand, the fermion Green's functions is not positive definite. The reduction in the phase space volume can therefore not be a strict upper bound by which the original estimate of a diagram is decreased. One should rather interpret the result as a measure for how much smaller the remaining interaction strength is within the expansion using RPA propagators compared to the original problem. We point out that the volume fraction does not yield any gain for $N \to \infty$ and cannot differentiate between diagrams which only differ by the number of internal boson lines. The phase space reduction does therefore not restore a unique ordering scheme for the perturbative expansion and cannot

realize a controlled expansion. Nevertheless, it readily explains why all singular corrections computed so far are parametrically small.

4.3 Breakdown of the scaling ansatz

The divergence of $\Pi^{(4c)}$ with the fifth power of a logarithm is somewhat surprising, but as we discussed in detail in Sec. 4.1 it can be traced back to the special momentum structure of the diagram. We further repeat that the complete correction to the susceptibility at four loop level might cancel the multilogarithmic divergence for one of both, even or odd interaction. This still leaves at least one case for which this divergence does not cancel and for which it requires a physical interpretation. The detected divergence cannot be incorporated into the scaling ansatz discussed in Sec. 2.2.4. In the following we present three possible consequences.

4.3.1 Interpretation as quantum anomaly

As a reminder we point out that the chiral anomaly in one dimensional systems is associated with a linear momentum dependence of the inverse fermion Green's function [182]. This anomaly appears in the calculation of the particle-hole bubble as long as a finite cutoff is imposed in momentum space. By taking the cutoff to infinity the anomaly can be removed after a variable shift (cf. Sec. 2.2.2).

The situation is not much different in the present case. Within the two-patch approximation, the dispersion is linearized for the x-momentum and in most explicit calculations, the boundaries of the patches are extended to infinity. In analogy to the one-dimensional case, one might therefore search for an anomaly in the SCM which deforms the low-energy theory. To this end we calculated a selection of low order corrections to the boson self-energy explicitly while keeping finite cutoffs, but without finding any new anomaly. This is in line with the discussion of contour integration in Sec. 2.3.1, where we explained that a finite integral will not lose any universal properties under contour integration as long as unrestricted variables are not shifted. Drawing from this insight, we conclude that a quantum anomaly which deforms the dependence on x-momenta, if it is present at all, can first appear in a singular diagram. The first singular diagrams for the boson self-energy are of course exactly the ones at four loops. At this loop order the main obstacle in the calculation of any anomalous terms is the enormous increase in complexity once the Fermi surface patches are kept finite: With finite cutoffs the entire approach based on contour integrations in the momentum variables becomes obsolete, and with this also the explicit expressions which were derived in chapter 3. Unfortunately, this complication is profound and we could not find a good way to analytically or

numerically approach the four-loop diagrams while keeping finite cutoffs on the fermionic momenta. The conclusion is therefore that a quantum anomaly concerning the x-momentum does not appear up to three loops in the corrections to the boson self-energy, but possibly at higher order.

4.3.2 Interpretation as symmetry breaking

Spontaneous symmetry breaking manifests in a way which is not dissimilar to the behavior discussed in the previous section. In a perturbative calculation for example, the instability of the ground state which induces symmetry breaking will appear as strong divergences. The major difference is the kind of regulation which should be employed to render the offending terms finite. In case of spontaneous symmetry breaking, this is achieved by the introduction of a small symmetry breaking term in the action. As we have seen in Sec. 4.1.2, the introduction of a term $\sim q_x^2/q_y^2$ does indeed reduce the $\log^5$ to a simple logarithm in $\Pi^{(4c)}$. This finding shows that the critical dynamics can be stabilized by a breaking of the sliding symmetry (Sec. 2.2.2). It does, however, not explain how the symmetry breaking term is introduced.

The easiest way to motivate a term like q_x^2/q_y^2 in the action is in reference to the nonanalyticity in the frequency dependence, $|q_0/q_y|$. For this, we remember that the original boson kinetic energy is usually motivated in a derivative expansion and thus quadratic in all variables,

$$D_0^{-1} \sim c_x q_x^2 + c_y q_y^2 + c_0 q_0^2, \tag{4.33}$$

where c_x, c_y and c_0 are constants. Upon approach the IR limit, the $|q_0/q_y|$-term can therefore be ascribed to a singular dependence $c_0 \sim 1/|q_y q_0|$ which is acquired by the coefficient of q_0^2. In the same way, the other irrelevant term q_x^2 may acquire a singular coefficient of $c_x \sim 1/q_y^2$. We stress that the precise form of the singularity structure is hard to calculate with a field-theoretic renormalization group, which is primarily suited to capture the evolution of critical exponents under scaling. If one indeed wants to track the evolution of the dependence on x-momentum in the boson propagator upon approaching the IR, it is recommendable to use a more sophisticated approach like the functional renormalization group [30], which can keep the full Fermi surface and resolve complicated momentum dependencies.

4.3.3 Destruction of the critical point

As the last possibility we discuss the destruction of the critical scaling. With regards to even interaction, this question relates to the instability of the Ising nematic QCP. As we have discussed in Sec. 2.1, many critical points are known where the metallic

criticality is destabilized due to fluctuations. Particularly illuminating in this context is the model for a ferromagnetic QCP in two dimensions. The low-energy action for this magnetic transition is closely related to the SCM considered here, but contains singular forward scattering in the spin channel, not the charge channel. The spin structure leads to a dissimilar symmetrization of diagrams due to the additional factors from spin sums. At one loop, this difference does not enter the equations very prominently so that the same one-loop fixed point is also found for the ferromagnetic transition. For higher order corrections, the effects are more profound. Most importantly, the spin structure implies the absence of the improved power counting I for symmetrized N-point loops which we derived in Sec. 3.2. For the ferromagnetic QCP it is therefore possible for higher order diagrams to contribute power law corrections to the model. Such power law corrections have indeed been found by Rech, Pépin, and Chubukov [31], leading to

$$D^{-1}(\mathbf{q}, q_0 = 0) \sim \mathbf{q}^2 - 0.25|\mathbf{q}|^{3/2}\sqrt{\Lambda}. \tag{4.34}$$

Since $|\mathbf{q}|^{3/2}$ has a negative coefficient and approaches zero slower than the bare quadratic momentum dependence, the ferromagnetic susceptibility is not positive definite. The authors therefore concluded that the QCP is unstable at the lowest scales.

Along the same lines, we notice that a term $\sim q_y^2 \log^5(\Lambda/|q_y|)$ is larger than q_y^2 for small enough scales, also making the susceptibility negative. The momentum scale q_m where this happens can be estimated by

$$0 = q_m^2 - c^{(4c)} q_m^2 \log^5 \frac{\Lambda}{q_m} \tag{4.35}$$

$$\frac{q_m}{\Lambda} = \exp\left(-(c^{(4c)})^{-1/5}\right) = 0.005. \tag{4.36}$$

Since this onset scale is exceedingly small, one can expect a sizable energy and momentum range where quantum critical scaling is preserved. At the lowest scales, the QCP might become unstable. Again, several possibilities exist what kind of behavior can result from such an instability (cf. Sec. 2.1.2). Firstly, the phase transition can deviate from the forward scattering channel and develop a finite ordering vector. The result is an incommensurate nematic order, also known as modulated bond order. Secondly, the phase transition can develop a small gap, making it weakly first order. This type of behavior can be observed in some cases of magnetic quantum criticality [23].

For odd interaction, i.e. fermions coupled to a $U(1)$ gauge field, the instability of the critical scaling is related to the possible confinement of gauge fields. A long time ago, Polyakov proved that noninteracting photons in 2+1 dimensions are strongly

influenced by the instanton plasma which is associated with the compact $U(1)$ gauge symmetry [189, 190]. He proved in particular that the originally massless theory acquires a mass, leading to a confinement of the bosons. The case we are interested in here of bosons in the presence of a Fermi surface was discussed intensely in the early 2000s, without a definite result [13].

While it is not possible to conclude that the behavior reported here leads to a confinement, we point out that all singular diagrams involve fermions from both patches. As we explained in Sec. 2.2.2, the use of two patches implies that the rotational degree of freedom along the Fermi surface becomes decompactified and broken apart into two local parts around $\mathbf{k}_F$ and $-\mathbf{k}_F$. Diagrams which contain fermions from either patch are therefore of instantonic nature with respect to a local expansion of the dispersion in the vicinity of one point on the Fermi surface.

To summarize, the four-loop contributions to the boson self-energy renormalize the low-energy theory in a way which is not consistent with the original scaling ansatz and can potentially destroy the critical scaling entirely at low energy scales.

5 Summary and Outlook

In this thesis we theoretically studied the low energy theory associated with both, a nematic QCP in a two-dimensional metal with critical forward scattering, and with metals coupled to a $U(1)$ gauge field in two dimensions. With the help of a field-theoretic renormalization group approach we investigated the effects of fluctuations in this model in the quantum critical regime. The primary angle of attack was the detailed analysis of the N-point density vertices in the low-energy limit.

To this end, we examined and sharpened the derivation of the effective field theory in chapter 2. In the course of the analysis we resolved the full momentum and frequency structure of the one-loop vertex correction. This extends earlier works regarding the next-to-leading order contributions [112, 113, 180]. Using this information we could corroborate the consistency of the chosen perturbative expansion based on RPA-renormalized propagators. Especially, we established precise criteria under which circumstances vertex corrections contribute on the same level as self-energy corrections. A simple proof was given for the finiteness of diagrams involving only chiral fermions from one patch. This proof complements the work in [181].

In chapter 3, we studied the general form of N-point loops in the appropriate low-energy limit. As the first main result we derived explicit expressions for the N-point loops. This formulation can be utilized in the calculation of higher order corrections not only for the problem studied here, but also in other cases of singular forward scattering. In particular, the expressions are not restricted to the case where the dynamical critical exponent is $z = 3$. With little extension, another possible application is a metal at a ferromagnetic QCP. With the new formulation of the N-point loops, we derived improved power counting rules for corrections involving symmetrized N-point loops, which allowed a sharp power counting at any loop order. Using this sharp power counting we restricted the possible singularities in diagrams to logarithms. This extends earlier efforts in this direction [114]. The proof of the absence of power-law divergences illuminates the prominent difference between the nematic and the ferromagnetic QCP in two dimensions, which was noticed previously, but not understood completely [31, 148]. Furthermore, with the improved power counting rules we could for the first time clarify the behavior which became visible in explicit calculations up to three loops. In particular, we exposed the special properties which guarantee the finiteness of the Aslamazov-Larkin correction. Along the same lines, we classified the self-energy corrections at four loop order and

established the appearance of singular corrections to the boson self-energy at four loops.

This gave way to the second part, presented in chapter 4, the calculation of a certain subset of four loop diagrams. The calculated class of diagrams can be seen as the four loop analogue of the Aslamazov-Larkin diagram. We constructed a momentum shell approach for the numerical integration which allowed to resolve the highly singular integrand. As the main result, we obtained a divergence for the boson self-energy with the fifth power of the logarithm. This divergence marks the first deviation from the dynamical critical exponent $z = 3$ found so far. The discovered singular term is inherently nonrenormalizable and cannot be interpreted within the chosen renormalization group approach. We could trace back the unexpected form of the divergence to the peculiar momentum dependence in the action which is related to the IR scaling within the two-patch approximation. Therefore, the newfound contribution at four loop level makes it necessary to modify the low-energy theory and might eventually destroy the critical scaling entirely.

Regarding the physical systems studied in this thesis, many questions remain open. This work fully exploited the very special properties which are associated with the two-patch approximation and the expansion based on RPA propagators. We demonstrated the intricate analytical insights and the immense computational possibilities offered by a systematic treatment of N-point loops and pushed the method to the limits with a partial four-loop calculation. In the future it is certainly desirable that the qualitatively new behavior which we found at four loops is investigated by another method. Presently, no other field-theoretic approach seems viable which could make four loops accessible for concrete calculations. We are also not aware of any efforts in this direction.

Recent studies regarding critical metals focused on the construction of a generic low-energy theory, mainly regarding systems in three or close to three dimensions [161, 162, 191]. This approach also uses an effective fermion-boson action and advocates the generalization of the model to a large number of boson flavors N_b, paired with an expansion for $3 - \epsilon$ dimensions.

A different promising approach is a sign-free Monte-Carlo simulation of the nematic QCP. This is presently undertaken by Schattner *et al.* [192]. They simulate a system where a quantum Ising model drives the nematic phase transition of tight-binding fermions on a square lattice. At the moment it is uncertain whether the model constructed in this way falls into the same universality class as the SCM. As a preliminary result, they obtain a dynamical critical exponent $z = 2$ and find no sign of the Landau damping term $|q_0/q_y|$ in the boson propagator.

Another important question is the interplay of nematic fluctuations and superconducting correlations. Studying the competition of multiple instabilities is inherently difficult due to the sensitivity of the result on the chosen methods and approxima-

tions. Recently, Metlitski *et al.* [121] investigated this problem with a renormalization group approach and found that critical nematic order-parameter fluctuations mediate an attractive interaction which invariably entails a superconducting instability. They concluded that the critical regime is always intercepted by a superconducting instability. Lederer *et al.* [120] on the other hand used a BCS-Eliashberg treatment and found a sizable region where the nematic quantum criticality remains which simultaneously enhances the superconducting transition temperature. Very close to the QCP, when the enhancement is strongest, their weak coupling approach breaks down. Drawing from our results in chapter 4 which demonstrated the instability of the low-energy theory at the lowest scales, we conclude that a detailed numerical analysis is recommendable for this study of competing orders which allows to keep track of the various intermediate scaling regimes. A promising method to achieve this in a systematic way is the functional renormalization group approach [30].

While the correct values of the critical exponents for a nematic QCP and fermions coupled to a $U(1)$ gauge field might be known in the near future from Monte Carlo simulations, the successful formulation of a low-energy theory remains so far elusive. In the meantime, metallic criticality from singular forward scattering persists as a difficult problem which keeps offering new surprises.

Bibliography

[1] S. L. Sondhi, S. M. Girvin, J. P. Carini, and D. Shahar, "Continuous quantum phase transitions," Rev. Mod. Phys. **69**, 315 (1997), arXiv:cond-mat/9609279.

[2] J. Zinn-Justin, *Quantum Field Theory and Critical Phenomena* (Clarendon Press, 2002).

[3] M. Vojta, "Quantum phase transitions," Rep. Prog. Phys. **66**, 2069 (2003), arXiv:cond-mat/0309604.

[4] X. G. Wen, *Quantum Field Theory of Many Body Systems* (Oxford Graduate Texts, 2004).

[5] P. Coleman and A. J. Schofield, "Quantum criticality," Nature **433**, 226 (2005), cond-mat/0503002.

[6] S. Sachdev, *Quantum Phase Transitions 2nd ed.* (Cambridge University Press, 2011).

[7] G. R. Stewart, "Non-Fermi-liquid behavior in d- and f-electron metals," Rev. Mod. Phys. **73**, 797 (2001).

[8] P. Gegenwart, Q. Si, and F. Steglich, "Quantum criticality in heavy-fermion metals," Nat. Phys. **4**, 186 (2008), arXiv:0712.2045 [cond-mat.str-el].

[9] S. Sachdev, "Colloquium: Order and quantum phase transitions in the cuprate superconductors," Rev. Mod. Phys. **75**, 913 (2003), cond-mat/0211005.

[10] J. R. Schrieffer and J. S. Brooks, eds., *Handbook of High -Temperature Superconductivity: Theory and Experiment* (Springer, 2007).

[11] S. Sachdev and B. Keimer, "Quantum criticality," Phys. Today **64**, 29 (2011), arXiv:1102.4628 [cond-mat.str-el].

[12] B. I. Halperin, P. A. Lee, and N. Read, "Theory of the half-filled Landau level," Phys. Rev. B **47**, 7312 (1993).

[13] P. A. Lee, N. Nagaosa, and X.-G. Wen, "Doping a Mott insulator: Physics of high-temperature superconductivity," Rev. Mod. Phys. **78**, 17 (2006).

[14] S. Sachdev, "Exotic phases and quantum phase transitions: model systems and experiments," ArXiv (2009), arXiv:0901.4103 [cond-mat.str-el].

[15] I. Bloch, J. Dalibard, and W. Zwerger, "Many-body physics with ultracold gases," Rev. Mod. Phys. **80**, 885 (2008), arXiv:0704.3011.

[16] K. R. A. Hazzard and E. J. Mueller, "Techniques to measure quantum criticality in cold atoms," Phys. Rev. A **84**, 013604 (2011), arXiv:1006.0969 [cond-mat.quant-gas].

[17] W. Zwerger, ed., *BCS-BEC Crossover and the Unitary fermi Gas* (Springer, 2012).
[18] D. J. Amit and V. Martin-Mayor, *Field Theory, the Renormalization Group and Critical Phenomena*, 3rd ed. (World Scientific Publishing, 2005).
[19] J. A. Hertz, "Quantum critical phenomena," Phys. Rev. B **14**, 1165 (1976).
[20] T. Moriya, *Spin Fluctuations in Itinerant Electron Magnetism* (Springer, 1985).
[21] A. J. Millis, "Effect of a nonzero temperature on quantum critical points in itinerant fermion systems," Phys. Rev. B **48**, 7183 (1993).
[22] D. Belitz, T. R. Kirkpatrick, and T. Vojta, "How generic scale invariance influences quantum and classical phase transitions," Rev. Mod. Phys. **77**, 579 (2005).
[23] H. V. Löhneysen, A. Rosch, M. Vojta, and P. Wölfle, "Fermi-liquid instabilities at magnetic quantum phase transitions," Rev. Mod. Phys. **79**, 1015 (2007).
[24] D. Belitz, T. R. Kirkpatrick, and J. Rollbühler, "Breakdown of the Perturbative Renormalization Group at Certain Quantum Critical Points," Phys. Rev. Lett. **93**, 155701 (2004), cond-mat/0406350.
[25] A. Abanov and A. Chubukov, "Anomalous Scaling at the Quantum Critical Point in Itinerant Antiferromagnets," Phys. Rev. Lett. **93**, 255702 (2004).
[26] D. V. Khveshchenko and P. C. E. Stamp, "Low-energy properties of two-dimensional fermions with long-range current-current interactions," Phys. Rev. Lett. **71**, 2118 (1993).
[27] C. Nayak and F. Wilczek, "Non-Fermi liquid fixed point in 2 + 1 dimensions," Nuc. Phys. B **417**, 359 (1994), cond-mat/9312086.
[28] C. M. Varma, Z. Nussinov, and W. van Saarloos, "Singular or non-Fermi liquids," Phys. Rep. **361**, 267 (2002), arXiv:cond-mat/0103393.
[29] J. Custers, P. Gegenwart, H. Wilhelm, K. Neumaier, Y. Tokiwa, O. Trovarelli, C. Geibel, F. Steglich, C. Pépin, and P. Coleman, "The break-up of heavy electrons at a quantum critical point," Nature **424**, 524 (2003), cond-mat/0308001.
[30] W. Metzner, M. Salmhofer, C. Honerkamp, V. Meden, and K. Schönhammer, "Functional renormalization group approach to correlated fermion systems," Rev. Mod. Phys. **84**, 299 (2012).
[31] J. Rech, C. Pépin, and A. V. Chubukov, "Quantum critical behavior in itinerant electron systems: Eliashberg theory and instability of a ferromagnetic quantum critical point," Phys. Rev. B **74**, 195126 (2006), cond-mat/0605306.
[32] P. W. Anderson, "The resonating valence bond state in La2CuO4 and superconductivity," Science **235**, 1196 (1987).
[33] P. A. Lee and N. Nagaosa, "Gauge theory of the normal state of high-T_c superconductors," Phys. Rev. B **46**, 5621 (1992).
[34] P. W. Anderson, *The Theory of Superconductivity in the High-Tc Cuprates* (Princeton University Press, 1997).

[35] G. Baskaran and P. W. Anderson, "Gauge theory of high-temperature superconductors and strongly correlated Fermi systems," Phys. Rev. B **37**, 580 (1988).

[36] I. Affleck and J. B. Marston, "Large-n limit of the Heisenberg-Hubbard model: Implications for high-T_c superconductors," Phys. Rev. B **37**, 3774 (1988).

[37] P. B. Wiegmann, "Superconductivity in strongly correlated electronic systems and confinement versus deconfinement phenomenon," Phys. Rev. Lett. **60**, 821 (1988).

[38] J. B. Marston and I. Affleck, "Large-n limit of the Hubbard-Heisenberg model," Phys. Rev. B **39**, 11538 (1989).

[39] J. Polchinski, "Low-energy dynamics of the spinon-gauge system," Nuc. Phys. B **422**, 617 (1994), arXiv:cond-mat/9303037.

[40] T. Senthil, A. Vishwanath, L. Balents, S. Sachdev, and M. P. A. Fisher, "Deconfined Quantum Critical Points," Science **303**, 1490 (2004), cond-mat/0311326.

[41] T. Senthil and P. A. Lee, "Cuprates as doped U (1) spin liquids," Phys. Rev. B **71**, 174515 (2005), cond-mat/0406066.

[42] Y. Shimizu, K. Miyagawa, K. Kanoda, M. Maesato, and G. Saito, "Spin Liquid State in an Organic Mott Insulator with a Triangular Lattice," Phys. Rev. Lett. **91**, 107001 (2003), cond-mat/0307483.

[43] J. S. Helton, K. Matan, M. P. Shores, E. A. Nytko, B. M. Bartlett, Y. Yoshida, Y. Takano, A. Suslov, Y. Qiu, J.-H. Chung, D. G. Nocera, and Y. S. Lee, "Spin Dynamics of the Spin-1/2 Kagome Lattice Antiferromagnet $ZnCu_3(OH)_6Cl_2$," Phys. Rev. Lett. **98**, 107204 (2007), cond-mat/0610539.

[44] T. Itou, A. Oyamada, S. Maegawa, M. Tamura, and R. Kato, "Quantum spin liquid in the spin- 1/2 triangular antiferromagnet $EtMe_3Sb[Pd(dmit)_2]_2$," Phys. Rev. B **77**, 104413 (2008).

[45] O. I. Motrunich, "Variational study of triangular lattice spin- 1/2 model with ring exchanges and spin liquid state in κ- $(ET)_2$ Cu_2 $(CN)_3$," Phys. Rev. B **72**, 045105 (2005), cond-mat/0412556.

[46] S.-S. Lee and P. A. Lee, "U(1) Gauge Theory of the Hubbard Model: Spin Liquid States and Possible Application to κ-$(BEDT\text{-}TTF)_2Cu_2(CN)_3$," Phys. Rev. Lett. **95**, 036403 (2005), cond-mat/0502139.

[47] Y. Ran, M. Hermele, P. A. Lee, and X.-G. Wen, "Projected-Wave-Function Study of the Spin-1/2 Heisenberg Model on the Kagomé Lattice," Phys. Rev. Lett. **98**, 117205 (2007), cond-mat/0611414.

[48] T. Senthil, M. Vojta, and S. Sachdev, "Weak magnetism and non-Fermi liquids near heavy-fermion critical points," Phys. Rev. B **69**, 035111 (2004), cond-mat/0305193.

[49] R. K. Kaul, M. A. Metlitski, S. Sachdev, and C. Xu, "Destruction of Néel order in the cuprates by electron doping," Phys. Rev. B **78**, 045110 (2008),

arXiv:0804.1794 [cond-mat.str-el].
[50] R. K. Kaul, Y. B. Kim, S. Sachdev, and T. Senthil, "Algebraic charge liquids," Nat. Phys. **4**, 28 (2008), arXiv:0706.2187 [cond-mat.str-el].
[51] T. Holstein, R. E. Norton, and P. Pincus, "de Haas-van Alphen Effect and the Specific Heat of an Electron Gas," Phys. Rev. B **8**, 2649 (1973).
[52] M. Y. Reizer, "Effective electron-electron interaction in metals and superconductors," Phys. Rev. B **39**, 1602 (1989).
[53] V. Kalmeyer and S.-C. Zhang, "Metallic phase of the quantum Hall system at even-denominator filling fractions," Phys. Rev. B **46**, 9889 (1992).
[54] S. H. Simon and B. I. Halperin, "Finite-wave-vector electromagnetic response of fractional quantized Hall states," Phys. Rev. B **48**, 17368 (1993), cond-mat/9307048.
[55] S. H. Simon and B. I. Halperin, "Response function of the fractional quantized Hall state on a sphere. I. Fermion Chern-Simons theory," Phys. Rev. B **50**, 1807 (1994), cond-mat/9402089.
[56] J. K. Jain, *Composite Fermions* (Cambridge University Press, 2007).
[57] S. A. Kivelson, E. Fradkin, and V. J. Emery, "Electronic liquid-crystal phases of a doped Mott insulator," Nature **393**, 550 (1998), cond-mat/9707327.
[58] I. J. Pomeranchuk, "On the stability of a Fermi liquid," JETP **8**, 361 (1958).
[59] P. Wölfle and A. Rosch, "Fermi Liquid Near a Quantum Critical Point," J. Low Temp. Phys. **147**, 165 (2007), arXiv:cond-mat/0609343.
[60] E. Fradkin, S. A. Kivelson, and V. Oganesyan, "Electron Nematic Phase in a Transition Metal Oxide," Science **315**, 196 (2007).
[61] V. Oganesyan, S. A. Kivelson, and E. Fradkin, "Quantum theory of a nematic Fermi fluid," Phys. Rev. B **64**, 195109 (2001), arXiv:cond-mat/0102093.
[62] Y. Ando, K. Segawa, S. Komiya, and A. N. Lavrov, "Electrical Resistivity Anisotropy from Self-Organized One Dimensionality in High-Temperature Superconductors," Phys. Rev. Lett. **88**, 137005 (2002), cond-mat/0108053.
[63] V. Hinkov, D. Haug, B. Fauque, P. Bourges, Y. Sidis, A. Ivanov, C. Bernhard, C. T. Lin, and B. Keimer, "Electronic Liquid Crystal State in the High-Temperature Superconductor YBa2Cu3O6.45," Science **319**, 597–600 (2008).
[64] Y. Kohsaka, C. Taylor, K. Fujita, A. Schmidt, C. Lupien, T. Hanaguri, M. Azuma, M. Takano, H. Eisaki, H. Takagi, S. Uchida, and J. C. Davis, "An Intrinsic Bond-Centered Electronic Glass with Unidirectional Domains in Underdoped Cuprates," Science **315**, 1380 (2007), cond-mat/0703309.
[65] R. Daou, J. Chang, D. Leboeuf, O. Cyr-Choinière, F. Laliberté, N. Doiron-Leyraud, B. J. Ramshaw, R. Liang, D. A. Bonn, W. N. Hardy, and L. Taillefer, "Broken rotational symmetry in the pseudogap phase of a high-T_c superconductor," Nature **463**, 519 (2010), arXiv:0909.4430 [cond-mat.supr-con].
[66] S. A. Kivelson, I. P. Bindloss, E. Fradkin, V. Oganesyan, J. M. Tranquada,

A. Kapitulnik, and C. Howald, "How to detect fluctuating stripes in the high-temperature superconductors," Rev. Mod. Phys. **75**, 1201 (2003), cond-mat/0210683.

[67] S. A. Kivelson and E. Fradkin, "How optimal inhomogeneity produces high temperature superconductivity," ArXiv (2005), cond-mat/0507459.

[68] M. Vojta, "Lattice symmetry breaking in cuprate superconductors: stripes, nematics, and superconductivity," Adv. Phys. **58**, 699 (2009), arXiv:0901.3145 [cond-mat.supr-con].

[69] N. P. Armitage, P. Fournier, and R. L. Greene, "Progress and perspectives on electron-doped cuprates," Rev. Mod. Phys. **82**, 2421 (2010), arXiv:0906.2931 [cond-mat.supr-con].

[70] E. Fradkin, "Electronic Liquid Crystal Phases in Strongly Correlated Systems," in *Modern Theories of Many-Particle Systems in Condensed Matter Physics*, edited by D. C. Cabra, A. Honecker, and P. Pujol (Springer, 2012) Chap. 2, pp. 53–116.

[71] T.-M. Chuang, M. P. Allan, J. Lee, Y. Xie, N. Ni, S. L. Bud'ko, G. S. Boebinger, P. C. Canfield, and J. C. Davis, "Nematic Electronic Structure in the "Parent" State of the Iron-Based Superconductor $Ca(Fe_{1-x}Co_x)_2As_2$," Science **327**, 181 (2010).

[72] S. Nandi, M. G. Kim, A. Kreyssig, R. M. Fernandes, D. K. Pratt, A. Thaler, N. Ni, S. L. Bud'Ko, P. C. Canfield, J. Schmalian, R. J. McQueeney, and A. I. Goldman, "Anomalous Suppression of the Orthorhombic Lattice Distortion in Superconducting $Ba(Fe_{1-x}Co_x)_2As_2$ Single Crystals," Phys. Rev. Lett. **104**, 057006 (2010), arXiv:0911.3136 [cond-mat.supr-con].

[73] J.-H. Chu, J. G. Analytis, K. De Greve, P. L. McMahon, Z. Islam, Y. Yamamoto, and I. R. Fisher, "In-Plane Resistivity Anisotropy in an Underdoped Iron Arsenide Superconductor," Science **329**, 824 (2010).

[74] R. M. Fernandes, A. V. Chubukov, and J. Schmalian, "What drives nematic order in iron-based superconductors?" Nat. Phys. **10**, 97 (2014).

[75] S. Kasahara, T. Shibauchi, K. Hashimoto, K. Ikada, S. Tonegawa, R. Okazaki, H. Shishido, H. Ikeda, H. Takeya, K. Hirata, T. Terashima, and Y. Matsuda, "Evolution from non-Fermi- to Fermi-liquid transport via isovalent doping in $BaFe_2(As_{1-x}P_x)_2$ superconductors," Phys. Rev. B **81**, 184519 (2010), arXiv:0905.4427 [cond-mat.supr-con].

[76] S. A. Grigera, R. S. Perry, A. J. Schofield, M. Chiao, S. R. Julian, G. G. Lonzarich, S. I. Ikeda, Y. Maeno, A. J. Millis, and A. P. Mackenzie, "Magnetic Field-Tuned Quantum Criticality in the Metallic Ruthenate $Sr_3Ru_2O_7$," Science **294**, 329 (2001).

[77] N. E. Hussey, "TOPICAL REVIEW: Phenomenology of the normal state in-plane transport properties of high-T_c cuprates," J. Phys. Cond. Mat. **20**, 123201

(2008), arXiv:0804.2984 [cond-mat.supr-con].
[78] D. N. Basov and A. V. Chubukov, "Manifesto for a higher T_c," Nat. Phys. **7**, 272 (2011).
[79] C. M. Varma, "Pseudogap Phase and the Quantum-Critical Point in Copper-Oxide Metals," Phys. Rev. Lett. **83**, 3538 (1999).
[80] S. Sachdev, "Where is the quantum critical point in the cuprate superconductors?" Phys. Status Solidi B **247**, 537 (2009), arXiv:0907.0008 [cond-mat.str-el].
[81] C. Fang, H. Yao, W.-F. Tsai, J. Hu, and S. A. Kivelson, "Theory of electron nematic order in LaFeAsO," Phys. Rev. B **77**, 224509 (2008), arXiv:0804.3843 [cond-mat.str-el].
[82] C. Xu, M. Müller, and S. Sachdev, "Ising and spin orders in the iron-based superconductors," Phys. Rev. B **78**, 020501 (2008), arXiv:0804.4293 [cond-mat.str-el].
[83] E.-A. Kim, M. J. Lawler, P. Oreto, S. Sachdev, E. Fradkin, and S. A. Kivelson, "Theory of the nodal nematic quantum phase transition in superconductors," Phys. Rev. B **77**, 184514 (2008), arXiv:0705.4099 [cond-mat.supr-con].
[84] T. Senthil, "Critical Fermi surfaces and non-Fermi liquid metals," Phys. Rev. B **78**, 035103 (2008), arXiv:0803.4009 [cond-mat.str-el].
[85] C. M. Varma and L. Zhu, "Helicity Order: Hidden Order Parameter in URu_2Si_2," Phys. Rev. Lett. **96**, 036405 (2006), cond-mat/0502344.
[86] M. P. Lilly, K. B. Cooper, J. P. Eisenstein, L. N. Pfeiffer, and K. W. West, "Evidence for an Anisotropic State of Two-Dimensional Electrons in High Landau Levels," Phys. Rev. Lett. **82**, 394 (1999), cond-mat/9808227.
[87] R. R. Du, D. C. Tsui, H. L. Stormer, L. N. Pfeiffer, K. W. Baldwin, and K. W. West, "Strongly anisotropic transport in higher two-dimensional Landau levels," Solid State Communications **109**, 389 (1999), cond-mat/9812025.
[88] R. A. Borzi, S. A. Grigera, J. Farrell, R. S. Perry, S. J. S. Lister, S. L. Lee, D. A. Tennant, Y. Maeno, and A. P. Mackenzie, "Formation of a Nematic Fluid at High Fields in $Sr_3Ru_2O_7$," Science **315**, 214 (2007), cond-mat/0612599.
[89] E. Fradkin, S. A. Kivelson, M. J. Lawler, J. P. Eisenstein, and A. P. MacKenzie, "Nematic Fermi Fluids in Condensed Matter Physics," Ann. Rev. Cond. Mat. **1**, 153 (2010), arXiv:0910.4166 [cond-mat.str-el].
[90] H. Yamase and H. Kohno, "Instability toward Formation of Quasi-One-Dimensional Fermi Surface in Two-Dimensional t-J Model," J. Phys. Soc. Jpn. **69**, 2151 (2000).
[91] H. Yamase and H. Kohno, "Possible Quasi-One-Dimensional Fermi Surface in $La_{2-x}Sr_xCuO_4$," J. Phys. Soc. Jpn. **69**, 332 (2000).
[92] C. J. Halboth and W. Metzner, "d-Wave Superconductivity and Pomeranchuk Instability in the Two-Dimensional Hubbard Model," Phys. Rev. Lett. **85**, 5162 (2000), cond-mat/0003349.

[93] W. Metzner, D. Rohe, and S. Andergassen, "Soft Fermi Surfaces and Breakdown of Fermi-Liquid Behavior," Phys. Rev. Lett. **91**, 066402 (2003), cond-mat/0303154.

[94] H.-Y. Kee, E. H. Kim, and C.-H. Chung, "Signatures of an electronic nematic phase at the isotropic-nematic phase transition," Phys. Rev. B **68**, 245109 (2003), cond-mat/0304467.

[95] I. Khavkine, C.-H. Chung, V. Oganesyan, and H.-Y. Kee, "Formation of an electronic nematic phase in interacting fermion systems," Phys. Rev. B **70**, 155110 (2004), cond-mat/0402565.

[96] H. Yamase, V. Oganesyan, and W. Metzner, "Mean-field theory for symmetry-breaking Fermi surface deformations on a square lattice," Phys. Rev. B **72**, 035114 (2005), arXiv:cond-mat/0502238.

[97] P. Jakubczyk, W. Metzner, and H. Yamase, "Turning a First Order Quantum Phase Transition Continuous by Fluctuations: General Flow Equations and Application to d-Wave Pomeranchuk Instability," Phys. Rev. Lett. **103**, 220602 (2009), arXiv:0908.2620 [cond-mat.str-el].

[98] H. Yamase, P. Jakubczyk, and W. Metzner, "Nematic quantum criticality without order," Phys. Rev. B **83**, 125121 (2011), arXiv:1101.1221 [cond-mat.str-el].

[99] Y. Huh and S. Sachdev, "Renormalization group theory of nematic ordering in d -wave superconductors," Phys. Rev. B **78**, 064512 (2008), arXiv:0806.0002 [cond-mat.str-el].

[100] P. Chandra, P. Coleman, and A. I. Larkin, "Ising transition in frustrated Heisenberg models," Phys. Rev. Lett. **64**, 88 (1990).

[101] L. Capriotti and S. Sachdev, "Low-Temperature Broken-Symmetry Phases of Spiral Antiferromagnets," Phys. Rev. Lett. **93**, 257206 (2004), cond-mat/0409519.

[102] N. Read and S. Sachdev, "Large-N expansion for frustrated quantum antiferromagnets," Phys. Rev. Lett. **66**, 1773 (1991).

[103] S. Sachdev and N. Read, "Large N Expansion for Frustrated and Doped Quantum Antiferromagnets," Int. J. Mod. Phys. B **5**, 219 (1991), cond-mat/0402109.

[104] M. J. Lawler, D. G. Barci, V. Fernández, E. Fradkin, and L. Oxman, "Nonperturbative behavior of the quantum phase transition to a nematic Fermi fluid," Phys. Rev. B **73**, 085101 (2006), cond-mat/0508747.

[105] J. Quintanilla and A. J. Schofield, "Pomeranchuk and topological Fermi surface instabilities from central interactions," Phys. Rev. B **74**, 115126 (2006), cond-mat/0601103.

[106] M. J. Lawler and E. Fradkin, "Local quantum criticality at the nematic quantum phase transition," Phys. Rev. B **75**, 033304 (2007), cond-mat/0605203.

[107] J. Quintanilla, M. Haque, and A. J. Schofield, "Symmetry-breaking Fermi

surface deformations from central interactions in two dimensions," Phys. Rev. B **78**, 035131 (2008), arXiv:0805.4623 [cond-mat.str-el].

[108] M. Zacharias, P. Wölfle, and M. Garst, "Multiscale quantum criticality: Pomeranchuk instability in isotropic metals," Phys. Rev. B **80**, 165116 (2009), arXiv:0907.0489 [cond-mat.str-el].

[109] T. Meng, A. Rosch, and M. Garst, "Quantum criticality with multiple dynamics," Phys. Rev. B **86**, 125107 (2012), arXiv:1205.3400 [cond-mat.str-el].

[110] P. A. Lee, "Gauge field, Aharonov-Bohm flux, and high-Tc superconductivity," Phys. Rev. Lett. **63**, 680 (1989).

[111] L. Dell'Anna and W. Metzner, "Fermi surface fluctuations and single electron excitations near Pomeranchuk instability in two dimensions," Phys. Rev. B **73**, 045127 (2006), cond-mat/0507532.

[112] B. L. Altshuler, L. B. Ioffe, and A. J. Millis, "Low-energy properties of fermions with singular interactions," Phys. Rev. B **50**, 14048 (1994), arXiv:cond-mat/9406024.

[113] Y. B. Kim, A. Furusaki, X.-G. Wen, and P. A. Lee, "Gauge-invariant response functions of fermions coupled to a gauge field," Phys. Rev. B **50**, 17917 (1994), cond-mat/9405083.

[114] M. A. Metlitski and S. Sachdev, "Quantum phase transitions of metals in two spatial dimensions. I. Ising-nematic order," Phys. Rev. B **82**, 075127 (2010), arXiv:1001.1153 [cond-mat.str-el].

[115] S.-S. Lee, "Low-energy effective theory of Fermi surface coupled with U(1) gauge field in 2+1 dimensions," Phys. Rev. B **80**, 165102 (2009), arXiv:0905.4532 [cond-mat.str-el].

[116] D. F. Mross, J. McGreevy, H. Liu, and T. Senthil, "Controlled expansion for certain non-Fermi-liquid metals," Phys. Rev. B **82**, 045121 (2010), arXiv:1003.0894 [cond-mat.str-el].

[117] C. Drukier, L. Bartosch, A. Isidori, and P. Kopietz, "Functional renormalization group approach to the Ising-nematic quantum critical point of two-dimensional metals," Phys. Rev. B **85**, 245120 (2012), arXiv:1203.2645 [cond-mat.str-el].

[118] D. Dalidovich and S.-S. Lee, "Perturbative non-Fermi liquids from dimensional regularization," Phys. Rev. B **88**, 245106 (2013), arXiv:1307.3170 [cond-mat.str-el].

[119] H. Yamase and W. Metzner, "Competition of Fermi surface symmetry breaking and superconductivity," Phys. Rev. B **75**, 155117 (2007), cond-mat/0701660.

[120] S. Lederer, Y. Schattner, E. Berg, and S. A. Kivelson, "Enhancement of Superconductivity near a Nematic Quantum Critical Point," Phys. Rev. Lett. **114**, 097001 (2015), arXiv:1406.1193 [cond-mat.supr-con].

[121] M. A. Metlitski, D. F. Mross, S. Sachdev, and T. Senthil, "Cooper pairing in non-Fermi liquids," Phys. Rev. B **91**, 115111 (2015).

[122] M. A. Metlitski and S. Sachdev, "Instabilities near the onset of spin density wave order in metals," New J. Phys. **12**, 105007 (2010), arXiv:1007.1968 [cond-mat.supr-con].

[123] S. Sachdev and R. La Placa, "Bond Order in Two-Dimensional Metals with Antiferromagnetic Exchange Interactions," Phys. Rev. Lett. **111**, 027202 (2013), arXiv:1303.2114 [cond-mat.supr-con].

[124] D. Chowdhury and S. Sachdev, "Density-wave instabilities of fractionalized Fermi liquids," Phys. Rev. B **90**, 245136 (2014), arXiv:1409.5430 [cond-mat.str-el].

[125] A. F. Ho and A. J. Schofield, "Effect of disorder on a Pomeranchuk instability," Europhys. Lett. **84**, 27007 (2008), arXiv:0706.1955 [cond-mat.str-el].

[126] J. Wang, G.-Z. Liu, and H. Kleinert, "Disorder effects at a nematic quantum critical point in d-wave cuprate superconductors," Phys. Rev. B **83**, 214503 (2011), arXiv:1101.1551 [cond-mat.str-el].

[127] S. A. Hartnoll, R. Mahajan, M. Punk, and S. Sachdev, "Transport near the Ising-nematic quantum critical point of metals in two dimensions," Phys. Rev. B **89**, 155130 (2014), arXiv:1401.7012 [cond-mat.str-el].

[128] T. Holder and W. Metzner, "Fermion loops and improved power-counting in two-dimensional critical metals with singular forward scattering," ArXiv e-prints (2015), arXiv:1509.07783 [cond-mat.str-el].

[129] T. Holder and W. Metzner, "Anomalous dynamical scaling from nematic and U(1) gauge field fluctuations in two-dimensional metals," Phys. Rev. B **92**, 041112 (2015), arXiv:1503.05089 [cond-mat.str-el].

[130] J. Polchinski, "Effective Field Theory and the Fermi Surface," ArXiv (1992), hep-th/9210046.

[131] R. Shankar, "Renormalization-group approach to interacting fermions," Rev. Mod. Phys. **66**, 129 (1994), cond-mat/9307009.

[132] S. Thier, *Fermion loops and effective action for nematic quantum phase transitions*, Diploma thesis, Max Planck Institute for Solid State Research, University of Stuttgart (2011).

[133] A. Houghton, H.-J. Kwon, and J. B. Marston, "Multidimensional bosonization," Adv. Phys. **49**, 141 (2000), cond-mat/9810388.

[134] A. Neumayr and W. Metzner, "Fermion loops, loop cancellation, and density correlations in two-dimensional Fermi systems," Phys. Rev. B **58**, 15449 (1998).

[135] A. Abanov, A. V. Chubukov, and J. Schmalian, "Quantum-critical theory of the spin-fermion model and its application to cuprates: normal state analysis," Adv. Phys. **52**, 119 (2003).

[136] M. A. Metlitski and S. Sachdev, "Quantum phase transitions of metals in two

spatial dimensions. II. Spin density wave order," Phys. Rev. B **82**, 075128 (2010), arXiv:1005.1288 [cond-mat.str-el].

[137] S. C. Thier and W. Metzner, "Singular order parameter interaction at the nematic quantum critical point in two-dimensional electron systems," Phys. Rev. B **84**, 155133 (2011), arXiv:1108.1929 [cond-mat.str-el].

[138] J. Feldman, H. Knörrer, R. Sinclair, and E. Trubowitz, "Evaluation of fermion loops by higher residues." Prog. in Math. **162**, 361 (1998).

[139] L. B. Ioffe, D. Lidsky, and B. L. Altshuler, "Effective lowering of dimensionality in the strongly correlated two dimensional electron gas," Phys. Rev. Lett. **73**, 472 (1994).

[140] T. R. Kirkpatrick and D. Belitz, "Quantum critical behavior of disordered itinerant ferromagnets," Phys. Rev. B **53**, 14364 (1996), cond-mat/9601008.

[141] T. Vojta, D. Belitz, R. Narayanan, and T. R. Kirkpatrick, "Quantum critical behavior of clean itinerant ferromagnets," Zeitschrift fur Physik B Condensed Matter **103**, 451 (1997), cond-mat/9612224.

[142] D. Belitz, T. R. Kirkpatrick, R. Narayanan, and T. Vojta, "Transport Anomalies and Marginal-Fermi-Liquid Effects at a Quantum Critical Point," Phys. Rev. Lett. **85**, 4602 (2000), cond-mat/0008431.

[143] D. Belitz, T. R. Kirkpatrick, M. T. Mercaldo, and S. L. Sessions, "Local field theory for disordered itinerant quantum ferromagnets," Phys. Rev. B **63**, 174427 (2001).

[144] D. Belitz, T. R. Kirkpatrick, M. T. Mercaldo, and S. L. Sessions, "Quantum critical behavior in disordered itinerant ferromagnets: Logarithmic corrections to scaling," Phys. Rev. B **63**, 174428 (2001), cond-mat/0010377.

[145] D. Belitz, T. R. Kirkpatrick, and T. Vojta, "Nonanalytic behavior of the spin susceptibility in clean Fermi systems," Phys. Rev. B **55**, 9452 (1997).

[146] D. Belitz, T. R. Kirkpatrick, and T. Vojta, "First Order Transitions and Multicritical Points in Weak Itinerant Ferromagnets," Phys. Rev. Lett. **82**, 4707 (1999), cond-mat/9812420.

[147] D. Belitz, T. R. Kirkpatrick, and J. Rollbühler, "Tricritical Behavior in Itinerant Quantum Ferromagnets," Phys. Rev. Lett. **94**, 247205 (2005), cond-mat/0410344.

[148] A. V. Chubukov, C. Pépin, and J. Rech, "Instability of the Quantum-Critical Point of Itinerant Ferromagnets," Phys. Rev. Lett. **92**, 147003 (2004), cond-mat/0311420.

[149] T. Vojta and R. Sknepnek, "Quantum phase transition of itinerant helimagnets," Phys. Rev. B **64**, 052404 (2001), cond-mat/0009441.

[150] A. V. Chubukov and D. L. Maslov, "Nonanalytic corrections to the Fermi-liquid behavior," Phys. Rev. B **68**, 155113 (2003), cond-mat/0305022.

[151] A. V. Chubukov and D. L. Maslov, "Singular corrections to the Fermi-liquid theory," Phys. Rev. B **69**, 121102 (2004), cond-mat/0304381.

[152] D. L. Maslov, A. V. Chubukov, and R. Saha, "Nonanalytic magnetic response of Fermi and non-Fermi liquids," Phys. Rev. B **74**, 220402 (2006), cond-mat/0609102.

[153] D. Belitz, T. R. Kirkpatrick, and A. Rosch, "Theory of helimagnons in itinerant quantum systems," Phys. Rev. B **73**, 054431 (2006), cond-mat/0510444.

[154] D. Belitz, T. R. Kirkpatrick, and A. Rosch, "Theory of helimagnons in itinerant quantum systems. II. Nonanalytic corrections to Fermi-liquid behavior," Phys. Rev. B **74**, 024409 (2006), cond-mat/0604427.

[155] J. Cardy, *Scaling and Renormalization in Statistical Physics* (Cambridge University Press, 1996).

[156] S. Caprara, R. Citro, C. di Castro, and G. Stefanucci, "Introduction to Renormalization Group and Ward Identities in Critical Phenomena and in Fermi and Bose Liquids," in *American Institute of Physics Conference Series*, American Institute of Physics Conference Series, Vol. 629, edited by F. Mancini (2002) pp. 3–78.

[157] R. Roussev and A. J. Millis, "Quantum critical effects on transition temperature of magnetically mediated p-wave superconductivity," Phys. Rev. B **63**, 140504 (2001), cond-mat/0005449.

[158] Z. Wang, W. Mao, and K. Bedell, "Superconductivity near Itinerant Ferromagnetic Quantum Criticality," Phys. Rev. Lett. **87**, 257001 (2001), cond-mat/0104097.

[159] M. Dzero and L. P. Gor'kov, "Breakup of a Stoner model for the two-dimensional ferromagnetic quantum critical point," Phys. Rev. B **69**, 092501 (2004), cond-mat/0310124.

[160] A. V. Chubukov, "Self-generated locality near a ferromagnetic quantum critical point," Phys. Rev. B **71**, 245123 (2005), cond-mat/0502302.

[161] A. L. Fitzpatrick, S. Kachru, J. Kaplan, and S. Raghu, "Non-Fermi-liquid fixed point in a Wilsonian theory of quantum critical metals," Phys. Rev. B **88**, 125116 (2013), arXiv:1307.0004 [cond-mat.str-el].

[162] A. L. Fitzpatrick, S. Kachru, J. Kaplan, and S. Raghu, "Non-Fermi-liquid behavior of large-N_B quantum critical metals," Phys. Rev. B **89**, 165114 (2014), arXiv:1312.3321 [cond-mat.str-el].

[163] F. Stern, "Polarizability of a Two-Dimensional Electron Gas," Phys. Rev. Lett. **18**, 546 (1967).

[164] L. B. Ioffe and A. I. Larkin, "Gapless fermions and gauge fields in dielectrics," Phys. Rev. B **39**, 8988 (1989).

[165] L. B. Ioffe and G. Kotliar, "Transport phenomena near the Mott transition," Phys. Rev. B **42**, 10348 (1990).

[166] L. B. Ioffe and P. B. Wiegmann, "Linear temperature dependence of resistivity as evidence of gauge interaction," Phys. Rev. Lett. **65**, 653 (1990).
[167] G. Baym, H. Monien, C. J. Pethick, and D. G. Ravenhall, "Transverse interactions and transport in relativistic quark-gluon and electromagnetic plasmas," Phys. Rev. Lett. **64**, 1867 (1990).
[168] N. Nagaosa and P. A. Lee, "Normal-state properties of the uniform resonating-valence-bond state," Phys. Rev. Lett. **64**, 2450 (1990).
[169] N. Nagaosa and P. Lee, "Experimental consequences of the uniform resonating-valence-bond state," Phys. Rev. B **43**, 1233 (1991).
[170] B. Blok and H. Monien, "Gauge theories of high-T_c superconductors," Phys. Rev. B **47**, 3454 (1993).
[171] J. Gan and E. Wong, "Non-Fermi-liquid behavior in quantum critical systems," Phys. Rev. Lett. **71**, 4226 (1993), cond-mat/9309044.
[172] C. Nayak and F. Wilczek, "Renormalization group approach to low temperature properties of a non-Fermi liquid metal," Nuc. Phys. B **430**, 534 (1994), cond-mat/9408016.
[173] S.-S. Lee, "Stability of the U(1) spin liquid with a spinon Fermi surface in 2+1 dimensions," Phys. Rev. B **78**, 085129 (2008), arXiv:0804.3800 [cond-mat.str-el].
[174] H. Bruus and K. Flensberg, *Many-Body Quantum Theory in Condensed Matter Physics: An Introduction* (Oxford University Press, 2004).
[175] J. Hofmann, E. Barnes, and S. Das Sarma, "Why Does Graphene Behave as a Weakly Interacting System?" Phys. Rev. Lett. **113**, 105502 (2014), arXiv:1405.7036 [cond-mat.mes-hall].
[176] A. Giuliani and G. Vignale, *Quantum Theory of the Electron Liquid* (Cambridge University Press, 2005).
[177] G. Mahan, *Many-Particle Physics* (Springer, 1990).
[178] W. Metzner and C. di Castro, "Conservation laws and correlation functions in the Luttinger liquid," Phys. Rev. B **47**, 16107 (1993).
[179] W. Metzner, C. Castellani, and C. Di Castro, "Fermi Systems with Strong Forward Scattering," Adv. Phys. **47**, 317 (1997), arXiv:cond-mat/9701012.
[180] A. V. Chubukov, "Ward identities for strongly coupled Eliashberg theories," Phys. Rev. B **72**, 085113 (2005), cond-mat/0411039.
[181] S. Sur and S.-S. Lee, "Chiral non-Fermi liquids," Phys. Rev. B **90**, 045121 (2014), arXiv:1310.7543 [cond-mat.str-el].
[182] A. Altland and B. Simons, *Condensed Matter Field Theory* (Cambridge University Press, 2006).
[183] T. Giamarchi, *Quantum Physics in One Dimension* (Clarendon Press, 2001).
[184] A. Neumayr and W. Metzner, "Reduction Formula for Fermion Loops and Density Correlations of the 1D Fermi Gas," J. Stat. Phys. **96**, 613 (1999).

[185] M. Peskin and C. Schroeder, *An Introduction to Quantum Field Theory* (Addison-Wesley, 1995).
[186] J. W. Negele and H. Orland, *Quantum many-particle systems*, Advanced book classics (Addison-Wesley, Boulder, CO, 1988).
[187] J. Feldman, M. Salmhofer, and E. Trubowitz, "Pertubation theory around nonnested fermi surfaces. I. Keeping the fermi surface fixed," J. Stat. Phys. **84**, 1209 (1996), cond-mat/9509006.
[188] T. Hahn, "CUBA - a library for multidimensional numerical integration," Comput. Phys. Commun. **168**, 78 (2005), hep-ph/0404043.
[189] A. M. Polyakov, "Compact gauge fields and the infrared catastrophe," Phys. Lett. B **59**, 82 (1975).
[190] Polyakov, *Gauge Fields and Strings* (Harwood Academic Publishers, 1987).
[191] R. Mahajan, D. M. Ramirez, S. Kachru, and S. Raghu, "Quantum critical metals in d=3+1 dimensions," Phys. Rev. B **88**, 115116 (2013), arXiv:1303.1587 [cond-mat.str-el].
[192] Y. Schattner, S. Lederer, S. A. Kivelson, and B. E., "Ising nematic quantum critical point in a metal: a quantum Monte Carlo study," unpublished (2015).

Acknowledgments

During the completion of this thesis I was supported by many people. I want to thank Walter Metzner for giving me the opportunity to join his group at the Max-Planck Institute in Stuttgart. He proposed this challenging topic and always encouraged me that my results are worth the expended effort. I want to thank him for his kind supervision and his refreshing straightforwardness. For co-refereeing this thesis I want to thank Maria Daghofer.

I also want to express my thanks to my office mates, Christoph Husemann and Damien Terrade, with whom I had a great time. They always offered encouragement and engaged in many useful discussions. Special thanks goes to my colleague Andreas Eberlein, who helped me tremendously when I first arrived at the institute and patiently answered my many questions about the wide field of condensed matter physics. He and also Benjamin Obert, Raquel Queiroz, Eslam Khalaf and Chia-Wei Huang were a constant inspiration through countless discussions, especially in our Journal Club. I especially thank Chia-Wei Huang for going through parts of the thesis. Roland Zeyher and Peter Horsch were always eager to share their knowledge and experience of many years and explain to us newcomers old and new ideas. Furthermore, a big thanks goes to Jeanette Schüller-Knapp for her competent help with all bureaucratic matters. I want to thank all members of the department for their kindness and the welcoming atmosphere they created.

For useful topical discussions I want to further thank Dietrich Belitz, Andrey Chubukov, Holger Gies, and Manfred Salmhofer.

Finally, I would not be who I am without the dedicated love of my family: my dad, mom, brother and sister. The strong bond connecting us carried me through sunny and rainy days since my earliest childhood until the present day.

And lastly, I am grateful to my Lord and God Jesus Christ for creating me and giving me my talent in physics. His grace and truth guided me through all tough phases in my life and his loving kindness I can clearly see in every part of my life.

Deutsche Zusammenfassung

Thema dieser Dissertation ist die theoretische Untersuchung der Niederenergietheorie für zweidimensionale Metalle, wenn singuläre Vorwärtsstreuung im Ladungskanal vorliegt. Dies ist entweder an einem nematischen quantenkritischen Punkt der Fall, oder wenn Elektronen an ein $U(1)$-Eichfeld gekoppelt werden.

Zweidimensionale Metalle mit singulärer Vorwärtsstreuung im Ladungskanal sind als idealisierte Modelle für viele stark korrelierte Elektronensysteme vorgeschlagen worden. So wurden sie herangezogen, um den normalleitenden Zustand von Hochtemperatursupraleitern sowohl vom Typ der Kuprate als auch der Pniktide bei optimaler Dotierung zu beschreiben. Des Weiteren wurde singuläre Vorwärtsstreuung mit Supraleitern mit schweren Fermionen und mit Systemen mit fraktionalem Quanten-Hall-Effekt bei einem halb gefüllten Landaulevel in Zusammenhang gebracht.

Das Zentrum der Arbeit bildet die Betrachtung des universellen Skalierungsverhaltens im quantenkritischen Regime und die Bestimmung der damit verbundenen kritischen Exponenten. Zu diesem Zweck analysieren wir den Einfluss von Quantenfluktuationen mithilfe eines feldtheoretischen Renormierungsgruppenansatzes. Eine wichtige Rolle nehmen hierbei die effektiven N-Punkt Dichtevertizes ein, da die detaillierte Untersuchung der Impuls- und Frequenzabhängigkeiten dieser Größen eine genaue Charakterisierung der auftretenden Fluktuationsbeiträge in jeder Schleifenordnung erlaubt.

In Kapitel 2 wird die Entwicklung der Niederenergietheorie für quantenkritische Metalle rekapituliert und die Herleitung des heute gebräuchlichen Zuganges skizziert. Ein wichtiges Element der Niederenergietheorie ist die Resummation der Selbstenergiebeiträge auf Ein-Schleifen-Niveau, welche dann als Startpunkt für die Berechnung weiterer Fluktuationsbeiträge dient. Die dabei benutzten Näherungen werden kritisch analysiert und deren Reichweite und Grenzen präzisiert. Wir präsentieren insbesondere eine vollständige Analyse der Vertexkorrektur auf Ein-Schleifen-Niveau und einen einfachen Beweis der Endlichkeit von Fluktuationsbeiträgen, die ausschließlich Elektronen von der lokalen Umgebung eines Punktes der Fermifläche enthalten.

In Kapitel 3 werden für den Niederenergielimes explizite Ausdrücke für die N-Punkt Dichtevertizes hergeleitet. Dazu wird die spezielle Frequenz- und Impulsstruktur dieser Dichtevertizes ausgenutzt, die mit den gewählten Näherungen im Niederenergielimes zusammenhängt und eine besonders geradlinige Auswertung

mithilfe von Konturintegrationen ermöglicht. Die Form dieser Ausdrücke erleichtert einerseits den numerischen Zugang zu Korrekturen höherer Ordnung, andererseits verbessern sie den analytischen Zugriff beträchtlich.

Wir beweisen zwei einfache Regeln, die beide zu einer Verbesserung des abgeschätzten UV-Verhaltens von N-Punkt Dichtevertizes führen. Die erste Regel gilt für symmetrisierte N-Punkt Dichtevertizes, bei denen ein oder zwei bosonische Beinchen kleine Impulse tragen. Die zweite Regel gilt für unsymmetrisierte N-Punkt Dichtevertizes, bei denen genau ein großer Impuls durch den Vertex läuft. Die so gewonnenen, verbesserten Abschätzungen des UV-Verhaltens erlauben eine scharfe Bestimmung des Divergenzgrades von Fluktuationsbeiträgen.

Wir zeigen, dass keine Beiträge zur bosonischen Selbstenergie auftreten können, die eine polynomiale Divergenz enthalten. Zudem ist es mit der verbesserten Abschätzung des UV-Verhaltens möglich, nicht nur die bereits bekannten Resultate bis zur Drei-Schleifen-Ordnung zu bestätigen, sondern auch das Auftreten neuer Korrekturen für die bosonische Selbstenergie von Diagrammen mit vier Schleifen vorherzusagen.

In Kapitel 4 wird diese Vorhersage durch eine explizite Rechnung bestätigt. Dazu wird eine bestimmte Teilmenge von Diagrammen mit vier Schleifen berechnet, welche genügt, um die Existenz eines singulären Beitrages zu etablieren. Wir dokumentieren die schwierige Auswertung dieser Diagramme und zeigen, mit welchen Kriterien die Korrektheit der numerischen Integration überprüft werden kann.

Im Ergebnis erhalten wir eine Singularität, was die allgemeine Vorhersage bestätigt, die mithilfe der Verbesserung des abgeschätzten UV-Verhaltens getroffen wurde. Überraschenderweise enthält die gefundene Singularität eine fünfte Potenz des Logarithmus, so dass es nicht möglich ist, sie als Beitrag zur Renormierung des dynamischen kritischen Exponenten in der Niederenergietheorie aufzufassen. Wir diskutieren die möglichen physikalischen Konsequenzen dieses Verhaltens für die betrachteten zweidimensionalen Metalle mit singulärer Vorwärtsstreuung im Ladungskanal. In Betracht kommen das Auftreten von Quantenanomalien, die spontane Symmetriebrechung der speziellen Impulsstruktur die im Niederenergielimes realisiert wird, oder die Instabilität des quantenkritischen Punktes bei sehr kleinen Skalen.